FRICTIONAL HEATING OF TRIBOLOGICAL CONTACTS

J. BOS

ISBN 90-9008920-9

FRICTIONAL HEATING OF TRIBOLOGICAL CONTACTS

PROEFSCHRIFT

ter verkrijging van
de graad van doctor aan de Universiteit Twente,
op gezag van de rector magnificus,
prof. dr. Th.J.A. Popma
volgens besluit van het College voor Promoties
in het openbaar te verdedigen
op donderdag 23 november 1995 te 13.15 uur

door

Johannes Bos

geboren op 21 januari 1968

te Hoogeveen

DIT PROEFSCHRIFT IS GOEDGEKEURD DOOR :

Promotor : Prof. ir. A.W.J. de Gee

Samenvatting

Overal waar wrijving optreedt, wordt mechanische energie omgezet in warmte. De temperatuurstijging die hiermee gepaard gaat kan een belangrijke invloed hebben op het gedrag van de elkaar rakende componenten. Behalve dat thermische verschijnselen de werking van tribologische contacten bepalen, hebben ze invloed op de betrouwbaarheid en kunnen ze falen ervan teweeg brengen.

In het eerste deel van dit proefschrift zal de nadruk liggen op de numerieke berekening van de contacttemperatuur, gegeven de distributie van een warmtebron, bijvoorbeeld in het geval van een gemeten wrijvingscoefficient.

Om deze contacttemperatuur te kunnen berekenen, is een multilevel algoritme ontwikkeld, dat een niet uniforme verdeling van de in het contact ontwikkelde warmte toestaat. Bovendien mogen de in contact staande lichamen verschillende massatemperaturen hebben.

Simulaties voor elliptische warmtebronnen met uniforme en half-ellipsoidale verdelingen, welke vooral van belang zijn voor contacten die onder condities van droge- en grenssmering opereren, hebben geresulteerd in nauwkeurige functie fits voor de gemiddelde en maximale contacttemperatuur. Deze functie fits zijn gebaseerd op asymptotische oplossingen voor lage en hoge Péclet kentallen en zijn geldig voor willekeurige Péclet kentallen.

De functie fits maken het mogelijke tribologische contacten eenvoudig als onderdeel van een thermisch netwerk te behandelen.

Het tweede deel van dit proefschrift behandelt het EHL-lijncontactprobleem. Eerst wordt een model beschreven, dat niet Newtons gedrag van het smeermiddel toestaat en dat het thermische gedrag van het smeermiddel en de lichamen beschrijft. Om dit model door te kunnen rekenen is een multilevel algoritme ontwikkeld. Dit algoritme is toegepast op een redelijk zwaar belast geval, gebruik makend van een vereenvoudigde energie vergelijking. Voor dit geval laten de resultaten zien dat er een significante reductie van de minimale filmdikte optreedt bij toenemende slip.

Tot slot worden er enkele aanbevelingen gedaan voor toekomstig onderzoek.

Abstract

Wherever friction occurs, mechanical energy is transformed into heat. The temperature rise associated with this heating can have an important influence on the tribological behaviour of the contacting components. Apart from determining performance, thermal phenomena affect reliability and may cause failure of the contact.

In the first part of this thesis the emphasis will be on the numerical calculation of the contact temperature given a heat source distribution, e.g. by means of a measured coefficient of friction.

In order to calculate this contact temperature, a multilevel algorithm has been derived which allows for a non-uniform division of the heat generated in the contact and different bulk temperatures.

Simulations for elliptic heat sources with uniform and semi-ellipsoidal distributions, which are of specific importance for contacts operating under conditions of dry and boundary lubrication, have resulted in accurate function fits for the average and maximum contact temperature. These function fits are based on asymptotic solutions for small and large Péclet numbers and are valid for arbitrary Péclet numbers.

The function fits enable simple treatment of tribological contacts as part of a thermal network.

The second part of this thesis deals with the EHL-line contact problem. First a model, which allows for Non-Newtonian lubricant behaviour and thermal effects, is described. For this model a multilevel algorithm is developed. The algorithm has been applied to a moderately loaded case, using a simplified energy equation. For this case, results show a significant decrease in minimum film thickness for increasing slip.

Finally this thesis is concluded with some recommendations for future research.

Contents

Nomenclature

chapters 1-5

a	semi-axis of the elliptic heat source in the direction of the velocity	m	
b	semi-axis of the elliptic heat source perpendicular to the velocity	m	
c	specific heat	J kg^{-1} K^{-1}	
F	rate of heat supply	W	
F_m	rate of heat flow due to bulk temperature differences	W	
F_n	Load	N	
G	Green's function		
h	film thickness	m	
K	thermal conductivity	W m^{-1} K^{-1}	
K_{ijkl}^{hhhh}	Discrete kernel		
p	convectivity ratio	-	$p = \sqrt{P_2/P_1}$
	pressure	Pa	
P	Péclet number	-	$P = aU/\kappa$
Q	rate of heat supplied per unit area	W m^{-2}	
Q_m	rate of heat flow per unit area of contact due to ϑ_m	W m^{-2}	
R	Radius	m	
$\mathbf{S}$	shape factor	-	
T	Temperature	K	
U	velocity relative to the heat source	m s^{-1}	
x	coordinate in the direction of the velocity	m	
x_1, x_2	boundaries of the heat source ellipse	m	$x_1, x_2 = \mp x_s$
x_s	local semi-length of the heat source	m	$x_s = a\sqrt{1 - y^2/b^2}$
y	coordinate perpendicular to the velocity	m	
z	coordinate	m	
α	heat partition function	-	
η	viscosity	Pa s	
θ	flash-temperature number	-	
ϑ	surface temperature rise	K	
$\bar{\vartheta}$	dimensionless surface temperature	-	$\bar{\vartheta} = \vartheta K_1 \sqrt{ab}/F$
ϑ_b	average interfacial bulk temperature rise	K	
ϑ_f	maximum or average flash temperature rise,	K	
ϑ_m	bulk temperature of body number 2,	K	
κ	diffusivity	m^2 s^{-1}	$\kappa = K/\rho c$
λ	conductivity ratio	-	$\lambda = K_2/K_1$
μ	coefficient of friction	-	
ρ	density	kg m^{-2}	
ϕ	aspect ratio of the contact ellipse	-	$\phi = b/a$
ψ	mass-temperature number	-	

Subscripts for θ and ψ

s	sliding asymptotic solution
h	high-speed asymptotic solution
r	rolling asymptotic solution
l	low-speed asymptotic solution
1	body number 1
2	body number 2

Superscripts for θ

a	average flash temperature over the interface
e	semi-ellipsoidal heat supply distribution
m	maximum flash temperature
u	uniform heat supply distribution

Supscripts for ϑ

b	temperature rise in the contact due to bulk temperature differences
m	bulk (mass) temperature difference
f	flash temperature, i.e. local temperature rise

Nomenclature

chapters 6 and 7.

A	constant	Pa^{-1}	
$\bar{A}$	dimensionless number	-	$\bar{A} = AE'U^{\frac{1}{4}}$
b	half contact width of the Herzian contact	m	$b = \sqrt{\frac{8wR}{\pi E'}}$
$\bar{b}$	dimensionless Herzian half contact width	-	$\bar{b} = \frac{b}{R}U^{-\frac{1}{4}}$
B	constant	Pa^{-1}	
$\bar{B}$	dimensionless number	-	$\bar{B} = BE'U^{\frac{1}{4}}$
c_p C_p	specific heat at constant pressure	$\mathrm{J\ K^{-1}\ kg^{-1}}$	
C_o	dimensionless number	-	$C_o = C_p\frac{\rho_0 u_+ R}{k}U^{\frac{3}{4}}$
e	specific internal energy per unit mass	$\mathrm{J\ kg^{-1}}$	
$\mathbf{e}_X$	unit vector in X-direction	-	
$\mathbf{e}_Y$	unit vector in Y-direction	-	
$\mathbf{e}_\zeta$	covariant unit vector in ζ-direction	-	
$\mathbf{e}_\xi$	covariant unit vector in ξ-direction	-	
E	Young's modulus	Pa	
	dimensionless number	-	$E = \varepsilon(\frac{k}{u_+^2\,\eta_0})^{-1}$
E'	reduced elastic modulus	Pa	
f	constitutive relation for $\dot{\gamma}$	$\mathrm{s^{-1}}$	$\dot{\gamma} = f(\tau, \eta)$
$\bar{f}$	non-dimensionalized f	-	$\bar{f} = f\frac{\eta_0}{E'}U^{-\frac{1}{2}}$
F	normalized $\bar{f}$	-	$F = \frac{\bar{f}}{\bar{p}_h}\frac{\bar{b}}{\bar{h}_h}$
F_1	parameter	-	
F_2	parameter	-	
$f_{i,j}$	"source-term" in energy-equation		
G	shear modulus	Pa	
	kernel in bc for energy equation		
$G1_{i,k}^{h_\xi h_\xi}$	discretized kernel in bc at solid 1		
$G2_{i,k}^{h_\xi h_\xi}$	discretized kernel in bc at solid 2		
$G_{i,k}^{hh}$	discretized kernel in bc for model-problem		
h	film thickness	m	
	mesh-size in model problem		
h_ξ	step-size in ξ-direction	-	
h_ζ	step-size in ζ-direction	-	
H	dimensionless normalized film thickness	-	$H = \frac{\bar{h}}{\bar{h}_h}$
h_h	maximal hertzian deformation	m	$h_h = \frac{b^2}{R} = \frac{8w}{\pi E'}$
$\bar{h_h}$	dimensionless hertzian deformation	-	$\bar{h}_h = \frac{h_h}{R}U^{-\frac{1}{2}}$
h_{00}	constant in film thickness equation	m	
$\bar{h}$	dimensionless film thickness	-	$\bar{h} = \frac{h}{R}U^{-\frac{1}{2}}$
k	thermal conductivity	$\mathrm{W\ m^{-1}\ K^{-1}}$	
K_0	modified Bessel function of second kind		
K_{f_s}	dimensionless number	-	$K_{fs} = \frac{k_f}{k_s}U^{-\frac{1}{4}}$

K^*_{fs}	dimensionless normalized number	-	$K^*_{fs} = K_{fs}\frac{\bar{b}}{h_h}$
$K^{h_\xi h_\xi}_{i,j}$	kernel in discretized film-thickness equation		
L_α	dimensionless number	-	$L_\alpha = \alpha E' U^{\frac{1}{4}}$
L_γ	dimensionless number	-	$L_\gamma = \gamma(\frac{k}{u_+^2\ \eta_0})^{-1}$
M	dimensionless number	-	$M = \frac{w}{E' R} U^{-\frac{1}{2}}$
n_ξ	number of points in ξ-direction		
n_ζ	number of points in ζ-direction		
$\mathbf{n}$	normal-vector		
p	pressure	Pa	
P	dimensionless normalized pressure	-	$P = \frac{\bar{p}}{\bar{p}_h}$
	Peclet number		
$\bar{p}$	dimensionless pressure	-	$\bar{p} = \frac{p}{E'} U^{-\frac{1}{4}}$
p_h	maximal hertzian pressure	Pa	$p_h = \sqrt{\frac{wE'}{2\pi R}}$
$\bar{p_h}$	dimensionless maximal hertzian pressure	-	$\bar{p}_h = \frac{p_h}{E'} U^{-\frac{1}{4}}$
p_0	constant in Roelands equation	Pa	1.9610^8
Pec	dimensionless number	-	$Pec = \frac{u_+ R}{2\kappa} U^{\frac{1}{4}}$
Pe	dimensionless normalized Peclet number	-	$Pe = Pec\ \bar{b}$
$\underline{\mathbf{q}}_r$	the radiation heat flux vector	W m^{-2}	
q	internal heat generation per unit volume	J m^{-3}	
	heat input on the surface of the bodies	W m^{-1}	
R	reduced radius of curvature	m	$R^{-1} = R_1^{-1} + R_2^{-1}$
$R_{i,j}$	residue of energy equation in (i,j)		
S	specific entropy	J K^{-1} kg^{-1}	
	dimensionless number	-	$S = \frac{u_-}{u_+}$
SR	slip to roll ration	-	$SR = 2\frac{U_2 - U_1}{U2 + U1} = -2\ S$
S_0	the temperature viscosity index	-	
T	temperature	K	
T_0	ambient temperature	K	
$\bar{T}$	dimensionless temperature	-	$\bar{T} = \frac{T}{u_+^2}\frac{k}{\eta_0}$
$\bar{T_0}$	dimensionless number	-	$\bar{T_0} = \frac{T_0}{u_+^2}\frac{k}{\eta_0}$
t	time	s	
u	velocity in x-direction	m s^{-1}	
$\bar{u}$	dimensionless velocity	-	$\bar{u} = \frac{u}{u_+}$
u_+	average velocity of the moving bodies	m s^{-1}	$(U_1 + U_2)/2$
u_-	half the difference velocity	m s^{-1}	$(U_1 - U_2)/2$
U	velocity relative to the heat source	m s^{-1}	
	D-H speed parameter	-	$(\eta_0 u_+)/(E'\ R)$
v	velocity in y-direction	m s^{-1}	
	specific volume	m^3 kg -1	
w	velocity in z-direction	m s^{-1}	
	applied load	N m^{-1}	

x	coordinate in direction of moving bodies	m	
X	normalized dimensionless x-coordinate	-	$X = \frac{\bar{x}}{b}$
X'	normalized dimensionless x-coordinate	-	
$\bar{x}$	dimensionless x-coordinate	-	$\bar{x} = \frac{x}{R} U^{-\frac{1}{4}}$
y	coordinate perpendicular to the velocity	m	
z	coordinate	m	
	the pressure viscosity index	-	
$\bar{z}$	dimensionless z-coordinate	-	$\bar{z} = \frac{z}{R} U^{-\frac{1}{2}}$
Z	dimensionless normalized z-coordinate	-	$Z = \frac{\bar{z}}{\bar{h}_h}$
α	the pressure viscosity coefficient	Pa^{-1}	
β	tangent of the angle between x- and ξ	-	
γ	the temperature viscosity coefficient	K^{-1}	
$\dot{\gamma}$	shear rate	s^{-1}	
$\delta_{i,j}$	changes applied using distributive relaxation		
η	viscosity	Pa s	
$\bar{\eta}$	dimensionless viscosity	-	$\bar{\eta} = \frac{\eta}{\eta_0}$
η^*	equivalent viscosity	Pa s	
$\bar{\eta^*}$	dimensionless equivalent viscosity	-	$\bar{\eta^*} = \frac{\eta^*}{\eta_0}$
η_0	viscosity at ambient conditions	Pa s	
Θ	dimensionless normalized temperature	-	$\Theta = \frac{\bar{T}}{T_0}$
θ	error frequency on 1d-grid		
ϵ_i	discretized parameter	-	$\epsilon_i = \Omega \left(\frac{\rho}{\eta}\right)_{e_i} H_i^3$
ε	thermal expansion coefficient	K^{-1}	
ζ	dimensionless normalized coordinate	-	$\frac{Z}{H(X)}$
κ	diffusivity	m^2 s^{-1}	$\kappa = K/\rho c_p$
λ	parameter		
μ	amplitude reduction factor		
	coefficient of friction	-	
$\bar{\mu}$	friction parameter	-	
ν	Poisson's ratio	-	
ξ	integration variable	m	
	dimensionless normalized coordinate	-	$\xi = X$
$\bar{\xi}$	dimensionless integration variable	m	
ρ	lubricant density	kg m^{-3}	
$\bar{\rho}$	dimensionless density	-	$\bar{\rho} = \frac{\rho}{\rho_0}$
ρ_0	density at ambient conditions	kg m^{-3}	
ρ^*	generalized density	kg m^{-3}	
$\boldsymbol{\rho^*}$	dimensionless normalized generalized density	-	
$\bar{\rho^*}$	dimensionless generalized density	-	$\bar{\rho^*} = \frac{\rho^*}{\rho_0}$
$\left(\frac{\rho}{\eta}\right)_e$		s m^{-2}	
$\overline{\left(\frac{\rho}{\eta}\right)_e}$		-	$\overline{\left(\frac{\rho}{\eta}\right)_e} = \left(\frac{\rho}{\eta}\right)_e \frac{\eta_0}{\rho_0}$

$\left(\frac{\rho}{\eta}\right)_e$		-	
τ	shear stress	Pa	
$\mathcal{T}$	dimensionless normalized shear stress	-	$\mathcal{T} = \frac{\bar{\tau}\,\bar{b}}{\bar{p}_h \bar{h}_h}$
$\bar{\tau}$	dimensionless shear stress	-	$\bar{\tau} = \frac{\tau}{E'} U^{-\frac{1}{2}}$
τ_r	representative stress	Pa	
Φ	viscous dissipation function	W m^{-3}	
Ψ	dimensionless normalized number	-	$\Psi = \frac{\bar{h}_h^2}{\bar{b}}$
Ω	dimensionless normalized number	-	$\Omega = \frac{\bar{h}_h^2 \bar{p}_h}{\bar{b}}$

Chapter 1

Introduction

Technological as well as economical trends result in tribo-systems operating under increasingly extreme conditions. Amongst these one finds higher loads, high operating temperatures and severe lubricant starvation. In addition, demands concerning size (weight), power consumption (viscosity) and manufacturing (surface roughness) may cause problems.

Due to these increasingly extreme conditions, designers need more accurate answers to more complicated problems. The latter frequently include thermal phenomena. In general, thermal aspects in tribology are important with respect to the determination of:

- the performance of the system (film thickness, power loss, etc.)
- magnitude and location of the maximum temperature
- effects of thermal gradients on the geometry of the contact
- heat flow to and from components of the system

Apart from determining performance, thermal phenomena affect bearing reliability and may cause failure, e.g. due to degradation of the bearing material or the lubricant. Also large temperature gradients may cause cracking, or by unequal thermal expansion of components, cause seizure.

Thermal aspects are closely related to friction and viscous dissipation in the contact. Friction, i.e. the resistance to motion, causes the conversion of mechanical work into thermal energy, thereby leading to a local temperature rise of the tribo-elements. The energy dissipation in the contact and the associated temperature rise in the contacting elements may be quite substantial. The good tribological behaviour of certain ceramic-steel contacts is for instance ascribed to local softening of a thin layer of the steel counter part. This softened steel is transferred to the ceramic counter part and is assumed to act as a lubricant film (see *He et. al.*, 1995).

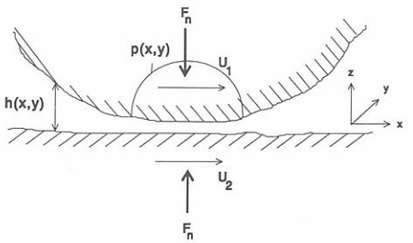

Figure 1.1: Schematic drawing of a concentrated contact.

The consequences of thermal effects for the operation of the contact strongly depend upon load and operating conditions. However, it is equally important to realize that the tribological contact is coupled to an overall mechanical system. For example, consider a bearing supporting a shaft which drives a cryogenic compressor. The heat generated in the bearing is conveyed away by the shaft, and chances of thermally initiated breakdown are relatively small. However, the situation is quite different if the shaft drives a steam turbine, where the bearing will be effectively heated.

1.1 Tribological Contacts

As stated before, thermal effects depend on the conditions in the contact. Figure 1.1 shows a schematic drawing of a so-called "concentrated contact".

The energy dissipation depends on the applied load, the coefficient of friction and the sliding velocity. Tribological contacts are often lubricated to avoid or minimize wear and, if required, to establish low friction between the two elements in relative motion. The coefficient of friction is a function of the operating conditions, i.e. the applied load, the lubricant properties, and the sliding velocity. This dependence can be illustrated in a so-called generalized Stribeck or Hersey curve, see figure 1.2, in which the coefficient of friction is plotted against the so-called Hersey number $\frac{\eta U}{\bar{p}}$, see for instance *Schipper* (1988).

In this figure three regions can be distinguished. Each region is characteristic for a lubrication regime with specific wear and friction behaviour. The regime is determined by the way the applied load is transferred from one solid to the other. At favourable operating conditions the surfaces will be fully separated by the lubricant, as shown in figure 1.3[a]. The load is transmitted by the pressure in the lubricant and all the shearing caused by the relative motion of the surfaces takes place in the lubricant. If the pressure in the lubricant is low compared to the elastic

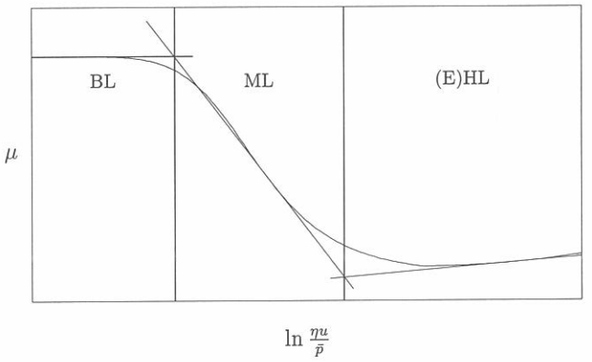

Figure 1.2: Generalized Stribeck curve

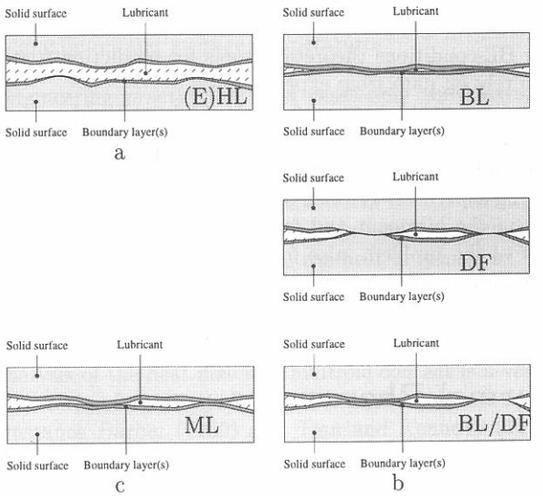

Figure 1.3: Lubrication modes

moduli of the bodies, the film shape is determined by the geometry of the surfaces. This lubrication regime is referred to as hydrodynamic lubrication (HL) and is characteristic for e.g. journal bearings. In concentrated contacts the pressures are generally high and the elastic deformation of the surfaces has a significant effect on the film shape. This special case of HL is generally referred to as elasto hydrodynamic lubrication (EHL). In both HL as well as EHL the surfaces are fully separated, hence wear is negligible for these modes of lubrication and the coefficient of friction is generally smaller than 0.01. Tribological contacts operating in these regimes have been analysed extensively, and over the past decades even theoretical models for the prediction of friction for EHL contacts have been developed.

If the load is fully transmitted by the interacting asperities, the lubrication mode is referred to as boundary lubrication (BL). Shear and wear depend on the effectiveness of the protecting boundary layer(s), see figure 1.3[b]. If the surfaces are mainly protected by the boundary layer, shear takes place in the boundary layers or at their interface and the coefficient of friction generally is of the order of 0.1.

If the boundary layers are absent or not effective in protecting the surfaces, direct contact of the unprotected asperities predominates. This regime is referred to as dry friction (DF). Shear will take place at the interface or in the weaker asperities, which may lead to substantial material transfer and wear. Generally the coefficient of friction is high, e.g. larger than 0.2. If the protective boundary layer is partially effective a combination of dry friction and boundary lubrication occurs. As can be seen from the generalized Stribeck curve (figure 1.2), in the boundary lubrication regime the coefficient of friction is constant. Unlike for EHL-conditions, for BL-conditions theoretical tools for predicting friction do not exist and one has to rely on data from experiments.

The intermediate regime between boundary lubricaton/dry friction and (elasto) hydrodynamic lubrication is referred to as mixed lubrication (ML); see figure 1.3[c]. In this case the load is partially carried by the pressure in the lubricant and partially by the interacting asperities. Friction in the mixed lubrication regime is a combined result of shear in the lubricant and friction due to asperity interactions. Due to the complexity of the problem, also for this regime theoretical models to predict friction are still lacking and most of the knowledge about contacts operating in the ML regime has been acquired by experiments.

1.2 Thermal Phenomena

Regardless of the lubrication regime, the temperature increase induced by friction affects the properties of the materials in a tribological contact, e.g. the viscosity of the lubricant, the reactivity of the additives in the lubricant, the oxidation of the bare surface materials and the geometry of the contact. These property changes may affect the tribo-element, regardless whether it is a ball bearing, a cam-follower

or a gear. In fact if the thermally induced changes are large, prediction of the performance of such an element is very complicated, if not impossible. In other cases the prediction of thermal phenomena may be feasable, but the result will strongly depend on the lubrication regime in which the contact operates.

Over the past decade a lot of attention has been paid to the development of rigorous solvers for thermo-elasto-hydrodynamic problems. One of the objectives of these studies is to be able to predict the coefficient of friction for a wide range of operating conditions. More powerful computers and numerical techniques enabled solving more and more complex models. However modelling the lubricant behaviour under the extreme pressures and high shear rates that may occur in EHL-contacts is still a topic under investigation.

Unlike the progress made in modelling and solving EHL, models for tribosystems operating in the boundary or mixed lubrication regime are at most rudimentary. In fact, determining the heat development in such a contact requires a measured coefficient of friction. In these cases only the total rate of heat flow is known, not the exact distribution. However, by the nature of the problem, fluctuations in the heat flow distribution are only important on the scale of the size of such a fluctuation and not on larger scales. This makes it possible to estimate the contact temperature distribution and thus the maximum and average temperature, without knowing the exact rate of heat flow distribution. The total heat flux and an idealized heat source distribution then suffice to obtain relatively accurate estimates of the maximum and average temperatures.

Indeed, in engineering practice, in most cases only the maximum and average surface temperatures are relevant and hence a model for the prediction of the surface temperatures in tribological contacts based on idealized heat source distributions is already very useful.

It may be argued that in boundary- or dry lubricated contacts the rate of heat flow distribution is not continuous, because the heat is generated by asperity interaction, i.e. in the real contact area instead of in the apparent contact area. However, in that case the real contact can be modelled as two bodies in multiple contact where each contact is the contact between two asperities of the mating surfaces. Full analysis of the heat flow in a multiple contact is a very complicated task, especially because of the limited information about contact interface conditions. See for instance *Barber* (1969) and *Tian and Kennedy* (1993). However, if the contact spots are relatively far apart, the local temperature rise caused by an individual heat source will not influence the local temperature rises at neighbouring contact spots and the single contact results can still be used. On a larger scale this is equivalent to a body in contact with several other bodies, e.g. a ball in contact with the inner and outer raceway and the cage of a ball bearing.

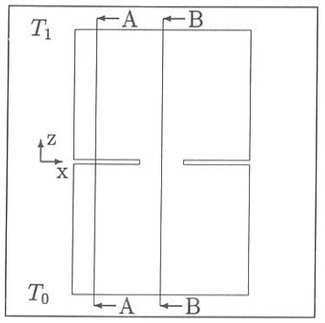

Figure 1.4: Cross section incised rod

1.3 Large and small scale Heat Flow Restrictions

It would be convenient if the complex problem of determining the contact temperature rise could be divided into smaller and easier problems which could then be studied separately. A possibility is given by the concept of small and large scale heat flow restrictions, known from the contact heat transfer field and extended by *Tian and Kennedy* (1993) to sliding frictional heating problems. This concept can be used to divide the contact temperature into a superposition of two temperature rises; a local temperature rise and a bulk temperature rise, each originating from heat flow restrictions on a specific scale.

1.3.1 Stationary Contact

The heat flow restriction concept for tribological contacts can be explained by the simple example of the heat flow through a rod kept at different end temperatures. In a homogeneous material heat flow obeys Fourier's heat transfer law: at steady-state the temperature drop within the rod is linearly proportional to the length in the direction of the heat flow and inversely proportional to the thermal conductivity of the material.

$$\Delta T \propto \frac{\Delta x}{K}$$

Now consider the situation in which a circumferential incision has been made in the rod and part of the material has been removed, see figure 1.4. Far away from the incision, the temperature drop will again be linearly proportional to the

T_1

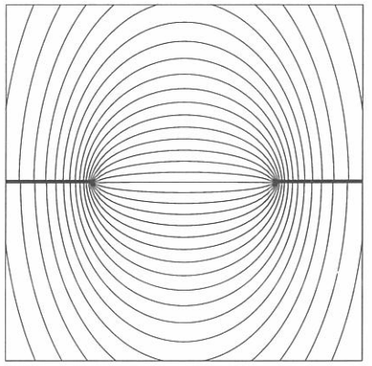

T_0

Figure 1.5: Contour plot of the temperature distribution in the vicinity of the contact for two bodies in contact, both bodies stationary.

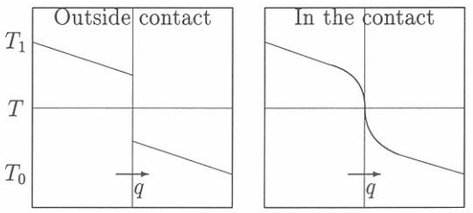

Figure 1.6: Temperature distributions across the interface in and outside the contact

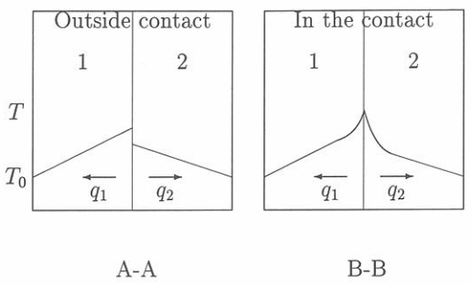

Figure 1.7: Temperature distributions across the interface in and outside the contact for heat generated by friction in the contact.

length in the direction of the heat flow. But in the vicinity of the incision the heat flow is confined to a smaller part than the original cross section of the rod. This causes a non-linear temperature distribution as shown in figure 1.5.

The 'surface' temperatures , i.e. the temperatures at $z = 0$, of the two parts of the rod must be equal in the 'contact' of the two parts, but are not necessarily equal outside the contact (figure 1.6). This possible temperature jump across the interface is generally known as the 'contact temperature jump'. Now suppose that the rod is cut in two along the plane $z = 0$, and the two parts are pressed together again. Then again in the center where previously the temperature changed smoothly, a temperature jump will occur. This is caused by the same phenomena as mentioned above: Now, the real contact, due to surface roughness, is much smaller than the apparent area. Only in the real contact area the contact temperatures of the two bodies are the same, not necessarily in the entire apparent area.

According to a theory developed by *Holm* (1948, 1958), the temperature drop at the contact interface can be attributed to the heat flow restriction at and near the real contact area, due to the convergence and subsequent divergence of the heat flow passing through this narrow contact area.

The heat flow restriction which causes the temperature drop at a contact interface is defined as a small scale heat flow restriction, based on the fact that the temperature drop is limited to a very small region at or near the real contact zone. The heat flow restriction which causes the linear temperature drop in the heat flow direction, outside the contact interface, is defined as a large scale heat flow restriction, because the temperature drop takes place through the entire thickness of the body. In the case of the rod, the heat flow is restricted to one direction

within thermally insulated boundaries.

In the above, the heat flow was caused by a fixed temperature difference between the end temperatures of the rod. However this is not the typical case for tribological contacts where the heat flow is generated by friction. The small and large scale restriction concept can be extended to the frictional heating situation as shown by *Tian and Kennedy* (1993). As an example consider two circular rods in contact at their ends, with one rod spinning about their common axis. Let us assume that the boundary parallel to the contact interface is thermally conducting and that the other boundaries are thermally insulated. The temperature drop can again be divided into two components, which result from large and small scale heat flow restrictions respectively. However, in contrast to the previous example in this case the heat is conducted away from the contact by both bodies. At and near the contact the small scale heat flow restriction causes a sharp nonlinear temperature drop. If a single real contact spot exists, centered at the contact interface, this temperature drop can be modelled by a stationary heat source on a semi-infinite medium. Far away from the contact interface, the temperature drop is caused by the large scale heat flow restriction, and is linear. As in the previous example, the surface temperatures of the two rods must be equal in the real contact but they need not be equal elsewhere. Figure 1.7 illustrates the temperature distributions in and outside the contact region for this case.

1.3.2 Moving Contact

So far the stationary situation has been considered, i.e. the contact between the two bodies was supposed to be stationary with respect to the bodies. However, in tribological contacts at least one of the bodies is likely to move relative to the contact and the heat generated in the contact will be divided between the two bodies, the heat partition depending on the operating and cooling conditions. The heat flow into each body is again subject to large scale and small scale heat flow restrictions. This leads to a sharp, nonlinear temperature drop at and near the contact, see also figure 1.7. Far away from the contact the temperature drop is caused by the large scale heat flow restriction which depends on the geometry of the body and the cooling conditions. For a single isolated real contact spot, the temperature distribution at and near the contact can be modelled as a concentrated heat source moving along the surface of a semi-infinite body.

1.4 Surface Temperatures for Sliding Contacts

Using the concept of small and large scale heat flow restrictions, the surface temperature can be divided in two contributions: the local surface temperature rise and the bulk temperature rise. The local temperature rise is defined as the temper-

ature rise due to the small scale heat flow restriction during the release of frictional heat within the real area of contact. The bulk temperature rise is defined as the temperature rise due to the large scale heat flow restriction of the frictional heat.

For a single heat source on the contact interface, the local surface temperature rise can be modelled by a concentrated heat source, acting on a semi-infinite medium. The semi-infinite body assumption describes the local temperature rise well. Studies, e.g. *Blok* (1937), show that for a concentrated heat source acting on a semi-infinite body, the surface temperature rise is basically limited to a very small region in the immediate vicinity of the contact interface. Therefore the local surface temperature rise can be modelled by a heat source acting on a semi-infinite body under the restriction that the size of the contact is small compared to the size of the body.

Although the temperatures at remote distances from the contact interface are scarcely affected by the conditions at the interface, the temperature at 'infinity', or the bulk temperature, *does* affect the temperature field near the contact. The material of the semi-infinite body acts as an infinite heat sink of negligible resistance. In the finite body reality this heat sink will be an actual heat transfer process, for instance convection by a cooling fluid, the large scale heat flow restriction. The heat flow the body can convey is therefore related to the temperature on the exterior boundaries. This will lead to an additonal heat flow, compared to the semi-infinite body situation, from the body with the highest bulk temperature to the body with the lowest bulk temperature. This heat flow often leads to a non uniform temperature rise in the contact, the bulk temperature rise.

In general the relationships for the large scale heat flow restriction will be known or may be found by independent experiments on the solids. These relationships depend on the geometry of the bodies and the cooling mechanisms.

1.5 History of Contact Temperature Studies

Studies investigating frictional heating and contact temperatures started as early as 1937. *Blok* (1937) was the first to study temperature rises due to concentrated heat sources, i.e. flash temperatures. He studied the quasi steady state temperature rise due to band-shaped heat sources for high Péclet numbers. The Péclet number is a measure for the relative importance of convection and lateral conduction, and in fact, Blok considered situations where the normal conduction and convection are the only mechanisms of heat transfer. Subsequently many studies were carried out to investigate frictional heating and flash temperatures, see *Kennedy* (1984). Blok's initial work needed extension in four directions.

- Flash temperatures for low and moderate Péclet numbers. In, for instance, gear-transmissions and cam-follower systems situations occur where conduction becomes important and cannot be neglected.

- Flash temperatures due to elliptic heat sources, because tribological contacts are rarely band shaped, and often elliptic.
- In the contact the surface temperatures of both bodies will be equal, but may vary over the contact. Blok approximated this condition of equal surface temperatures in the interface by equating only the maximum surface temperatures of the two bodies. A more accurate approach is to equate all the temperatures in the contact.
- Incorporation of the effect of the bulk temperature rise on the contact temperature.

1.5.1 Conduction

Jaeger (1943) and *Carslaw and Jaeger* (1959) [§10.7] extended Blok's model to contacts with limited Péclet numbers, that is, for band-shaped contacts, they extended Blok's model to situations where lateral conduction becomes an important heat transfer mechanism.

1.5.2 Heat Source Shape

Until 1959, most of these studies considered the contact temperature between two semi-infinite solids under steady state conditions assuming a band shaped contact, although *Jaeger's* (1943) already included rectangular contacts as well. For circular contact areas *Archard* (1959) introduced an approximate solution on the basis of Jaeger's work together with a simple rule of thumb for the partitioning of the generated heat. However, most practical contacts are neither band shaped nor circular, but elliptic. Initially this was accounted for by using *Jaeger*'s (1943) solution for rectangular contacts as an approximation. For conditions where the lateral conduction can be neglected, this approach will yield good approximations. However for situations where the lateral conduction becomes an important factor, ambiguous decisions have to be made regarding the dimensions and the distribution of the rectangular heat source in order to assure a good approximation, since in this situation the entire heat source distribution and shape determines e.g. the maximum temperature, not just some cross section in the direction of the velocity. The elliptic problem itself was addressed much later, e.g. by *Kuhlmann-Wilsdorf* (1986, 1987) who introduced approximate solutions for elliptic contacts, that are generally applicable. Accurate solutions for elliptic contacts are still lacking though.

1.5.3 Frictional Heat Partition

The partition of the frictional rate of heat flow at the contact interface is such that the surface temperatures in the contact interface are equal. For two semi-infinite

bodies with zero bulk temperatures, this heat partition depends on the material properties of the bodies and their velocities. *Blok* (1937) approximated the condition of equal surface temperatures in the interface by equating the maximum surface temperatures of the two bodies whilst *Jaeger* (1942) equated the average temperature over the contact. To some extend, the latter method takes into account the variation of temperature over the contact area; it is thus less likely to fail under unusual conditions. However the correct approach for the steady state heat partition and the associated contact temperatures for arbitrarily shaped contacts is to match the surface temperatures of the two contacting solids at all points inside the contact area, thus allowing for variation of the heat distribution with position. The solution of this problem generally requires a numerical approach, see 1.6.

1.5.4 Bulk Temperature Rise

For finite bodies the frictional heat flow partition also depends on the large scale heat flow restriction. For instance, if one of the bodies is fully insulated except for the contact interface, the net heat flow entering this body through the contact interface must be zero. This can be achieved by studying the problem of two semi-infinite bodies with different bulk temperatures, without heat generation at their interface. *Holm* (1948, 1958), conducted studies on this problem but for stationary solids only. *Elshof* (1994) studied the problem for bodies moving relative to the (elliptic) contact.

1.6 Outline of this Thesis

This thesis can be divided in two parts. In the first part, i.e. chapters 2 to 5, the essential tools for the calculation of contact temperatures for known heat sources in elliptical contacts will be derived. The emphasis will be on how, given a heat source distribution, the contact temperatures can be calculated. The results presented here are of specific practical importance for BL and ML contacts, i.e. situations where, due to the complexity of the phenomena, no models are available, see section 1.1. The second part of the thesis, i.e. chapters 6 and 7, deal with the EHL-line contact problem for which the heat generation can be calculated from fundamental equations like the Reynolds equation and the energy equation.

In chapter 2 a numerical algorithm will be introduced for the calculation of the surface temperature of a semi-infinite body moving along an arbitrary heat source. Subsequently the algorithm will be applied to elliptic heat sources with either a uniform or a semi-ellipsoidal distribution. For these heat sources accurate curvefit formulas for the maximum and average contact temperature will be presented. The formulas are valid for the entire range of Péclet numbers.

In chapter 3 the algorithm of chapter 2 will be extended to the situation where two semi-infinite bodies are in contact, moving relative to each other. Heat is generated in the contact as a result of friction. Since the heat flow into each body is not known a priori, it must be calculated by matching all the temperatures in the contact. Once the two heat flows have been calculated the contact temperatures can be calculated by using the algorithm explained in chapter 2. Again the results for the maximum and average contact temperatures are curvefitted, resulting in formulas for elliptic contacts with either a uniform or a semi-ellipsoidal heat source.

In chapter 4 the algorithm derived in chapter 3 will be applied to the situation where the two semi-infinite bodies in contact have different bulk temperatures. There is no heat generation in the contact, but due to the bulk temperature difference, heat will flow from the body with the highest bulk temperature to the body with the lowest bulk temperature, the bulk temperature difference heat flow. In general this will lead to a non-uniform contact temperature distribution.

In chapter 5 it will be demonstrated how the curvefit formulas derived in the previous chapters can be applied to estimate the contact temperature of bodies in contact with different bulk temperatures. First the extreme case of an insulated body in contact with a semi-infinite body with zero bulk temperature will be treated. Since in the steady state the net heat flow entering the insulated body must be zero, the insulated body must have a high bulk temperature in order to prevent heat, generated in the contact, from flowing into this body. It will be shown how the curvefit formulas derived in chapter 3 and chapter 4 can be used to estimate the maximum and average contact temperature. Further it will be shown, by means of an example, how the contact temperatures of multiple bodies in contact, or bodies in multiple contact, can be calculated by using the curvefit formulas.

Although it is necessary to assume the heat source distribution for bodies in contact under conditions of dry, mixed and boundary lubrication, this is not necessary for (elasto) hydrodynamically lubricated contacts.

In chapter 6 a model for EHL-line contacts will be proposed. This model takes into account non-Newtonian lubricant behaviour and thermal effects when calculating the film thickness, the pressure distribution, the coefficient of fricton and the temperature.

In chapter 7 thermal effects will be addressed. Although the model described in chapter 6 allows for non-Newtonian behaviour of the lubricant, Newtonian lubricant behaviour is assumed in order not to mix non-Newtonian effects with thermal effects.

References

Archard, J.F., 1959, "The temperature of rubbing surfaces", *Wear*, Vol. 2, pp. 438-455.

Barber, J.R., 1970, "The Conduction of Heat From Sliding Solids", *Int. J. Heat Mass Transfer*, Vol. 13, pp. 857-869.

Blok, H., 1937, "Theoretical study of temperature rise at surface of actual contact under oiliness lubricating conditions", Instn. Mech. Engrs., *Proceedings of general discussion on lubrication and lubricants*, Vol. 2, pp. 222-235.

Carslaw, H.S. and Jaeger, J.C., 1959, "Conduction of Heat in Solids", Oxford University Press, Oxford, UK.

Elshof, H.L.J., 1994, "Heat fluxes between semi-infinite solids", Masters Thesis, University of Twente, Enschede.

He, Y.J., Winnubst, A.J.A., Schipper, D.J., Bakker, P.M.V., Burggraaf, A.J. and Verweij, H., 1995, " Friction and Wear Behaviour of Ceramic-hardened Steel Couples under Reciprocating Sliding Motion," *Wear*, Vol. 185, pp. 33-43.

Holm, R., 1948, "Calculation of the Temperature Development in a Contact Heated in the Contact Surface, and Application to the Problem of the Temperature Rise in a Sliding Contact", *J. of Appl. phys.*, Vol. 19, pp. 361-366.

Holm, R., 1958, *Electric Contacts Handbook*, Springer-Verlag, Berlin.

Jaeger, J.C., 1943, "Moving sources of heat", *J. and Proc. Roy. Soc. N.S.W.*, Vol. 76, pp. 203-224.

Kennedy, F.E., 1984, "Thermal and thermomechanical effects in dry sliding", *Wear*, Vol. 100, pp. 453-467.

Kuhlmann-Wilsdorf, D., 1986, "Sample calculations of flash temperatures at a silver-graphite electric contact sliding over copper" , *Wear*, Vol. 107, pp. 71-90.

Schipper, D.J., 1988, "Transitions in the lubrication of concentrated contacts", Ph.D. thesis, Twente University, Enschede, The Netherlands.

Tian, X. and Kennedy, F.E., 1993, "Contact Surface Temperature Model for Finite Bodies in Dry and Boundary Lubricated Sliding", *J. of Tribology*, Vol. 115, pp. 411-418.

Chapter 2

Local Temperature Rise

In this chapter the part of the contact temperature due to the small scale heat flow restriction, i.e. the local temperature rise, will be addressed. Over the years, this subject has been studied extensively. The studies started in 1937 with a study by *Blok* that stimulated numerous subsequent works. *Kennedy* (1984) gives a comprehensive literature review. It is now generally accepted that the local temperature rise can be modelled well by the surface temperature rise of a semi-infinite solid moving past a heat source. The basic theory for this problem is well established; see for instance *Carslaw and Jaeger* (1959), and analytical results have been derived for some simple heat distributions e.g. uniformly heated rectangles at high Péclet number. However, for heat sources with arbitrary shape and heat flow distribution or arbitrary Péclet number, numerical simulations are needed for the computation of the surface temperature. The model will be described in section 2.1 after which the numerical algorithm is explained in section 2.2. Although for tribological contacts the shape of the heat source will in general be known, this is not true for the heat source distribution as seen by the individual bodies in contact. This is due to the fact that the known heat source in the contact will be distributed between the two bodies in contact, according to an a priori unknown partition function. The partition problem itself will be addressed in the next chapter. For now it suffices to realize that heat sources with arbitrary distribution will occur and the algorithm to be developed should be able to deal with these heat sources.

Subsequently the algorithm will be applied to heat sources covering an ellipse with either a uniform or a semi-ellipsoidal distribution. These heat sources play an important role in tribology, but accurate formulas for the maximum and average surface temperature are still lacking. Such formulas will be derived, using the numerically obtained values and asymptotic solutions.

As an illustration the maximum and average temperature in the contact between a ceramic ball and a steel surface will be calculated using these formulas.

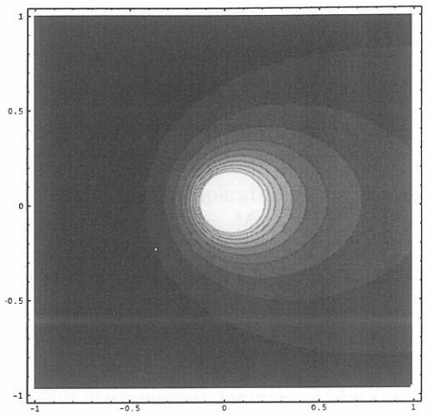

Figure 2.1: Contour plot of the Greens function for $\frac{U}{2\kappa} = 2$

2.1 Model

For the calculation of the quasi-steady state surface temperature of a semi-infinite homogeneous solid the solution for a moving point source of unit strength, i.e. the Greens function is particularly usefull.

Suppose that heat is emitted at the origin at the rate of one heat unit per unit time, and that a semi-infinite homogeneous medium moves uniformly past the origin with velocity U parallel to the x-axis. Then according to *Carslaw and Jaeger* (1959), the quasi-steady state surface temperature distribution is given by:

$$\begin{aligned} G(x,y) &= \frac{1}{2\pi KR}\exp(-\frac{U}{2\kappa}(R-x)) \\ R &= \sqrt{x^2+y^2} \end{aligned} \tag{2.1}$$

where K is the conductivity of the solid and $\kappa = K/\rho c$ its diffusivity. To illustrate the distribution of this function, a contour plot of the function $G(x,y) = \frac{1}{R}\exp(-2(R-x))$ is shown in figure 2.1.

This expression can easily be extended to heat sources of arbitrary shape and distribution by integrating with respect to the appropriate spatial coordinates. For the situation shown in figure 2.2, the quasi-steady state surface temperature rise is given by:

$$\vartheta(x,y) = \int_{S_q} q(x',y')\; G(x-x',y-y')\; dx'dy' \tag{2.2}$$

where S_q is the area over which the heat source extends.

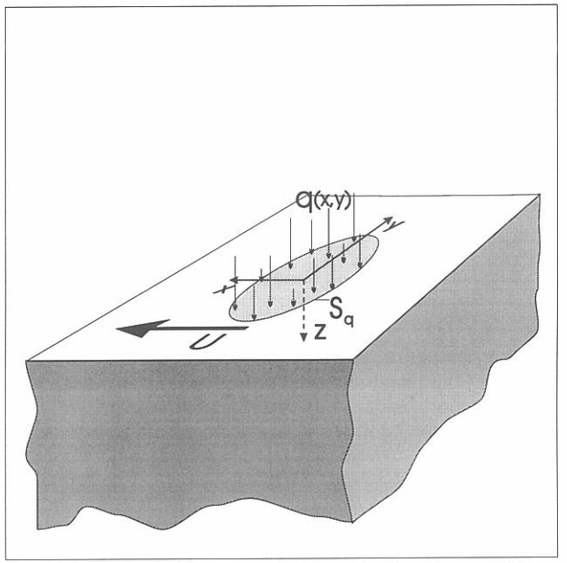

Figure 2.2: Schematic drawing of a semi-infinite body moving past an elliptic heat source of arbitrary distribution.

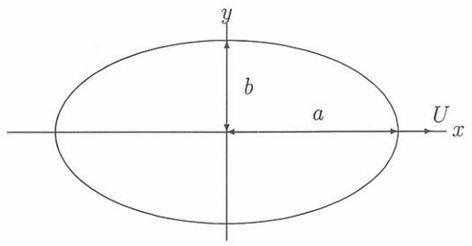

Figure 2.3: Definitions for the geometry of the contact ellipse.

Generally there are two heat transfer mechanisms operating simultaneously: convection and conduction. The Péclet number P, i.e. the ratio between the convective and the conductive heat transfer, is a measure for the relative importance of convection, compared to conduction. It is defined by

$$P \equiv \frac{LU}{\kappa}, \tag{2.3}$$

where L represents some characteristic heat source length. The heat sources are assumed to be elliptic, the usual shape of concentrated tribological contacts. The definitions for the contact geometry are shown in figure 2.3. The aspect ratio of the ellipse is defined by

$$\phi = b/a. \tag{2.4}$$

In the literature (*Kuhlmann-Wilsdorf* 1987, *Greenwood* 1991), the semi-axes of the contact ellipse in the direction of the velocity, a, is often chosen as the characteristic heat source length. In that case

$$P \equiv \frac{aU}{\kappa}. \tag{2.5}$$

This definition of the Péclet number will be used in this thesis.

To present solutions that are generally applicable, the number of parameters determining the surface temperature rise should be reduced to a minimum. Therefore the optimum similarity analysis introduced by *Moes* (1992) has been applied. This leads to the following dimensionless equation:

$$\overline{\vartheta}(\overline{x},\overline{y}) = \frac{1}{2\pi}\frac{1}{\sqrt{\phi}}\int_{S_q} \frac{\overline{Q}(\overline{x}',\overline{y}')\exp(-\frac{1}{2}P\{\overline{R}-(\overline{x}-\overline{x}')\})}{\overline{R}} d\overline{x}'\, d\overline{y}' \tag{2.6}$$

where

$$\overline{\vartheta} \equiv \vartheta\frac{K\sqrt{ab}}{F},\ \ \overline{Q} \equiv Q\frac{ab}{F} \tag{2.7}$$

$$\overline{x} \equiv \frac{x}{a} \text{ and } \overline{y} \equiv \frac{y}{a}. \tag{2.8}$$

2.2 Numerical Algorithm

In this section an algorithm will be presented for the fast numerical evaluation of equation (2.6). First the equation will be discretized in section 2.2.1. Since the equation at hand is an integral equation this leads to a dense matrix multiplication. As will be shown, straightforward multiplication is very expensive from a computational point of view. Instead a more efficient algorithm, i.e. Multilevel Multi Integration, introduced by *Brandt and Lubrecht* (1990), will be used. This algorithm is discussed briefly in section 2.2.2.

2.2.1 Discretization

Equation (2.6) is discretized on a uniform grid with meshsize h. When the heat source distribution is approximated by a piecewise constant function on the subspaces surrounding each grid point, i.e. $\overline{x}_k' - h/2 \le \overline{x}' \le \overline{x}_k' + h/2 \wedge \overline{y}_l' - h/2 \le \overline{y}' \le \overline{y}_l' + h/2$, the integral in equation (2.6) can be written as the following summation,

$$\overline{\vartheta}(\overline{x}_i,\overline{y}_j) = \frac{1}{2\pi}\frac{1}{\sqrt{\phi}}\sum_{k=0}^{n_x}\sum_{l=0}^{n_y} K_{ijkl}^{hhhh}\overline{Q}_{kl}, \tag{2.9}$$

where

$$K_{ijkl}^{hhhh} \equiv \int_{x_m}^{x_p}\int_{y_m}^{y_p} \frac{dvdu}{\sqrt{u^2+v^2}}\exp\left(-\frac{1}{2}P(\sqrt{u^2+v^2}-u)\right), \tag{2.10}$$

with

$$\begin{aligned} u = \overline{x}_i - \overline{x} \quad &, \quad v = \overline{y}_j - \overline{y}, \\ x_p = \overline{x}_i - \overline{x}_k + h/2 \quad &, \quad x_m = \overline{x}_i - \overline{x}_k - h/2, \\ y_p = \overline{y}_j - \overline{y}_l + h/2 \quad &, \quad y_m = \overline{y}_j - \overline{y}_l - h/2. \end{aligned}$$

Carslaw and Jaeger (1959) found an analytical expression for the integral in equation (2.10) which reduces it to a line integral. However, as their expression contains infinite integrals, it is less suited for use in a numerical process. Mathematica 2.0 reduces (2.10) to a line integral which, apart from exponential integrals, consists of finite integrals only. For those who have a sound sceptical attitude towards computer generated results, a formal derivation of the following result can be found in

appendix A

$$\int_{x_m}^{x_p}\int_{y_m}^{y_p}\frac{dvdu}{\sqrt{u^2+v^2}}\exp\left(-\frac{1}{2}P(\sqrt{u^2+v^2}-u)\right) = \tag{2.11}$$

$$y_m \mathrm{E}_1\left\{\frac{1}{2}P\left(\sqrt{x_m^2+y_m^2}-x_m\right)\right\} - y_m \mathrm{E}_1\left\{\frac{1}{2}P\left(\sqrt{x_p^2+y_m^2}-x_p\right)\right\} -$$

$$y_p \mathrm{E}_1\left\{\frac{1}{2}P\left(\sqrt{x_m^2+y_p^2}-x_m\right)\right\} + y_p \mathrm{E}_1\left\{\frac{1}{2}P\left(\sqrt{x_p^2+y_p^2}-x_p\right)\right\} -$$

$$\int_{y_m}^{y_p}\frac{\exp\left(-\frac{1}{2}P(\sqrt{v^2+x_m^2}-x_m)\right)v^2}{\sqrt{v^2+x_m^2}(\sqrt{v^2+x_m^2}-x_m)}dv + \int_{y_m}^{y_p}\frac{\exp\left(-\frac{1}{2}P(\sqrt{v^2+x_p^2}-x_p)\right)v^2}{\sqrt{v^2+x_p^2}(\sqrt{v^2+x_p^2}-x_p)}dv$$

Where E_1 is the *exponential integral*, defined by

$$E_1(x) \equiv \int_x^\infty \frac{\exp(-t)}{t}dt \quad (x>0)\ .$$

Polynomial as well as rational approximations exist for the exponential integral e.g. *Abramowitz and Stegun*, (1965).

The line integrals of equation (2.11) have been solved numerically using the double adaptive algorithm of *Oliver* (1972).

2.2.2 Multilevel Multi Integration

Equation (2.9) in itself represents a straightforward way to calculate the surface temperatures, simply by carrying out all the summations. However from a computational point of view this approach is inefficient. The calculation of each temperature $\overline{\vartheta}_{ij}$ costs $O(N)$ operations, N being the number of nodes on the grid. So, the calculation of the N temperatures costs $O(N^2)$ operations. Hence, if the evaluation must be done frequently, e.g. in the course of the iterative solution of an integral problem, it will consume the major part of the total computing time. *Brandt and Lubrecht* (1990) developed an algorithm called Multilevel Multi Integration for the fast numerical evaluation of such integrals. They showed that for sufficiently smooth kernels the complexity can be reduced from $O(N^2)$ to $O(N)$, whereas for potential type kernels such as $\ln|x-y|$ and $|x-y|^{-1}$ a reduction to $O(N\log N)$ can be obtained without loss of accuracy. This reduction is obtained by effectively performing part of the "integration" on coarser grids. Exploiting the smoothness properties of the discrete kernel, K_{ijkl}^{hhhh}, this can be done in such a way that the error introduced by the coarse grid integration remains small compared to the original discretization error on grid h.

Brandt and Lubrecht's approach can be summarized as follows: when the function u_i^h is defined on a grid of meshsize h, one wants to evaluate in $O(N)$ operations:

$$w_i^h = \sum_j K_{ij}^{hh}\, u_j^h \quad \forall i. \tag{2.12}$$

This can be achieved by the following four recursive steps, see *Balsara and Brandt*, (1991). Assume there exists a coarse grid of size $H = 2h$ and that a p order interpolation matrix I_H^h is being used to transfer solutions from grid H to h.

1. Adjoint Interpolation to Coarse Grid

   Evaluate

   $$u^H = \frac{1}{2^d}(I_H^h)^T\, u^h \tag{2.13}$$

   on the course grid H. Here d is the dimensionality of the space.

2. Solve on Coarse Grid

   On the coarse grid evaluate

   $$w^H = 2^d\, K^{HH}\, u^H \tag{2.14}$$

   Here K^{HH} is the injection of K^{hh} onto the coarse grid, i.e. $K_{IJ}^{HH} = K_{2i,2j}^{h\ h}$

3. Interpolate to Fine Grid

   Interpolate the coarse grid solution to the fine grid as follows

   $$\tilde{w}^h = I_H^h\, w^H \tag{2.15}$$

4. Make local Corrections on the Fine Grid

   Combination of (2.12), (2.13), (2.14) and (2.15) gives

   $$w^h - \tilde{w}^h = (K^{hh} - [I_H^h\, K^{HH}\, (I_H^h)^T])u^h \tag{2.16}$$

Written like this the summation in (2.16) extends over all points in the domain and thus no gain of efficiency is obtained. However, for asymtotically smooth kernels, i.e. kernels that have the property that

$$||\partial_x^p\, K(x,y)|| < C_p \xi^{q-p} \tag{2.17}$$

for all $\xi \geq O(h)$, efficiency can be gained. Here $\xi = ||x-y||$, ∂_x^p is any p order derivative with respect to x, q is independent of p and C_p depends only on p. If (2.17) is satisfied unconditionally the kernel is smooth troughout and corrections need not be made at all. For asymptotically smooth kernels and p order interpolation,

$$K_{ij}^{hh} - [I_H^h\, K^{HH}\, (I_H^h)^T]_{ij} \approx O(h^p\, \xi^{q-p}) \tag{2.18}$$

and $|h^p\, \xi^{q-p}|$ is a rapidly decreasing function of $\xi = ||i-j||$. Thus for suitable p (depending on the accuracy ϵ) there exists an m such that for $||i-j|| > mh$ [1],

[1] For potential-type kernels m is not independent of the meshsize and thus depends on the number of grid points. However it can be shown that for potential-type kernels $m = c_1 + c_2 \ln N$ where c_1 and c_2 are constants. So for large N, m becomes negligible compared to N.

Thus for singular smooth kernels the correction of each point after interpolation from a coarser grids costs $O(\ln N)$ operations resulting in $O(N \ln N)$ operations for the interpolation and correction of every point.

$|K^{hh}_{ij} - [I^h_H\ K^{HH}\ (I^h_H)^T]_{ij}|$ is smaller than a fraction of ϵ and can be neglected, so corrections are needed only for $||i-j|| \leq mh$.

Realizing that every step in the procedure takes $O(N)$ operations except for step 2, it is clear that if this step can be accomplished in $O(N)$ operations as well, the evaluation of (2.12) is done in only $O(N)$ operations. Since the procedure is recursive, the recursion can be continued down to a level which has only $O(\sqrt{N})$ grid points, so here the multi integration can be accomplished in $O(N)$ operations by direct evaluation.

The Multilevel Multi integration algorithm needs to be modified if it is to be applied for high Péclet numbers. First will be explained why and how the characteristics of the kernel change for high Péclet numbers and how these changes influence the performance of the Multilevel Multi Integration algorithm. Then a remedy will be given.

The elements of the kernel are given by equation (2.10). From this equation it is clear that for high Péclet numbers, the only elements of the kernel that differ substantialy from zero are the elements with $v \approx 0$ and $u > 0$ ($j = l$ and $i > k$), i.e. the kernel becomes an almost one dimensional function, independent of y. Thus if one looks at the kernel in the y-direction, it will look more and more like a delta function for increasing Péclet number. Such a function can not be approximated by a polynomial, the smoothness properties in the y-direction are lost. Therefore from coarsening in this direction no efficiency is gained since all points need to be corrected with m being $O(n)$ as stated in equation (2.16).

So for high Péclet numbers coarsening in the y-direction should not be applied. Just coarsening in the x-direction would result in an algorithm with a complexity of $O(N\sqrt{N}\ln N)$ because on the coarsest grid one would have $n\sqrt{n}$ points (n is the number of points in 1 direction, i.e. $N = n^2$), and the evaluation of the temperature in one such a point would require $n\sqrt{n}\ln N$ operations. However the summation now need not extend over the entire number of point on the coarsest grid. There are only $O(\sqrt{n})$ elements of the kernel on the coarsest grid that differ from zero (see Figure 2.4). Therefore, evaluation of the temperature in one point on the coarsest grid requires only $O(\sqrt{n}\ln N)$ operations, and the evaluation in all coarse grid points requires $O((n\sqrt{n}).\sqrt{n}\ln N) = O(N\ln N)$ operations as before.

2.2.3 Results

To verify the consistency of the discretization, the integrals are solved on a series of increasingly finer grids, each next grid having half the meshsize of the previous grid. The resulting integrals should then converge to the exact solution. The difference between two subsequent solutions should decrease with the meshsize and the ratio of two such successive differences should become a constant, 2^p, where p is the discretization order. The discretization as used here is of second order, i.e. $p = 2$, and the constant should be 4.

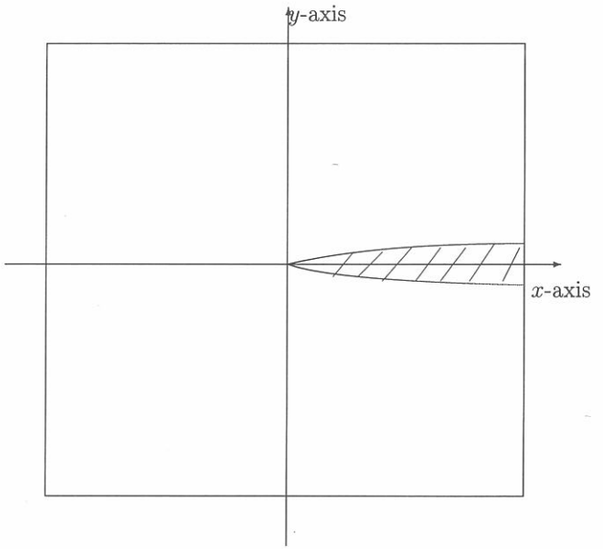

Figure 2.4: Sketch of the region over which the kernel extends for high Péclet numbers.

	ϑ_f		
grid	$\overline{Q} = \frac{1}{\pi}$	$\overline{Q} = \frac{3}{2\pi}\sqrt{1-x^2-y^2}$	$\overline{Q} = \frac{6}{2\pi}(1-x^2-y^2)^2$
1	0.31908	0.34846	0.5004611
2	0.31329	0.36875	0.5047230
3	0.31483	0.37318	0.5078755
4	0.31682	0.37465	0.5089108
5	0.31790	0.37490	0.5091957
6	0.31812	0.37498	0.5092704
7	0.31819	0.37499	0.5092894
exact	0.31831	0.375	0.5092958

Table 2.1: Maximum dimensionless temperatures for different heat distributions on increasingly finer grids for $P = 10^{-10}$

The discretization is checked for the Péclet numbers $P = 10^{-10}$ and $P = 10^4$, to make sure the discretization order is independent of the Péclet number. Furthermore three different heat distributions are considered, all on the unit circle. The first heat distribution is the uniform one. This heat source is discontinuous at $x^2 + y^2 = 1$. The second one is the semi-ellipsoidally shaped heat source. This heat source is continuous throughout, but the first derivative is discontinuous at $x^2 + y^2 = 1$. Finally a third heat source distribution is considered that is zero on the boundary of the unit circle and continuous throughout, as well as in the first derivative. The results are presented in table 2.1. The first grid (grid 1) has (1+4)x(1+4) nodal points. Grid 2 has (1+8)x(1+8) nodal points, etc. For the first two heat distributions table 2.1 shows that the maximum dimensionless temperature converges to its exact solution. However, if one looks at the differences between the solutions on each pair of subsequent grids, see table 2.2, one has to conclude that for the uniform heat distribution, and to a lesser extent for the semi-ellipsoidally shaped heat distribution, the ratio between subsequent differences does not converge to a constant. This phenomenon is explained by the way the circular region over which the heat source extends is discretized. The circle is divided into squares. On the boundary of the circle the squares will partially extend over the boundary. And since the heat source is assumed constant within each square, an error is introduced. This error decreases when the area of the squares becomes smaller, so the discretization still is consistent, although not of second order. The third case shows results for an artificially constructed heat distribution described by a fourth order polynomial which smoothly tends to zero at the boundary. This heat distribution (which has no practical relevance) does not suffer from discretization errors at the boundary of the domain and is seen to be of second order as follows from the nice convergence to the constant 4 in table 2.2 for the ratio of succesive

	$\overline{Q} = \frac{1}{\pi}$		$\overline{Q} = \frac{3}{2\pi}\sqrt{1-x^2-y^2}$		$\overline{Q} = \frac{6}{2\pi}(1-x^2-y^2)^2$	
grid	diff.	rat.	diff.	rat.	diff.	rat.
1-2	579e-5		2029e-5		42689e-7	
2-3	54e-5	10.7	443e-5	4.6	31525e-7	1.4
3-4	199e-5	0.3	147e-5	3.0	10353e-7	3.0
4-5	108e-5	1.8	25e-5	5.9	2849e-7	3.6
5-6	22e-5	4.9	8e-5	3.1	746e-7	3.8
6-7	7e-5	3.1	1e-5	8	190e-7	3.9

Table 2.2: Maximum dimensionless temperature differences for $P = 10^{-10}$

	$\overline{Q} = \frac{3}{2\pi}\sqrt{1-x^2-y^2}$		
grid	$\vartheta_f \cdot \sqrt{\phi P}$	diff.	rat.
1	0.54803		
2	0.57162	2359e-5	
3	0.58484	1322e-5	1.8
4	0.58763	279e-5	4.7
5	0.58885	122e-5	2.3
6	0.58919	34e-5	3.6
7	0.58931	12e-5	2.8
$\vartheta_f \cdot \sqrt{\phi P}(P \to \infty) =$	0.589487		

Table 2.3: Maximum dimensionless temperature and differences for $P = 10^4$

error differences. Thus, in conclusion, the consistency of the dicretization scheme has been validated, even though the approximation of the circle on a cartesian mesh slightly affects the order of the overall scheme.

For high Péclet numbers the results show the same phenomena. For high Péclet numbers the product $\overline{\vartheta} \cdot \sqrt{\phi P}$ converges to a known constant. As an example the case with $P = 10^4$ and a semi-ellipsoidal shaped heat source has been calculated; see table 2.3.

2.3 Function Fits

For engineering practice general formulas for the maximum and average temperature will be particularly usefull. In this section such a formula based on function fits of the numerically obtained data, will be derived. These function fits use the

asymptotic solutions for small and large Péclet numbers as building blocks. The asymptotic solutions will be presented in a way suitable for combining them into a general function fit. The general function fit is then compared with numerically obtained values.

Two heat source distributions will be considered, the uniform and the semi-ellpsoidal heat source distribution. A uniform heat supply seems to be a fair approximation if EHL-conditions prevail, i.e. for full film conditions.

In case of dry contact or boundary lubrication conditions a semi-ellipsoidal heat supply seems a good approximation, since for a constant coefficient of friction the heat supply has the same distribution as the elastic (Herzian) contact pressure.

For a uniform heat source distribution over an elliptic area the heat generated per unit area is given by

$$Q(x,y) = \frac{1}{\pi}\frac{F}{ab} \quad (|x| < x_s(y),\ |y| < b).$$

F is the total heat generated in the contact. For an elliptic contact with a semi-ellipsoidal source

$$Q(x,y) = \frac{3}{2\pi}\frac{F}{ab}\sqrt{1-\left(\frac{x}{a}\right)^2\left(\frac{y}{b}\right)^2}$$
$$(|x| < x_s(y),\ |y| < b)$$

applies with x_s given by

$$x_s(y) = a\sqrt{1-\left(\frac{y}{b}\right)^2} \quad (|y| < b).$$

2.3.1 Stationary Asymptotic Solutions

The asymptotic solution for small Péclet numbers is the temperature of a semi-infinite solid due to some specified stationary heat source distribution. One is generally interested in the average and maximum temperature in the contact. For elliptical contacts the average and maximum temperature rise can be written as

$$\vartheta_f = \theta_l \mathbf{S}(\phi)\frac{F}{K\sqrt{ab}}. \tag{2.19}$$

Where θ_l (l refers to low speed) has different values, depending on the distribution of the heat source (e.g. uniform versus semi-ellipsoidal) and depending on whether the average or maximum temperature is considered. The effect of the ellipticity of the contact is taken into account by the shape factor $\mathbf{S}(\phi)$, which reduces to $\mathbf{S}(1) = 1$ for the circular case ($\phi = b/a$, the aspect ratio of the contact ellipse).

For a circular contact area and a uniform heat source distribution the maximum dimensionless surface temperature rise of a stationary solid is $\theta_l^{um} = 1/\pi =$

0.318310... [2] (*Blok*, 1937). The average dimensionless contact temperature is $\theta_l^{ua} = 8/3\pi^2 = 0.270190...$ (*Carslaw and Jaeger*, 1959). The solution for the actual temperature distribution has been presented by *Francis* (1971) in terms of complete elliptic integrals.

For a circular contact area and a semi-ellipsoidal heat source distribution the maximum dimensionless contact temperature is given by $\theta_l^{em} = 3/8 = 0.375$ and the average dimensionless contact temperature is $\theta_l^{ea} = 9/32 = 0.28125$. This according to the analogy of the theory for concentrated elastic contacts of *Hertz* (1881) as proposed by *Francis* (1971). In the thermo-elastic analogy Q represents the contact pressure, ϑ the deformation and K the elasticity parameter $E/2(1-\nu^2)$. It is clear that transforming the shape of the heat source has an effect on the resulting temperature distribution, even if the total rate of heat supply and the heat source area remain unaltered. For an elliptic contact area and either a uniform or a semi-ellipsoidal heat source distribution, the dimensionless contact temperature can be calculated by applying the shape factor:

$$\mathbf{S}(\phi) = \frac{2\sqrt{\phi}}{1+\phi}\frac{2}{\pi}\mathbf{K}\left(\frac{|1-\phi|}{1+\phi}\right); \tag{2.20}$$

where $\mathbf{K}(k)$ represents the complete elliptic integral of the first kind and k its modulus; see *Abramowitz, e.a.* (1965). This exact solution for $\mathbf{S}(\phi)$ applies to the maximum contact temperature as well as the average contact temperature. In figure 2.5 the variation of $\mathbf{S}(\phi)$ is shown for $\phi \in [0.1, 10]$.

Holm (1958) found the same shape factor for the constriction resistance of an elliptic contact divided by the constriction resistance of a circular contact.

2.3.2 Large Péclet Numbers

In the previous section the low speed asymptotic solution has been discussed. There the prevailing heat transfer mechanism was conduction. Now, consider the case where only convection is of importance, thus neglecting any lateral conduction.

Because of the essentially one-dimensional nature of the heat transport for the Péclet numbers considered, a contact of any shape may be treated as a band contact. An asymptotic solution for large Péclet numbers that applies to a band shaped contact with a uniform distribution has been derived by *Jaeger* (1943). This solution is readily extended to contacts with other distributions by solving

$$\vartheta(x,y) = \frac{1}{\sqrt{\pi}}\frac{1}{K\rho cU}\int_{x_1(y)}^{min(x,x_2(y))}\frac{Q(\xi,y)d\xi}{\sqrt{x-\xi}}. \tag{2.21}$$

In this equation the integration boundaries are defined by

$$x_1(y) = -x_s(y)\ ,\ x_2(y) = x_s(y).$$

[2] For a summary of the asymptotic solutions see table 2.4

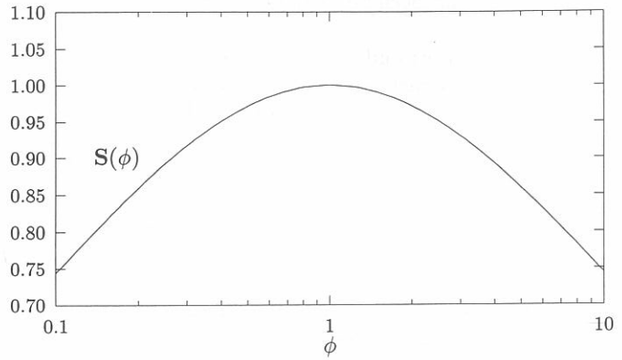

Figure 2.5: The shape factor $S(\phi)$.

The solution of (2.21) is identical to the end temperature variation with time of a one-dimensional rod, see *Carslaw and Jaeger* (1959), where time equals the residence time during which the heat input is felt, i.e. the distance from the moving heat front divided by its velocity.

Using the dimensionless variables given in (2.7) and (2.8), equation (2.21) can be written as

$$\overline{\vartheta}(\overline{x},\overline{y})\sqrt{\phi P} = \frac{1}{\sqrt{\pi}}\int_{\overline{x}_1(\overline{y})}^{min(\overline{x},\overline{x}_2)} \frac{\overline{Q}(\overline{\xi},\overline{y})d\overline{\xi}}{\sqrt{\overline{x}-\overline{\xi}}} \tag{2.22}$$

Thus for elliptic contacts the maximum and average temperature can, in analogy with (2.19), be obtained from

$$\vartheta_f = \frac{F}{K\sqrt{ab}}\frac{1}{\sqrt{\phi P}}\theta_r. \tag{2.23}$$

The flash temperature numbers θ_r that for elliptic contacts follow from the integral (2.22) will now be summerized. *Jaeger's* (1943) result for the maximum temperature in a uniformly heated band contact also applies to a uniformly heated elliptic contact resulting in $\theta_r^{um} = 2\sqrt{2}/\pi\sqrt{\pi} = 0.507949...$ For the semi-ellipsoidal heat distribution *De Winter* (1967) obtained for the maximum temperature $\theta_r^{em} = 0.589487...$

Less interesting, although more generally applied, is the average temperature of the contact area that, for a uniform heat source distribution, has been calculated

as

$$\theta_r^{ua} = \frac{32\sqrt{2}\Gamma(\frac{3}{4})}{5\pi^2}\Gamma(\frac{1}{4}) = 0.309955... \tag{2.24}$$

Consequently *Archard's* (1959) approximated solution of the average temperature, i.e. $\theta_r = 0.31$, is quite to the point. Also quite to the point is the maximum temperature according to *Archard and Rowntree* (1988), viz. 1.64 times the average temperature. The solution according to *Kuhlmann-Wilsdorf* (1986) though, viz. $\theta_r = 9/32 \approx 0.281$, underestimates the average temperature by about 10 %.

For the sake of completeness the average temperature of the contact area for a semi-ellipsoidal heat source distribution has been calculated as $\theta_r^{ea} = 0.322991...$ This differs only 7% from the average temperature for a uniform distribution. For general applications though, the maximum temperature is of more importance.

The solution that has been presented is a generalization to elliptic contacts of the asymptotic solution that applies to a band shaped heat source. However, the maximum local temperature rise for an elliptic contact is much larger than the average temperature rise over the contact area. Thus for elliptic contacts, whether the heat source is uniform or semi-ellipsoidal, the average temperature is a bad approximation for the maximum local temperature rise, an approximation frequently used for band contacts.

2.3.3 General Curvefit Function

For the asymptotic cases, i.e. very small and very high Péclet numbers, the analytic solutions have been given in the previous sections. For intermediate Péclet numbers neither of the asymtotic solutions decribes the local temperature rise well by itself. In this range both convection and conduction act as heat transfer mechanisms. If one can argue that the mechanisms of heat transfer are distinct and both operative, then an interpolation law can be found by assuming that both mechanisms are working in parallel, i.e.

$$\frac{1}{\vartheta_f} = \frac{1}{\vartheta_l} + \frac{1}{\vartheta_r}$$

where ϑ_l and ϑ_r are the temperatures due to, respectively, conduction only and convection only. For ϑ_l and ϑ_r expressions (2.19) and (2.23) have been derived in the foregoing sections. However the division of the heat flow into convection and conduction is spurious, the attribution of the two heat flows is wrong. This does not lead to accurate approximations of the local surface temperature rise in the intermediate range of Péclet numbers. Based on the results for a square source *Greenwood* (1991) found that the interpolation rule given above did indeed not lead to good approximations. He suggested that the local surface temperature rise of a source of any shape may be estimated by interpolation of the stationary and

uniform			
maximum		average	
θ_l^{um}	θ_r^{um}	θ_l^{ua}	θ_r^{ua}
0.318310	0.507949	0.270190	0.309955
semi-ellipsoidal			
maximum		average	
θ_l^{em}	θ_r^{em}	θ_l^{ea}	θ_r^{ea}
0.375000	0.589487	0.281250	0.322991

Table 2.4: Survey of the flash temperature numbers in six digits

high speed solutions, ϑ_l and ϑ_r according to the following rule:

$$\frac{1}{\vartheta_f^2} = \frac{1}{\vartheta_l^2} + \frac{1}{\vartheta_r^2}$$

This interpolation formula showed a remarkably good agreement with numerically calculated temperatures. Comparing the curvefit with numerical data, it was found that the following interpolation formula gives even better results for elliptic heat sources:

$$\vartheta_f^s = \vartheta_l^s + \vartheta_r^s \tag{2.25}$$

with

$$s = 0.5 \cdot \exp(1 - \phi) - 2.5, \tag{2.26}$$

or, equivalently,

$$\boxed{\vartheta_f \approx \frac{F}{K\sqrt{ab}} \left[\{\theta_l \mathrm{S}(\phi)\}^s + \left\{ \theta_r / \sqrt{\phi P} \right\}^s \right]^{1/s}} \tag{2.27}$$

where θ_l and θ_r represent the asymptotic flash temperature numbers for low and high Péclet numbers respectively. Equation (2.25), or (2.27), is a generalization of Greenwood's interpolation fomula and for circular contacts, $\phi = 1$, it is actually the same formula.

The asymptotic flash temperature numbers θ_l and θ_r still depend on the shape of the heat supply distribution and on the kind of temperature concerned, i.e. the maximum or the average temperature. Table 2.4 gives a list of the different flash temperature numbers.

2.3.4 Comparison with Numerical Data

Figures 2.6 and 2.7 show the numerically calculated surface temperatures and values obtained from the function fit for elliptic heat sources with, respectively,

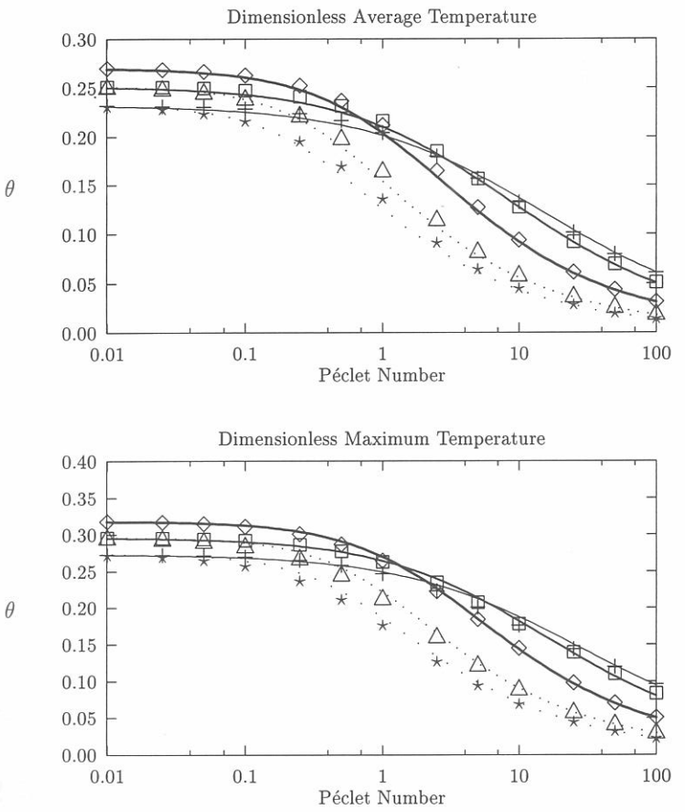

Figure 2.6: Average- and maximum temperature, uniform heat source. Markers denote numerically calculated values. The lines represent the curvefit function. $+$: $\phi = 1/5$, $\square$: $\phi = 1/3$, $\diamond$: $\phi = 1$, $\triangle$: $\phi = 3$, $\star$: $\phi = 5$.

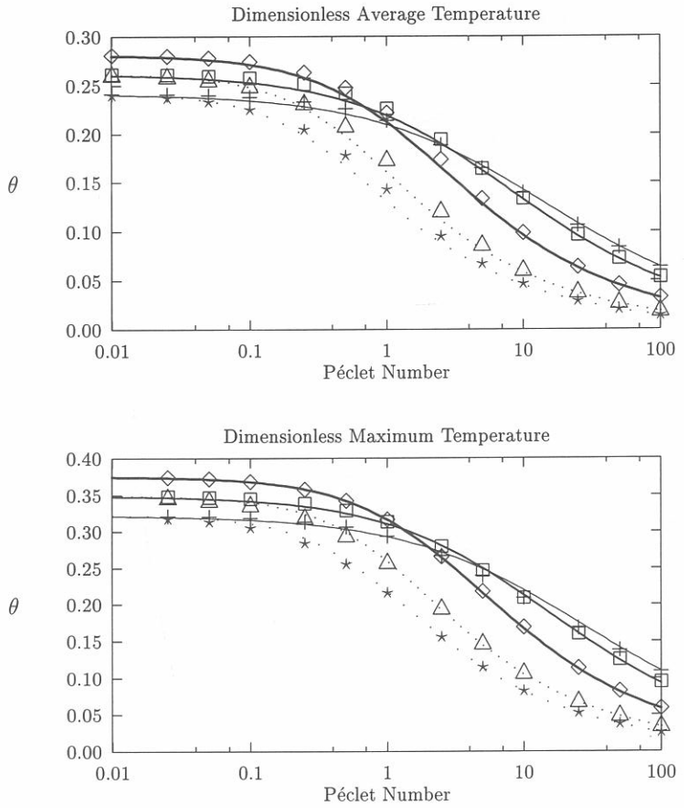

Figure 2.7: Average- and maximum temperature, semi-ellipsoidal heat source. Markers denote numerically calculated values. The lines represent the curvefit function. $+$: $\phi = 1/5$, $\square$: $\phi = 1/3$, $\diamond$: $\phi = 1$, $\triangle$: $\phi = 3$, $\star$: $\phi = 5$.

uniform and semi-ellipsoidal distributions. As can be seen from these figures, there is a very good agreement between the numerically obtained values and the approximate values from the function fit. The error is always less than 5% in the range of $\phi \in [1/5, 5]$.

2.4 Example

As an illustration the maximum contact temperature of a zirconia ball with a diameter of 10.0 mm sliding against a steel plate will be calculated as function of the sliding velocity. Table 2.5 lists the material properties of the bodies. As the conductivity of steel is about 20 times higher than the conductivity of zirconia, the contact temperature can be estimated reasonably well by assuming that all the heat generated in the contact will flow into the steel plate.

First the dimensions of the contact need to be calculated. According to the Hertzian theory the radius of the circular ($\phi = 1$) contact area is 0.15 mm, for a load of $F_n = 100\ N$. For the coefficient of friction a value of $\mu = 0.38$ is taken (*He, et. al.*, 1995). The rate of heat flow follows from:

$$F = \mu\ F_n\ U$$

Due to the elastic deformation of the bodies the rate of heat flow will have a semi-ellipsoidal distribution, so θ_l^{em} and θ_r^{em} should be used for θ_l and θ_r in equation (2.27). Substitution of these values leads to the following expression for the maximum contact temperature as function of the sliding speed:

$$\vartheta_f(U) \approx \frac{\mu F_n U}{K_{steel}\sqrt{ab}} \left[\{\theta_l^{em}\}^{-2} + \left\{ \theta_r^{em} / \sqrt{\frac{aU}{\kappa_{steel}}} \right\}^{-2} \right]^{-1/2}$$

This expression is plotted in figure 2.8. It can be seen that for $U > 0.1\ m/s$ the local temperature rise exceeds $200°C$, indicating that tempering of the metal and therefore softening is likely to occur at and just below the surface.

2.5 Conclusion

An algorithm, able to calculate the surface temperature of a semi-infinite body, moving past a heat source of arbitrary shape and distribution, has been developed.

By applying the algorithm to elliptic heat sources with uniform and semi-ellipsoidal distributions, function fits for these heat sources were constructed and verified for the maximum and average temperature, see equation (2.27).

For practical engineering use, the function fits can be used to calculate the maximum or average temperature rise, without having to perform complicated numerical simulations.

Material Properties				
			AISI52100 hardened steel	ZrO_2
Young's modulus	$[GPa]$	E	213	191
Poisson's ratio		ν	0.3	0.3
Thermal conductivity	$[W/mK]$	K	45	2.5

Table 2.5: Relevant material properties for ball bearing steel and zirconia. From *He et. al.* (1995)

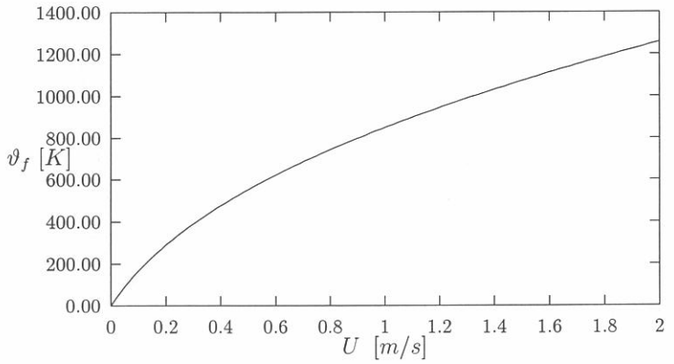

Figure 2.8: Maximum contact temperature rise in the contact between a zirconia ball and a steel plate. $F_n = 100N$; $\kappa_{steel} = 13e-6$

References

Abramowitz, M. and Stegun, I.A., 1965 (eds), Handbook of Mathematical Functions, New York.

Archard, J.F., 1959, "The temperature of rubbing surfaces", *Wear*, Vol. 2, pp. 438-455.

Archard, J.F., and Rowntree, R.A., 1988, " The temperature of rubbing bodies; part 2, the distribution of temperatures," *Wear*, Vol. 128, pp. 1-17.

Balsara, S. and Brandt, A. , 1991, "Multilevel Methods for Fast Solution of N-body and Hybrid Systems", *Int. Series of Num. Math.*, Birkhäuser Verlag, Vol. 98, pp. 131-142, Basel.

Brandt, A. and Lubrecht, A.A., 1990, "m Multilevel Matrix Multiplication and Fast Solution of Integral Equations," *J. of Comp. Physics*, Vol. 90, No. 2, pp. 348-370.

Blok, H., 1937, "Theoretical study of temperature rise at surface of actual contact under oiliness lubricating conditions", Instn. Mech. Engrs., *Proceedings of general discussion on lubrication and lubricants*, Vol. 2, pp. 222-235.

Bos, J., and Moes, H., 1994, "Frictional heating of elliptic contacts," *Dissipative processes in tribology*, Proc. 20th Leeds-Lyon Symposium on Tribology, Elsevier, Amsterdam, pp. 491-500.

Brandt, A. and Lubrecht, A.A., 1990, " Multilevel matrix multiplication and fast solution of integral equations," *J. of Comp. Phys.*, Vol. 90, No. 2, pp. 348-370.

Carslaw, H.S. and Jaeger, J.C., 1959, "Conduction of Heat in Solids," Oxford University Press, Oxford, UK.

Francis, H.A., 1971, "Interfacial Temperature Distribution Within a Slidng Hertzian Contact," *ASLE Trans.*, Vol. 14, pp. 41-54.

Greenwood, J.A., 1991, " An Interpolation Formula for Flash Temperatures," *Wear*, Vol. 150, pp. 153-158.

He, Y.J., Winnubst, A.J.A., Schipper, D.J., Bakker, P.M.V., Burggraaf, A.J. and Verweij, H., 1995, " Friction and Wear Behaviour of Ceramic-hardened Steel Couples under Reciprocating Sliding Motion," *Wear*, Vol. 184, No. 1, pp. 33-43.

Hertz, H., 1881, "Über die Berührung fester elastischer Körper," *Journal für die reine und angewandte Mathematik*, Vol.92, pp.156-171.

Holm, R., 1958, Electric Contacts Handbook, Berlin/New York.

Jaeger, J.C., 1943, "Moving sources of heat", *J. and Proc. Roy. Soc. N.S.W.*, Vol. 76, pp. 203-224.

Kennedy, F.E., 1984, "Thermal and thermomechanical effects in dry sliding," *Wear*, Vol. 100, pp. 453-467.

Kuhlmann-Wilsdorf, D., 1986, "Sample calculations of flash temperatures at a silver-graphite electric contact sliding over copper" , *Wear*, Vol. 107, pp. 71-90.

Kuhlmann-Wilsdorf, D., 1987, " Temperatures at interfacial contact spots: dependence on velocity and on role reversal of two materials in sliding contact, *J. of Tribology*, Vol. 109, pp. 321-329.

Moes, H., 1992, "Optimum similarity analysis with applications to elastohydrodynamic lubrication," *Wear*, Vol. 159, pp. 57-66.

Oliver, J., 1972, " A doubly-adaptive Clenshaw-Curtis quadrature method," *Computer Journal*, Vol. 15, pp. 141-147.

Winter, A. de, 1967, "De berekening van de flitstemperatuurverdelingen in en aan weerszijden van een bandvormig contactvlak (tevens warmtebron) tussen twee over elkaar glijdende loopvlakken", Masters Thesis (in Dutch), Technical University of Delft.

Chapter 3

Partition Problem

In chapter 2 the surface temperature rise of a semi-infinite body moving past a heat source was studied. In tribological contacts this represents the local temperature rise of two bodies in sliding contact, where one of the bodies has a much higher conductivity than the other, e.g. a metal in contact with a ceramic material or a plastic. However, in many tribological contacts the bodies will have conductivities of the same order of magnitude and the heat developed in the contact will be distributed between the two bodies in contact according to an a priori unknown partition function. As an example consider the following two situations; 1) two identical bodies, well cooled in sliding contact where one body is stationary and the other is moving relative to the contact, 2) both bodies are moving in the same direction relative to the contact with the same speed as in situation 1. If the total heat, generated in the contact, is the same for both situations, then the contact temperature is expected to be highest in situation 1. The only heat transfer mechanism for the stationary body is conduction whereas in situation 2 for both bodies convection too is available as a heat transfer mechanism. So in situation 1 the moving body has to convey more heat compared to either body in situation 2 resulting in a higher contact temperature. From this example it becomes clear that, depending on the Péclet numbers of the bodies, different contact temperatures can be expected, even if the total heat generated in the contact is the same. This implies that the heat flow is divided differently for the two situations described.

This more general problem of determining the local temperature rise for two bodies with conductivities of the same order of magnitude in contact, i.e. the heat partition between the two bodies, was addressed numerically by *Allen* (1962) for band shaped contacts. This work was later improved upon by *Cameron et al.* (1965). These studies considered the contact temperature between two semi-infinite solids under steady state conditions. For circular contact areas *Archard* (1959) introduced an approximate solution on the basis of Jaeger's work together with a simple rule of thumb for the partition problem. However, most practical contacts are neither band shaped nor circular, but elliptic. Initially this was ac-

counted for by using *Jaeger*'s (1943) solution for rectangular contacts by way of an approximation. For conditions where the lateral conduction can be neglected, this approach yields good approximations. For situations where the lateral conduction becomes an important factor, i.e. for low and intermediate Péclet numbers, ambiguous decisions have to be made regarding the dimensions and the distribution of the rectangular heat source in order to assure a good approximation.

In this chapter an algorithm will be developed for the heat partition problem. It computes the heat partition by matching the surface temperatures of the bodies at all points within the apparent contact area. Furthermore, asymptotic solutions for the local temperature rise in the case of opposing velocities are calculated for both uniform and semi-ellipsoidal circular heat sources. Subsequently, using these asymptotic solutions, numerically calculated local temperature rises and asymptotic solutions known from the literature, closed-form function fits will be derived to predict the maximum local temperature rise in the contact for the entire range of possible values of Péclet numbers.

3.1 Equations

In dimensionless variables, the steady state surface temperature rises of the contacting semi-infinite solids can be written as (see chapter 2 section 2.1):

$$\overline{\vartheta}_1(\overline{x},\overline{y}) = \frac{1}{2\pi}\frac{1}{\sqrt{\phi}}\int_{S_q}\frac{\overline{Q_1}(\overline{x}',\overline{y}')\exp\left(-\frac{P_1}{2}\{R-(\overline{x}-\overline{x}')\}\right)}{R}d\overline{x}'\,d\overline{y}' \tag{3.1}$$

$$\overline{\vartheta}_2(\overline{x},\overline{y}) = \frac{1}{2\pi}\frac{1}{\lambda}\frac{1}{\sqrt{\phi}}\int_{S_q}\frac{\overline{Q_2}(\overline{x}',\overline{y}')\exp\left(-\frac{P_2}{2}\{R-(\overline{x}-\overline{x}')\}\right)}{R}d\overline{x}'\,d\overline{y}' \tag{3.2}$$

where P_1 and P_2 are the Péclet numbers, $\lambda = K_2/K_1$ is the conductivity ratio, S_q the contact area, i.e. an ellipse, and

$$R \equiv \sqrt{(\overline{x}-\overline{x}')^2+(\overline{y}-\overline{y}')^2}.$$

The two bodies are assumed to have the same bulk temperature, i.e. the local temperature rise is considered. Further it is assumed that the bodies cannot exchange heat outside the contact area.

By definition, the partition function α, describes the part of the heat flowing into body 1:

$$\overline{Q}_1(\overline{x}',\overline{y}') = \overline{Q}(\overline{x}',\overline{y}')\,\alpha(\overline{x}',\overline{y}') \tag{3.3}$$

$$\overline{Q}_2(\overline{x}',\overline{y}') = \overline{Q}(\overline{x}',\overline{y}')\,(1-\alpha(\overline{x}',\overline{y}')) \tag{3.4}$$

In the contact the surface temperatures are assumed to be equal, so temperature drops over intermediate layers of any kind, like oxides or oil films, are neglected:

$$\overline{\vartheta}_1(\overline{x},\overline{y}) - \overline{\vartheta}_2(\overline{x},\overline{y}) = 0, \qquad (\overline{x},\overline{y}) \in S_q \tag{3.5}$$

Substitution of equations (3.1 - 3.4) in this equation results, after simplification, in:

$$\int_{S_q}\frac{\overline{Q}(\overline{x}',\overline{y}')\;\alpha(\overline{x}',\overline{y}')\;\exp\left(-\frac{P_1}{2}\{R-(\overline{x}-\overline{x}')\}\right)}{R}d\overline{x}'\,d\overline{y}' =$$
$$\frac{1}{\lambda}\int_{S_q}\frac{\overline{Q}(\overline{x}',\overline{y}')\;(1-\alpha(\overline{x}',\overline{y}'))\;\exp\left(-\frac{P_2}{2}\{R-(\overline{x}-\overline{x}')\}\right)}{R}d\overline{x}'\,d\overline{y}' \tag{3.6}$$

or written in terms of Q_1

$$\int_{S_q}\overline{Q_1}(\overline{x}',\overline{y}')\;\frac{\lambda\exp\left(-\frac{P_1}{2}\{R-(\overline{x}-\overline{x}')\}\right)+\exp\left(-\frac{P_2}{2}\{R-(\overline{x}-\overline{x}')\}\right)}{R}d\overline{x}'\,d\overline{y}' =$$
$$\int_{S_q}\overline{Q}(\overline{x}',\overline{y}')\;\frac{\exp\left(-\frac{P_2}{2}\{R-(\overline{x}-\overline{x}')\}\right)}{R}d\overline{x}'\,d\overline{y}' \tag{3.7}$$

From this equation the dimensionless heat flux $\overline{Q}_1$ can be solved for a given $\overline{Q}$ and thus the local temperature rise in the contact can be found by applying equation (3.1). The partition function α then immediately follows from (3.3).

3.2 Numerical Approach

In recent years it has been amply demonstrated that multigrid techniques yield fast and efficient solvers for tribological problems, e.g. EHL see *Lubrecht*, (1986). The first step in the development of a multigrid solver is the discretization of the problem on a grid, followed by the development of a stable relaxation scheme which reduces the high frequency error components effectively. Once such a relaxation scheme is devised, the multilevel schemes can be applied (see *Brandt* 1984 and references therein). The discretization is the same as in the previous chapter and the details will not be repeated here. The relaxation scheme for the partition problem will be described in section 3.2.2.

3.2.1 Discrete Equation

In order to solve the dimensionless heat flux from equation (3.7), the discretization from section 2.2.1 is used, resulting in a set of linear equations from which $\overline{Q}_{1_{ij}}$ in each grid point can be solved.

This linear set of equations can be written compactly in index notation as:

$$\sum_{k=0}^{n_x}\sum_{l=0}^{n_y}[K_{ijkl}^{hhhh}]\overline{Q}_{1_{kl}} = f_{ij} \tag{3.8}$$

Here

$$f_{ij} = \sum_{k=0}^{n_x} \sum_{l=0}^{n_y} [K_{ijkl}^{hhhh}]_2 \overline{Q}_{kl} \tag{3.9}$$

and

$$[K_{ijkl}^{hhhh}] = [K_{ijkl}^{hhhh}]_1 + [K_{ijkl}^{hhhh}]_2 \tag{3.10}$$

The $[K_{ijkl}^{hhhh}]$ matrix is a full matrix and thus solving this set of equations for $\overline{Q}_1$ in fact requires inverting this full matrix, either directly or by means of an iterative scheme.

3.2.2 Relaxation Scheme

This section describes the relaxation scheme. For convenience, the multi summations at the left hand side of equation (3.8) are denoted by t_{ij}. Equation (3.8) can then be written as:

$$t_{ij} = f_{ij} \tag{3.11}$$

with

$$t_{ij} = \sum_{k=0}^{n_x} \sum_{l=0}^{n_y} [K_{ijkl}^{hhhh}] \ \overline{Q}_{1_{kl}} \tag{3.12}$$

This equation is very similar to the equation for the dry contact problem described in *Lubrecht and Ioannides*, (1989) and, indeed, their numerical approach can be applied here.

Equation (3.11) can be solved by means of the following second order distributive relaxation scheme: Given an approximation $\tilde{\overline{Q}}_{1_{ij}}$ to $\overline{Q}_{1_{ij}}$ and the associated integrated values $\tilde{t}_{ij}$, all grid points are visited in lexicographic order and changes δ_{ij} are calculated according to:

$$\delta_{ij} = \frac{f_{ij} - \tilde{t_{ij}}}{\Delta K_{iijj}^{hhhh}} \tag{3.13}$$

where:

$$\Delta K_{iijj}^{hhhh} = K_{iijj}^{hhhh} - (K_{ii-1jj}^{hhhh} + K_{ii+1jj}^{hhhh} + n_{iijj-1}^{hhhh} + K_{iijj-1}^{hhhh})/4 \tag{3.14}$$

Once all the changes δ_{ij} have been calculated, they are applied at sites (i, j) and the adjacent sites $(i \pm 1, j)$ and $(i, j \pm 1)$ according to the following distribution:

$$\frac{1}{4}\delta_{ij} \begin{bmatrix} 0 & -1 & 0 \\ -1 & 4 & -1 \\ 0 & -1 & 0 \end{bmatrix} \tag{3.15}$$

The changes are applied simultaneously after the sweep is completed, a so called "Jacobi relaxation". The new approximation $\hat{\overline{Q}}_{1_{ij}}$ to $\overline{Q}_{1_{ij}}$ is thus given by:

$$\hat{\overline{Q}}_{1_{ij}} = \tilde{\overline{Q}}_{1_{ij}} + \delta_{ij} - (\delta_{i-1j} + \delta_{i+1j} + \delta_{ij-1} + \delta_{ij+1})/4 \tag{3.16}$$

The relaxation sweep is followed by an update of the multi summations, for which the multi level multi integration algorithm described in chapter 2 is used in order to obtain all $\hat{t}_{ij}$, the values of the multi-summations associated with the new approximations to $\hat{\overline{Q}}_{1_{ij}}$.

The distributive relaxation ensures stability of the relaxation by keeping the accumulated changes in the multi summations small. It is also very effective in reducing high frequency error components in both x- and y-direction see *Venner and Lubrecht*, (1993).

3.2.3 Verification

Although in general the partition function cannot be derived analytically, for two bodies moving in the same direction with the same Péclet number, the partition problem simplifies to:

$$(1+\lambda) \int_{S_q} \frac{\overline{Q}(\overline{x}', \overline{y}') \ \alpha(\overline{x}', \overline{y}') \ \exp\left(-\frac{P}{2}\{R - (\overline{x} - \overline{x}')\}\right)}{R} d\overline{x}' \, d\overline{y}' \ = \int_{S_q} \frac{\overline{Q}(\overline{x}', \overline{y}') \ \exp\left(-\frac{P}{2}\{R - (\overline{x} - \overline{x}')\}\right)}{R} d\overline{x}' \, d\overline{y}', \tag{3.17}$$

and for any $\overline{Q}$ the solution for α is:

$$\alpha(\overline{x}', \overline{y}') = \frac{1}{1+\lambda}, \tag{3.18}$$

i.e. α is independent of the position in the contact. In particular for $\lambda = 1$ the heat is divided evenly and $\alpha = \frac{1}{2}$ everywhere in the contact. For a circular contact the partition function for this situation is shown in figure 3.1.

Another interesting situation is the following: two bodies moving in opposite direction with the same Péclet number and $\lambda = 1$. If the heat supply in the contact is symmetric around the origin then α should be asymmetric around the line $x = 0$ with $\alpha(0, \overline{y}') = \frac{1}{2}$. This situation is shown in figure 3.2

Figure 3.3 shows the partition function at $y = 0$, to demonstrate the asymmetry around $x = 0$ and to show that $\alpha(\overline{x}' = 0) = \frac{1}{2}$, something that is not immediately clear from figure 3.2. This figure shows another interesting aspect of the partition function; it does not vary between zero and one, but between $-\infty$ and ∞. Since for two bodies sliding in opposite directions, in each half of the contact most of the heat will go into the cooler incoming body, it is clear that the division of heat

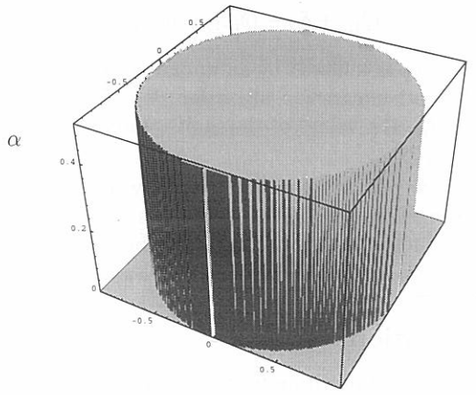

Figure 3.1: Partition function for two bodies moving in the same direction with equal Péclet numbers and $\lambda = 1$

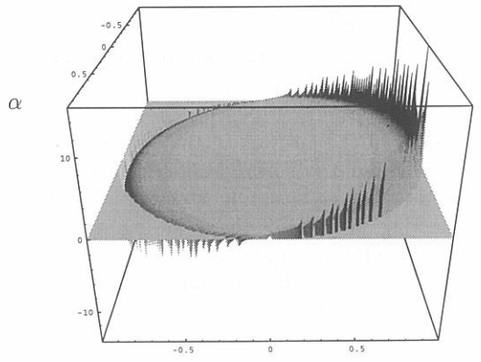

Figure 3.2: Partition function for two bodies moving in opposite directions with equal Péclet numbers, $P = 20$, $\lambda = 1$

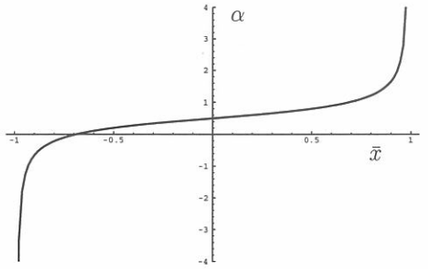

Figure 3.3: Centre line partition function values for two bodies moving in opposite directions with equal Péclet numbers, $P = 20$, $\lambda = 1$

is not uniform over the contact. However by assuming the range of the partition function to be between zero and one, circulation of heat is excluded, i.e. heat flowing from body 1 to body 2 at some place and vice versa at another with a net zero result. For band contacts these aspects of the partition function have already been observed by *De Winter* (1967).

3.3 Results

Figure 3.4 shows the surface temperature distributions for both contacting surfaces due to a uniform heat source for the combination of Péclet numbers $P_1 = 5, P_2 = 0$. Both the temperature distribution in the contact region and part of the temperature distribution outside the contact are shown. Note that, because of the boundary condition in the contact (3.5), the surface-temperatures for both bodies only differ outside the contact area.

The temperature distribution of solid 2 (figure 3.4.B) shows a groove at the right edge of the contact region. These local minima of the temperature are caused by a negative heat flux for solid 2. At these positions the temperature of solid 1 (figure 3.4.A) has to rise from almost ambient temperature (the heat source has not yet passed the surface there) to the elevated temperature of solid 2. This results in an additional heat flux from solid 2 into solid 1, i.e. the partition function is larger than 1. The corresponding local negative heat flux for solid 2 leads to a the local temperature drop.

Figures 3.5 and 3.6 show center-line ($y = 0$) temperatures for a uniform and a semi-ellipsoidal heat source respectively. In both figures the combination $P_1 = 5, P_2 = 0$ shows, as expected from the example in the introduction of this chapter, the highest maximum temperature. For the uniform heat source the maximum temperatures for the combinations $P_1 = 5, P_2 = 5$, a situation which might occur

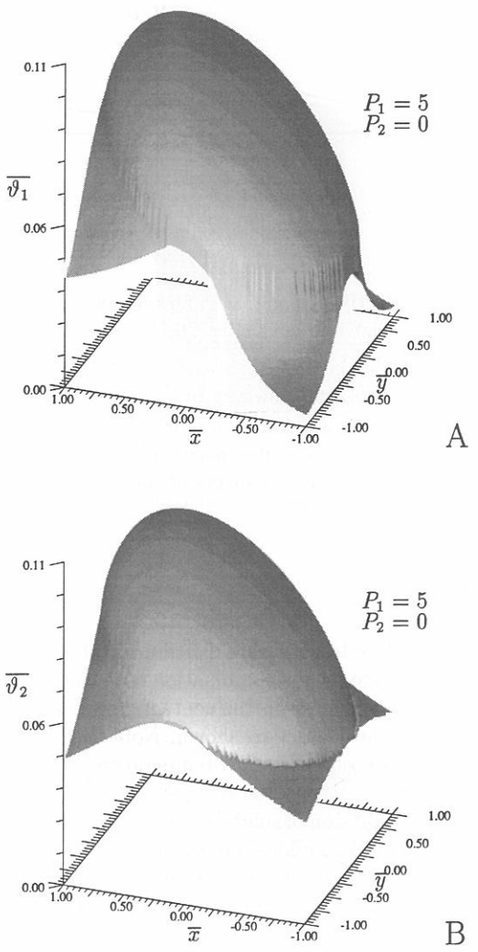

Figure 3.4: Temperature distributions of both bodies for the combination of $P_1 = 5$ and $P_2 = 0$, $\lambda = 1$

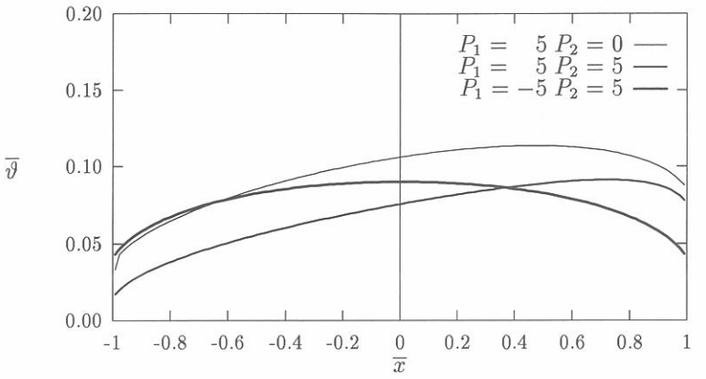

Figure 3.5: Center-line temperatures for different Péclet numbers, uniform heat source, $\lambda = 1$.

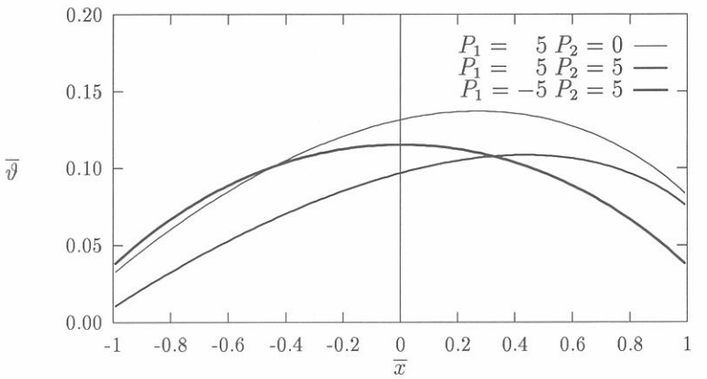

Figure 3.6: Center-line temperatures for different Péclet numbers, semi-ellipsoidal heat source, $\lambda = 1$.

for two sliding bodies with different specific heats, and $P_1 = -5, P_2 = 5$ are, suprisingly almost identical although located at different positions. From the point of view of available heat transfer mechanisms the fact that the maximum temperatures are (almost) the same makes sense; ignoring the distributions of Q_1 and Q_2, the available heat transfer mechanisms are the same for both situations. In general, the distributions Q_1 and Q_2 cannot be ignored or replaced by their average values. This follows from the situation where the total heat supply has a semi-ellipsoidal distribution.

Figure 3.6 shows that for the semi-ellipsoidal heat source, the maximum temperature for the combination $P_1 = -5, P_2 = 5$ is higher than that for the combination $P_1 = 5, P_2 = 5$. Apparently, for semi-ellipsoidal heat sources, heat transfer is hampered by opposing velocities.

3.4 Function fits

The closed-form function fits of chapter 2 cover only part of the situations that can occur for two bodies in sliding contact with conductivities of the same order of magnitude. If the two bodies have the same Péclet number and are moving in the same direction, the partition function is a constant. Also for two bodies moving in the same direction with asymptotically high Péclet numbers the partition function becomes a constant, which can be calculated without performing the full numerical simulation decribed in section 3.2 and thus the function fits of chapter 2 can be applied for these situations as soon as the partition constant is determined.

In this section generally applicable function fits will be derived, i.e. function fits that also apply for bodies moving in opposite direction or for situations of intermediate Peclet numbers. These function fits use the asymptotic solutions for small and large Péclet numbers as building blocks. As in the previous chapter, the asymptotic solutions will be presented in a way suited to combine them into a general function fit. The general function fit is then verified against numerically obtained values, using the algorithm described in section 3.2

3.4.1 Asymptotic solutions

Velocities in the same direction

For two bodies moving in the same direction with a high Peclet number *Blok* (1937) has shown that the rate of heat supply is partitioned over the two solids in contact according to the simple relation

$$F_i = \frac{\sqrt{K_i \rho_i c_i U_i}}{\sum \sqrt{K \rho c U}}; \tag{3.19}$$

where $\sum \sqrt{K \rho c U} \equiv \sqrt{K_1 \rho_1 c_1 U_1} + \sqrt{K_2 \rho_2 c_2 U_2}$. The heat supply to the individual bodies has the same shape as the total heat supply. The flash temperature for two solids in contact, moving in the same direction, can be calculated from the asymptotic solution for the surface temperature at large Péclet numbers:

$$\vartheta(x,y)_i = \frac{1}{\sqrt{\pi}} \frac{1}{\sqrt{K_i \rho_i c_i U_i}} \int_{-x_s(y)}^{min(x, x_s(y))} \frac{Q_i(\xi, y) d\xi}{\sqrt{x - \xi}} \quad . \tag{3.20}$$

The flash temperature follows from the maximum for the contact temperature after substituting equation (3.19) into (3.20) and reads:

$$\vartheta_f = \theta_r \frac{F}{b\sqrt{a}} \frac{1}{\sum \sqrt{K \rho c U}} \quad . \tag{3.21}$$

This is in fact applying *Archard*'s rule of thumb. In this relation θ_r is the flash temperature factor derived in chapter 2 which takes into account the distribution of the heat supply and the temperature concerned, i.e. maximum or average. The subscript r indicates a predominantly rolling movement of the bodies in contact.

Velocities in opposite directions

The temperature distribution for $K_2 \rho_2 c_2 U_2 = K_1 \rho_1 c_1 U_1$ with U_1 and U_2 in opposite directions, *e.g.* two identical bodies moving at equal speeds in opposite directions and a uniform heat supply, has been calculated numerically for high Peclet numbers by applying the following integral equation defining Q_1—and thus the partition of the heat flow:

$$\int_{-x_s(y)}^{x_s(y)} \frac{Q_1(\xi, y) d\xi}{\sqrt{|\xi - x|}} = \int_{x}^{x_s(y)} \frac{Q(\xi, y) d\xi}{\sqrt{\xi - x}}, \tag{3.22}$$

This is *Abels's integral equation with constant integral limits.* This equation was solved numerically. With the proper adjustments for the one dimensionality of the problem, the numerical approach is similar to the one described in section 3.2 for the general two dimensional problem. For more details on the subject see *Bos and Moes*, (1995)

Equation (3.22) was solved for both a uniform and a semi-ellipsoidal heat supply. Surprisingly, for a uniform heat distribution, the numerically obtained maximum temperature rise was very similar (7 decimal places) to the maximum temperature rise for two bodies moving in the same direction. Recently *Greenwood* (1995) showed by means of an analytic proof that for an uniform heat supply, the maximum temperature rise for bodies moving at high speeds in opposite directions is exactly the same as for bodies moving at high speeds in the same direction. So

$$\vartheta_f = \theta_s \frac{F}{b\sqrt{a}} \frac{1}{2\sqrt{K \rho c U}}, \tag{3.23}$$

with $\theta_s^{um} = \theta_r^{um} = 2\sqrt{2}/\pi\sqrt{\pi} = 0.507949\cdots$.

The maximum flash temperature is not independent of the direction of the velocities in general, as was already indicated by the results shown in section 3.3. For a semi-ellipsoidal supply of heat and two identical bodies moving at equal, high, speeds in opposite directions the maximum local temperature rise is substantially higher than the maximum local temperature rise for two identical bodies moving in the same direction at equal, high, speeds, i.e. $\theta_s^{em} = 0.700792\cdots$ (whereas $\theta_r^{em} = 0.589487\cdots$).

For the average flash temperatures the discrepancies are even stronger; because $\theta_s^{ua} \equiv 8\sqrt{2}/5\pi\sqrt{\pi} = 0.406359\cdots$ (whereas $\theta_r^{ua} = 0.309954\cdots$) and $\theta_s^{ea} = 0.437504\cdots$ (whereas $\theta_r^{ea} = 0.322991\cdots$) have been calculated for a uniform and a semi-ellipsoidal heat supply distribution, respectively. The index **s** was introduced in order to indicate the predominating *sliding* movement of the two mating surfaces; the index **r** introduced in chapter 2 indicates a predominating *rolling* movement of the two mating surfaces. Both indices indicate high speed asymptotic solutions, i.e. the only lateral heat transfer mechanism is convection.

Stationary solids

The heat partition for two stationary solids follows from

$$F_i = \frac{K_i}{\sum K} F \quad (i = 1, 2) \ ; \tag{3.24}$$

where $\sum K \equiv K_1 + K_2$. Although academic, since there is no heat generation in the contact for this situation, the results are needed for the general function fit. This leads to the following equation for the flash temperature for two solids in contact:

$$\vartheta_f = \theta_l S(\phi) \frac{F}{\sqrt{ab}} \frac{1}{\sum K} \ . \tag{3.25}$$

Where θ_l is the flash temperature factor from chapter 2.

3.4.2 General function fit

Archard's (1959) rule of thumb for the partitioning of the heat flow also holds when maximum temperatures instead of average temperatures are used. It then reads

$$\frac{1}{\vartheta_f} \approx \frac{1}{\vartheta_1} + \frac{1}{\vartheta_2} \ ;$$

where the two temperatures at the right hand side are the maximum temperatures that would occur if all the heat was supplied to either solid 1 or solid 2. These

temperatures can be determined with the curve-fit relation derived in the previous chapter;

$$\vartheta_i = \frac{F}{K_i \sqrt{ab}} \left[\{\theta_l S(\phi)\}^s + \left(\frac{\theta_r}{\sqrt{\phi P_i}} \right)^s \right]^{1/s} \quad (i = 1, 2) \ ; \tag{3.26}$$

This rule of thumb invariably represents the exact solution for the heat partitioning at the asymptotic conditions. Therefore, accepting this rule of thumb as a general condition will probably yield good approximations for the general case, see section 3.4.3. Consequently the flash temperature may be represented by the simple equation

$$\boxed{\vartheta_f \approx \frac{F}{\sqrt{ab}} \frac{1}{\sum (K/\theta)} \ ,} \tag{3.27}$$

$$\boxed{\theta_i \approx \left[\{\theta_l S(\phi)\}^s + \left(\frac{\theta_h}{\sqrt{\phi P_i}} \right)^s \right]^{1/s} \quad (i = 1, 2) \ ;} \tag{3.28}$$

with $s = 0.5 * \exp(1 - \phi) - 2.5$. In this equation the auxiliary flash temperature factor θ_h represents the flash temperature solution for **h**igh velocities. Contrary to the 1 body situation the direction of the velocities of the bodies with respect to the contact *is* important if two bodies are in contact. θ_h is a function fit based on the asymptotic solutions θ_r and θ_s and takes into account the sliding conditions which prevail when the bodies are moving in opposite direction. It is defined as

$$\theta_h = \frac{\theta_r + t\theta_s}{1 + t}. \tag{3.29}$$

In this expression t represents:

$$t = \max\left(0, \frac{-q}{1+q}\right) \quad \text{with} \quad q = \text{sign}(U_1 \cdot U_2) \min\left(p, \frac{1}{p}\right), \tag{3.30}$$

and

$$p \equiv \sqrt{\frac{P_2}{P_1}}. \tag{3.31}$$

For convenience, situations with velocities in opposite directions have been, and will be, indicated by a combination of a positive and negative Péclet number. Please note that when using the formulas (3.26), (3.28) and (3.31), positive Péclet numbers should always be applied.

Further it is convenient to observe that for velocities in the same direction equation (3.29) reduces to

$$\theta_h = \theta_r,$$

so for velocities in the same direction equations (3.30) and (3.31) need not be evaluated.

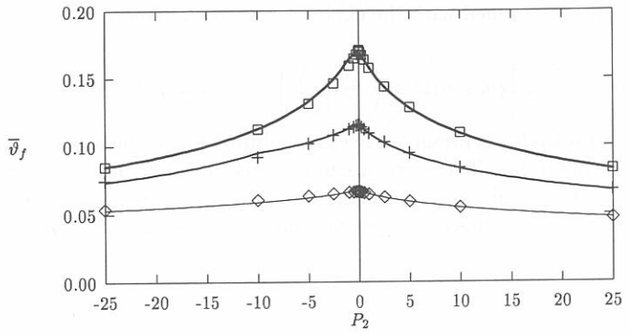

Figure 3.7: Maximum temperature, semi-ellipsoidal heat source. Markers denote numerically calculated values. The lines represent the curvefit function. $\diamond$: $P_1 = 50$; $+$: $P_1 = 10$; $\square$: $P_1 = 1$, $\lambda = 1$

The heat fluxes entering bodies 1 and 2, respectively, can be approximated by

$$F_1 \approx \frac{1/\theta_1}{1/\theta_1 + \lambda/\theta_2} F \qquad F_2 \approx \frac{\lambda/\theta_2}{1/\theta_1 + \lambda/\theta_2} F \tag{3.32}$$

3.4.3 Comparison with numerical results

Figures 3.7 and 3.8 show numerically calculated maximum contact temperatures and function fit values for circular, i.e. $\phi = 1$, semi-ellipsoidal and uniform heat sources respectively. Each figure shows the maximum contact temperature for three different Péclet numbers of one body and a range of Péclet numbers of the second body, i.e. $P_1 = 1$, $P_1 = 10$ and $P_1 = 50$ and P_2 varies from -25 to 25. Thus velocities in opposite direction and velocities in the same direction are both considered.

As can be seen from these figures for circular contacts, the approximated curvefit values agree very well with the numerically obtained values. The error is always less than 5%, as was found previously for the situation where only one body moves past a heat source.

Indeed, the curvefit formula accurately predicts the value of the flash temperature, but the shape of the curves at some points is less accurate, e.g. notice the wiggle in the curve for the semi-ellipsoidal heat source at $P_1 = 10$ and $P_2 = -10$. Such a wiggle can not be physical. Here it is an artefact resulting from the use of (3.29) (t becomes infinite for this situation). By choosing a more gradual transition between the asymptotic solutions one can easily avoid this wiggle. However, this generally results in a decreased overall accuracy of the curvefit.

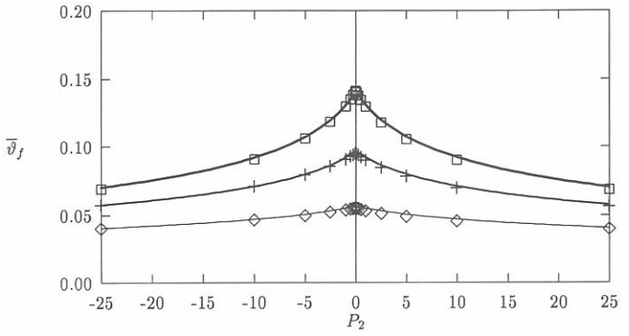

Figure 3.8: Maximum temperature, uniform heat source. Markers denote numerically calculated values. The lines represent the curvefit function. $\diamond$: $P_1 = 50$; $+$: $P_1 = 10$; $\square$: $P_1 = 1$, $\lambda = 1$

3.5 Example

In the previous chapter (par. 2.4) the maximum contact temperature of a zirconia ball with a diameter of 10.0 mm, sliding against a steel plate has been calculated as a function of the sliding velocity. As the conductivity of steel is about 20 times higher than the conductivity of zirconia, the heat flowing into the zirconia ball was neglected. Now, with the formulas derived in this chapter, this heat flow can be taken into account.

Consider the same situation as in chapter 2. If the zirconia ball is purely sliding against the steel plate then the Péclet number for the ball is zero. From equations (3.30) and (3.31) one obtains $t = 0$ and therefore by using eq. (3.29), $\theta_h = \theta_r$. If the steel plate is denoted as body 1 and the zirconia ball as body 2 then θ_1 and θ_2 can be calculated by using equation (3.28):

$$\begin{aligned} \theta_1 &= \left[\{\theta_l^{em}\}^{-2} + \left\{ \theta_r^{em} / \sqrt{\frac{aU}{\kappa_{steel}}} \right\}^{-2} \right]^{-\frac{1}{2}} \\ \theta_2 &= \theta_l^{em} \end{aligned}$$

Substitution of θ_1 and θ_2 in equation (3.27) results in the following expression for the maximum local temperature rise as a function of the sliding velocity:

$$\vartheta_f(U) = \frac{\mu F_n U}{\sqrt{ab}} \frac{1}{\frac{K_{steel}}{\theta_1} + \frac{K_{zirconia}}{\theta_2}}$$

This expression is shown in figure 3.9 together with the relation derived in the previous chapter. As is clearly indicated by the figure, the assumption made in the

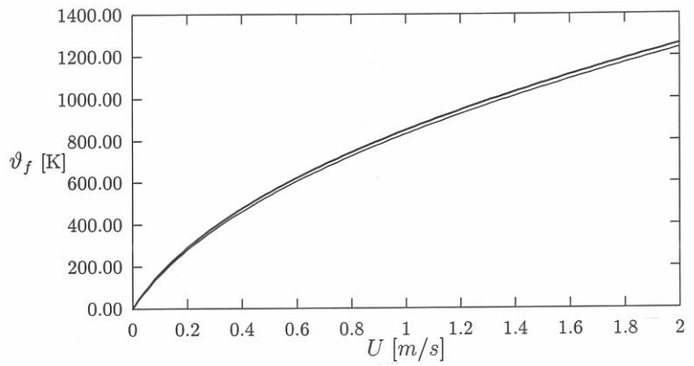

Figure 3.9: Maximum contact temperature rise in the contact between a zirconia ball and a steel plate. Conditions as in figure 2.7. The thin line is the full approximation. The thick line shows the result when the heat, flowing into the zirconia ball, is neglected.

previous chapter, i.e. that the heat flowing into the zirconia ball can be neglected, is justified.

3.6 Conclusion

A numerical algorithm has been developed for the heat partition problem. It matches the temperatures in all points in the contact and thus allows for a variable partition of heat in the contact. Furthermore a closed-form function fit (3.27) has been derived, based on numerical calculations and asymptotic solutions for large and small Péclet numbers, as well as an asymptotic solution for opposing velocities, see the equations (3.21), (3.23) and (3.25). This function fit approximates the flash temperature for an arbitrarily chosen Péclet number combination with an error less than 5%. Both uniform and semi-ellipsoidal heat sources are covered. This implies that Archard's rule of thumb also holds for opposing velocities.

Finally, it was found that for semi-ellipsoidal heat sources the maximum local temperature rise is substantially higher if the surfaces of the bodies move in opposite directions, compared to the case of velocities in the same direction.

Note that the results of this chapter apply only to situations where both bodies

have the same bulk temperature. If the bodies have different bulk temperatures an additional heat flux due to the bulk temperature difference will occur, which in turn influences the contact temperature. This topic will be addressed in the next chapter.

References

Allen, D.N. de G., 1962, " A suggested approach to finite-difference representation of differential equations, with an application to determine temperature-distribution near a sliding contact", *Quart. J. Mech. and Applied Math.*, Vol. 15, pp. 11-33.

Archard, J.F., 1959, "The temperature of rubbing surfaces", *Wear*, Vol. 2, pp. 438-455.

Blok, H., 1937, "The surface temperatures under extreme pressure lubricating conditions", *Contributions by the Delft laboratory of the Royal Dutch/Shell to the 2nd World Petroleum Congress*, Paris 1937, the Hague 1939, pp. 151-182.

Bos, J., and Moes, H., 1994, "Frictional heating of elliptic contacts," *Dissipative processes in tribology*, Proc. 20th Leeds-Lyon Symposium on Tribology, Elsevier, Amsterdam, pp. 491-500.

Bos, J., and Moes, H., 1995, "Frictional heating of tribological contacts," *ASME J. of Tribology*, Vol. 117, pp. 171-177

Brandt, A., 1984, "Multigrid Techniques: 1984 Guide with applications to fluid dynamics," available as G.M.D.-studien No. 85, from G.M.D.-F1T, Postfach 1240, D-5205, St. Augustin1, Germany.

Cameron, A., Gordon, A.N., and Symm, G.T., 1965, "Contact temperatures in sliding/rolling surfaces", *Proc. Roy. Soc. A*, Vol. 286, pp. 45-61.

Greenwood, J.A., 1995, "Flash temperatures for bodies moving at equal, high, speeds in opposite direction.", *submitted to ASME J. of Tribology*

Jaeger, J.C., 1943, "Moving sources of heat", *J. and Proc. Roy. Soc. N.S.W.*, Vol. 76, pp. 203-224.

Lubrecht, A.A., ten Napel, W.E. and Bosma, R., 1986, "Multigrid, an alternative method for calculating film thickness and pressure profiles in elastohydrodynamically lubricated line contacts",*ASME J. of Tribology.*, Vol. 108, 551-556.

Lubrecht, A.A. and Ioannides, E., 1989, "A fast solution of the dry contact problem and the associated sub-surface stress field", using multilevel techniques, *ASME J. of Tribology*, Vol. 113, pp. 128-133.

Tian, X. and Kennedy, F.E., 1993, "Maximum and Average Flash Temperatures in Sliding Contacts", *J. of Tribology*, to appear.

Venner, C.H. and Lubrecht, A.A., 1993, "Multilevel solvers for Integro and integro-differential problems in contact mechanics and lubrication", *Proceedings 4th European Multigrid Conference*, Amsterdam, The Netherlands, pp. 111-127, Editors Hemker, P.W. and Wesseling, P., published by Birkhauer Verlag.

Winter, A. de, 1967, "De berekening van de flitstemperatuurverdelingen in en aan weerszijden van een bandvormig contactvlak (tevens warmtebron) tussen twee over elkaar glijdende loopvlakken", Masters Thesis (in Dutch), Technical University of Delft.

Chapter 4

Bulk Temperature Differences

In chapters 2 and 3 the local temperature rise in the contact has been considered, i.e. the temperature due to the small scale heat flow restriction. By assuming the bodies to be semi-infinite, large scale heat flow restrictions were neglected; by definition the materials of the semi-infinite bodies act as infinite heat sinks of negligible resistance. In practice, however, the bodies in contact will be finite and instead of an infinite heat sink there will be a cooling mechanism, e.g. a cooling fluid. In the steady state situation the bodies will have a bulk temperature such that heat is transferred from the contact to the cooling medium. In general the relation between the bulk temperature and the rate of heat flow transferred to the environment of the solid will be known or may be found from independent experiments on the solids. Such a relation will depend on the geometry of the body and the cooling mechanism (air, water, forced or free convection).

The bulk temperatures are not necessarily the same for both bodies in contact. If they are, the contact temperature is simply the superposition of the local contact temperature rise and the bulk temperature. In all other cases, the temperature distribution in the contact is affected by the bulk temperature difference. The maximum temperature, as well as its location in the contact, will change. As an example, consider the situation in which one of the bodies is insulated. All the heat generated in the contact will flow into the other body. This however, does not imply that locally the heat flux through the contact surface of the insulated body is zero, only the net heat flow entering the insulated body must be zero.

If the contact is small compared to the size of the bodies, the effect of bulk temperature differences can be modelled by two semi-inifinite bodies in contact with different bulk temperatures. The effect of a bulk temperature difference can be separated from the conditions at the contact interface by considering two semi-infinite bodies in contact with a bulk temperature difference but without heat supply in the contact. Due to the bulk temperature difference heat will flow from the body with the highest bulk temperature through the contact to the other body. If this heat flow is superimposed on the heat flows following from the partition

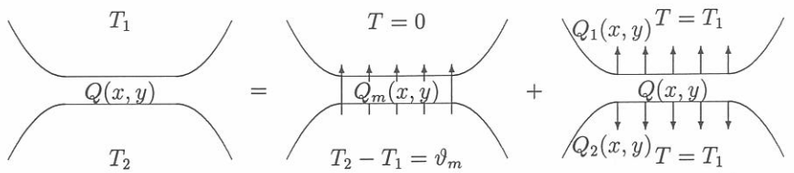

Figure 4.1: General problem as superposition of two simpler problems

problem, the heat flows for each body are found and the contact temperature can be calculated. See figure 4.1

4.1 Equations

The rate of heat flow between two bodies in contact with different bulk temperatures depends on the difference in bulk temperature, not on their absolute values. Therefore the rate of heat flow can be examined by considering a body (body 1) with zero bulk temperature in contact with a body (body 2) of positive bulk or mass temperature, ϑ_m. To distinguish the temperature rise in the contact from the bulk temperature difference, the subscribt b is used for the temperature rise in the contact and the subscript m for the bulk temperature difference (= mass temperature difference).
For the situation described above, the surface temperatures of the two bodies are given by (*Carslaw and Jaeger*, 1959):

$$\vartheta(x,y)_1 = \frac{1}{2\pi K_1}\int_{S_q} Q_m(x',y')\frac{\exp(-U_1(R-(x-x'))/2\kappa_1)}{R}\,dx'\,dy' \qquad (4.1)$$

$$\vartheta(x,y)_2 = \vartheta_m - \frac{1}{2\pi K_2}\int_{S_q} Q_m(x',y')\frac{\exp(-U_2(R-(x-x'))/2\kappa_2)}{R}\,dx'\,dy' \qquad (4.2)$$

where Q_m is the unknown rate of heat flow due to the bulk temperature difference. This rate of heat flow acts as a heat source for solid 1 and as a heat sink for solid 2.

If temperature drops across layers like oxides or reaction products are neglected, the temperatures in the contact must be equal and Q_m can be found from:

$$\frac{1}{2\pi K_1}\int_{S_q} Q_m(x',y')\frac{\exp(-U_1(R-(x-x'))/2\kappa_1)}{R}\,dx'\,dy' =$$
$$\vartheta_m - \frac{1}{2\pi K_2}\int_{S_q} Q_m(x',y')\frac{\exp(-U_2(R-(x-x'))/2\kappa_2)}{R}\,dx'\,dy' \qquad (4.3)$$

In dimensionless form this equation reads:

$$\frac{1}{2\pi}\frac{1}{\sqrt{\phi}}\int_{S_q}\overline{Q}_m(\overline{x}',\overline{y}')\frac{\exp\left(-\frac{P_1}{2}\{R-(\overline{x}-\overline{x}')\}\right)}{R}d\overline{x}'\,d\overline{y}' \quad +$$
$$\frac{1}{2\pi}\frac{1}{\sqrt{\phi}}\int_{S_q}\overline{Q}_m(\overline{x}',\overline{y}')\frac{\frac{1}{\lambda}\exp\left(-\frac{P_2}{2}\{R-(\overline{x}-\overline{x}')\}\right)}{R}d\overline{x}'\,d\overline{y}' = \overline{\vartheta}_m \qquad (4.4)$$

where (see chapter 2)

$$\overline{\vartheta} \equiv \vartheta\frac{K_1\sqrt{ab}}{F},\quad \overline{Q} \equiv Q\frac{ab}{F} \qquad (4.5)$$

$$\overline{x} \equiv \frac{x}{a} \text{ and } \overline{y} \equiv \frac{y}{a} \qquad (4.6)$$

For a given $\overline{\vartheta}_m$, $\overline{Q}_m$ can be found by solving equation (4.4) for $\overline{Q}_m$. The contact temperature can then be found by applying equation (4.1), which in dimensionless form reads:

$$\overline{\vartheta}(\overline{x},\overline{y})_1 = \frac{1}{2\pi}\frac{1}{\sqrt{\phi}}\int_{S_q}\frac{\overline{Q}_m(\overline{x}',\overline{y}')\exp\left(-\frac{1}{2}P_1\{R-(\overline{x}-\overline{x}')\}\right)}{R}d\overline{x}'\,d\overline{y}' \qquad (4.7)$$

From a numerical point of view equation (4.4) is similar to equation (3.7). Therefore the numerical algorithm, derived in the previous chapter can be used here as well.

4.2 Function Fits

4.2.1 Asymptotic solutions

Like in the preceding chapters, first a set of asymptotic solutions will be derived to use them as the building blocks of a general function fit.

Velocities in the same direction

Analogous to equation (3.20), for high speeds the relation between the bulk temperature difference and the surface temperature in the interface can be written as:

$$\vartheta(x,y) = \vartheta_m - \frac{1}{\sqrt{\pi}}\frac{1}{\sqrt{K_2\rho_2c_2U_2}}\int_{-x_s(y)}^{min(x,x_s(y))}\frac{Q_m(\xi,y)d\xi}{\sqrt{x-\xi}}; \qquad (4.8)$$

with $Q_m(x,y)$ the rate of heat flow from body 2 into body 1 and $x_s = a\sqrt{1-\left(\frac{y}{b}\right)^2}$, see chapter 2. At the interface this heat flow represents a source for body 1 and a sink for body 2. If both velocities U_1 and U_2 are in the same direction one obtains the following equation for the surface temperature in the interface for body 1:

$$\vartheta(x,y) = \frac{1}{\sqrt{\pi}}\frac{1}{\sqrt{K_1\rho_1c_1U_1}}\int_{-x_s(y)}^{min(x,x_s(y))}\frac{Q_m(\xi,y)d\xi}{\sqrt{x-\xi}}. \qquad (4.9)$$

From (4.8) it follows

$$\frac{1}{\sqrt{\pi}} \sum \left(\frac{1}{\sqrt{K \rho c U}} \right) \int_{-x_s(y)}^{min(x, x_s(y))} \frac{Q_m(\xi, y) d\xi}{\sqrt{x - \xi}} = \vartheta_m, \tag{4.10}$$

where $\sum \left(\frac{1}{\sqrt{K \rho c U}} \right) = \frac{1}{\sqrt{K_1 \rho_1 c_1 U_1}} + \frac{1}{\sqrt{K_2 \rho_2 c_2 U_2}}$.
According to *Abel* (1823) this equation can be inverted as

$$Q_m(x, y) = \frac{1}{\sqrt{\pi}} \frac{\vartheta_m}{\sum \left(\frac{1}{\sqrt{K \rho c U}} \right)} \frac{d}{dx} \left(\int_{-x_s(y)}^{min(x, x_s(y))} \frac{d\xi}{\sqrt{x - \xi}} \right).$$

This leads to the following closed form analytical solution for the additional rate of heat flow distribution over the interface:

$$Q_m(x, y) = \frac{1}{\sqrt{\pi}} \frac{\vartheta_m}{\sum \left(\frac{1}{\sqrt{K \rho c U}} \right)} \{x + x_s(y)\}^{-1/2}. \tag{4.11}$$

Finally, by integrating Q_m over the elliptic interface, a relation is obtained between the bulk temperature difference and the total rate of heat flow, F_m, that it induces;

$$\vartheta_m = \psi_r \frac{F_m}{b \sqrt{a}} \sum \left(\frac{1}{\sqrt{K \rho c U}} \right). \tag{4.12}$$

Where ψ_r is derived as (see *Elshof*, 1994):

$$\psi_r \equiv \frac{3}{4\pi} \Gamma^2 (3/4) = 0.358491 \cdots.$$

According to this equation and the equations (4.9), (4.10) and (4.11) the temperature at the interface due to the bulk temperature difference, ϑ_m, reads:

$$\vartheta_b = \frac{\sqrt{K_2 \rho_2 c_2 U_2}}{\sum \sqrt{K \rho c U}} \vartheta_m. \tag{4.13}$$

The temperature rise over the interface is uniform, therefore this solution can simply be added to the local temperature rise, as discussed in the previous chapter. Consequently the maximum contact temperature for two bodies moving in the same direction with high Péclet numbers follows from $\vartheta_b + \vartheta_f$.

Velocities in opposite directions

The temperature distribution for $K_1 \rho_1 c_1 U_1 = K_2 \rho_2 c_1 U_2 = K \rho c U$ with U_1 and U_2 in opposite directions, *e.g.* for two identical bodies moving at equal high speeds

in opposite directions is defined by the following integral equation for the rate of heat flow distribution:

$$\frac{1}{\sqrt{\pi}} \frac{1}{\sqrt{K \rho c U}} \int_{-x_s(y)}^{x_s(y)} \frac{Q_m(\xi, y) d\xi}{\sqrt{|\xi - x|}} = \vartheta_m, \tag{4.14}$$

with a constant value for ϑ_m. Since according to *Hijmans* (1992), see appendix B:

$$\int_{-1}^{1} \frac{|\xi - x|^{2r-1}}{(1 - \xi^2)^r} d\xi = \frac{\pi}{\sin(\pi r)} \qquad (-1 \le x \le 1\ ,\ 0 < r < 1) \tag{4.15}$$

which reduces to

$$\int_{-1}^{1} \frac{(1 - \xi^2)^{-\frac{1}{4}}}{\sqrt{|\xi - x|}} = \pi \sqrt{2} \qquad (-1 \le x \le 1\ ,\ 0 < r < 1)$$

for $r = \frac{1}{4}$, this equation can be solved by recognising

$$Q_m = (1 - \xi^2)^{-\frac{1}{4}}$$

as:

$$Q_m(x, y) = \frac{1}{\sqrt{2\pi}} \vartheta_m \sqrt{K \rho c U} \left[\{x_s(y)\}^2 - \{x\}^2 \right]^{-1/4}. \tag{4.16}$$

This solution for the heat flux leads to a temperature distribution over the interface, $\vartheta(x, y)$, which, in contrast to the situation where two bodies move in the same direction is far from uniform. However, in the center of the contact, because of symmetry conditions, $\vartheta_b = \frac{1}{2} \vartheta_m$. Figure 4.2 shows the dimensionless temperature distribution for the line $y = 0$.

Integration of equation (4.16) over the elliptic contact leads to the following relation for the bulk temperature difference and the total rate of heat flow it induces:

$$\vartheta_m = \psi_s \frac{F_m}{b \sqrt{a}} \sum \left(\frac{1}{\sqrt{K \rho c U}} \right). \tag{4.17}$$

Where ψ_s is given by (see *Elshof*, 1994):

$$\psi_s \equiv \frac{3}{4\sqrt{2\pi}} = 0.299206 \cdots$$

The highly non-uniform distribution of the temperature at the interface complicates the estimation of the actual maximum contact temperature, i.e. the sum of the local temperature rise derived in the previous chapter and the temperature rise at the interface due to a bulk temperature difference. If the bulk temperature difference is small compared to the maximum local temperature rise, the actual maximum contact temperature can be approximated by $\vartheta_f + \frac{1}{2} \vartheta_m$ since for this

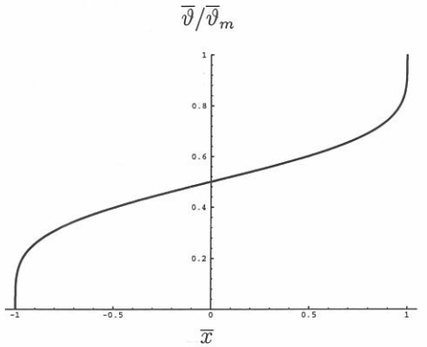

Figure 4.2: Temperature distribution at the line of symmetry for two equal bodies with equal high Péclet numbers, moving in opposite directions

situation the maximum local temperature rise occurs in the center of the contact. However, if the total rate of heat flow due to the bulk temperature difference exceeds the heat generated in the contact, only the average contact temperature can be approximated accurately. For more details on this subject one is referred to chapter 5.

Two bodies at rest

The asymptotic solution for low velocities is the solution for two bodies at rest. To this situation *Holm*'s (1958) analogous solution for electrical resistances can be applied

$$\vartheta_m = \psi_l \mathbf{S}(\phi) \frac{F_m}{\sqrt{ab}} \sum (1/K)\,; \tag{4.18}$$

with $\psi_l \equiv \frac{1}{4}$. The corresponding uniform temperature over the interface is:

$$\vartheta_b = \frac{K_2}{\sum K} \vartheta_m. \tag{4.19}$$

To obtain the actual maximum interface temperature this solution can simply be superimposed on the analytical curve fit for the flash temperature introduced in chapter 3. Thus the actual maximum contact temperature is $\vartheta_b + \vartheta_f$.

4.2.2 General solution

Equation (4.4) has been solved numerically with the algorithm described in chapter 3. Based on such numerical solutions and the asymptotic solutions of equations (4.12), (4.17) and (4.18) for arbitrary Péclet numbers, the following relation between the bulk temperature difference and the resulting rate of heat flow is proposed:

$$\boxed{\bar{\vartheta}_m \equiv \vartheta_m \frac{K_1\sqrt{ab}}{F} \approx \frac{F_m}{F}(\psi_1 + \psi_2/\lambda),} \tag{4.20}$$

with

$$\boxed{\psi_i = \left[\{\psi_l \mathbf{S}(\phi)\}^s + \left\{\psi_h/\sqrt{\phi P_i}\right\}^s\right]^{1/s}.} \tag{4.21}$$

Here $s = 0.5 \cdot \exp(1-\phi) - 2.5$. In this equation the auxiliary bulk temperature number ψ_h represents the bulk temperature number for high velocities. It takes into account the rolling or sliding conditions depending on the direction and the value of the velocities of the bodies relative to the contact. Since ψ_s is substantially smaller than ψ_r, an expression similar to equation (3.29) will apply for ψ_h,

$$\psi_h = \frac{\psi_r + t\psi_s}{1+t}. \tag{4.22}$$

Where

$$t = \frac{1-q}{1+q} \quad \textit{with} \quad q = \operatorname{sign}(U_1 U_2) \min\left(p, \frac{1}{p}\right), \tag{4.23}$$

and

$$p \equiv \sqrt{\frac{P_2}{P_1}}. \tag{4.24}$$

Please note that the expression for the parameter t differs from the expression for t as obtained for the partition problem. For a survey of the bulk temperature numbers see table 4.1.

Although the total rate of heat flow due to a bulk temperature difference is approximated well by equation (4.20), see section 4.2.3, the calculation of the corresponding temperature rise over the interface, ϑ_b, leads to complications. Actually ϑ_b varies over the interface. As a consequence only the average temperature rise in the contact, due to the bulk temperature difference can be predicted. From equations (4.13), (4.19) and (4.21) it follows that the average temperature rise over the interface due to the bulk temperature difference ϑ_m can be approximated by:

$$\boxed{\bar{\vartheta}_b \approx \frac{\psi_1}{\psi_2/\lambda + \psi_1} \bar{\vartheta}_m.} \tag{4.25}$$

	ψ
ψ_l	$\frac{1}{4} = 0.25$
ψ_r	$\frac{3}{4\pi}\Gamma^2(3/4) = 0.358491\cdots$
ψ_s	$\frac{3}{4\sqrt{2\pi}} = 0.299206\cdots$

Table 4.1: *Survey of the bulk temperature numbers.*

The relation is exact for two bodies at rest and for two bodies with high Péclet numbers and velocities in the same direction. For arbitrary Péclet number combinations this formula represents an accurate approximate rule, see section 4.2.3.

As stated earlier, the contact temperature is the sum of the local temperature rise, i.e. the temperature rise due to the small scale heat flow restriction, and the bulk temperature rise, i.e. the temperature rise due to the large scale heat flow restriction. For the approximation of the maximum contact temperature a problem arises in case of two bodies moving in opposite directions; the location of the maximum local temperature rise does not coincide with the location of the maximum bulk temperature rise. However, since the maximum local temperature generally occurs at or near the center of the interface area, a fair approximation for the maximum interface temperature may be obtained by superimposing the flash temperature according to the equation (3.27) on the average bulk temperature over the interface according to the equation (4.25), *i.e.* $\vartheta_b + \vartheta_f$

$$\boxed{\bar{\vartheta}_b + \bar{\vartheta}_f \approx \frac{\psi_1}{\psi_2/\lambda + \psi_1}\bar{\vartheta}_m + \frac{1}{1/\theta_1 + \lambda/\theta_2}.} \tag{4.26}$$

However, to predict the actual maximum rise of the interface temperature for opposed velocities will invariably be somewhat more complicated.

4.2.3 Comparison with numerical results

Figure 4.3 shows numerically calculated and function fit values for the bulk temperature difference which causes a rate of heat flow $F_m = F$. The figure shows the bulk temperature difference for three distinct Péclet numbers of one body and a range of Péclet numbers of the second body, i.e. $P_1 = 1$, $P_1 = 10$ and $P_1 = 25$ and P_2 varies from -25 to 25.

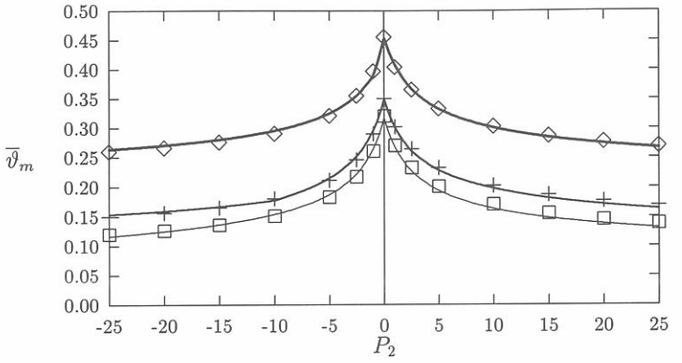

Figure 4.3: Dimensionless bulk temperature difference for $F = F_m$ and a circular contact. Markers denote numerically calculated values. The lines represent the curvefit function. $\diamond$: $P_1 = 1$; $+$: $P_1 = 10$; $\square$: $P_1 = 25$, $\lambda = 1$

As can be seen from this figure, the values obtained from the curvefit agree very well with the results numerically obtained. The error is always less than 5%.

Figure 4.4 shows the average temperature rise over the contact due to a dimensionless bulk temperature difference of 1, ($\overline{\vartheta}_m = 1$) for the same cases. The numerically calculated values are compared with the values, obtained from relation (4.25). From this figure it is clear that the average temperature rise in the contact due to the bulk temperature difference is well approximated by equation (4.25). In fact, the error is always less than 5%.

4.3 Example

To illustrate the practical value of the results presented in this chapter, consider the following example, the calculation of the rate of heat flow through the contact of two bodies in rolling contact with different bulk temperatures. The quasi steady state is considered, i.e. the bulk temperatures of the bodies are not affected by the heat transfer. Furthermore, heat generation in the contact, e.g. due to elastic hysteresis, is neglected.

Consider a steel ball with a diameter of 10.0 *mm* in rolling contact with a steel plate. If a normal force of 100 *N* is applied, according to the Hertzian theory the radius of the contact circle is 0.147 *mm* (a Young's modulus of 213 *GPa* and a

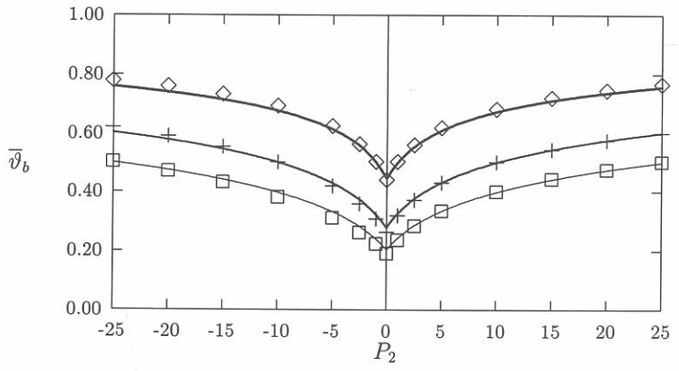

Figure 4.4: Average dimensionless contact temperature rise, due to a dimensionless bulk temperature difference of 1. Markers denote numerically calculated values. The lines represent the curvefit function. $\diamond$: $P_1 = 1$; $+$: $P_1 = 10$; $\square$: $P_1 = 25$, $\lambda = 1$

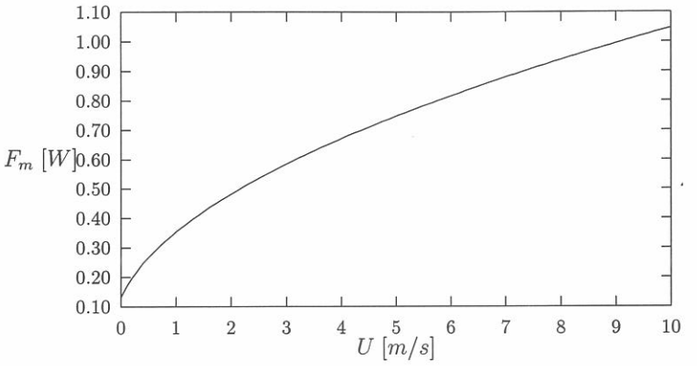

Figure 4.5: Rate of heat flow as function of the rolling speed, for a steel ball in contact with a steel plate. The bulk temperature difference is 10 degrees Kelvin.

Poisson's ratio of 0.3 are assumed).

Given the diffusivity, $\kappa_{steel} = 13\ 10^{-6}\ m^2/s$, the Péclet number of the bodies can now be expressed as a function of the rolling velocity, U:

$$P_1 = P_2 = \frac{aU}{\kappa_{steel}}$$

Since the Péclet numbers are the same for this situation, $\psi_1 = \psi_2$. With $\lambda = 1$ and $K_1 = K_{steel}$, equation (4.20) can be rewritten as:

$$F_m(P) = \vartheta_m \frac{K_{steel}\sqrt{ab}}{2\psi(P)}$$

For $\vartheta_m = 10$, this relation is presented graphically in figure 4.5 ($K_{steel} = 45\ W/mK$).

4.4 Conclusion

A formula has been derived (eq. 4.20) which enables accurate approximation of the rate of heat flow due to a difference in bulk temperature of two bodies in contact or vice versa. To apply this formula, the bulk temperature numbers of the two

bodies in contact must be known. They can be calculated by applying equation (4.21).

The proposed relation is a function fit, based on asymptotic solutions for low and high Péclet numbers and numerical solutions. The asymptotic solution for high Péclet numbers is again a function fit based on two asymptotic cases; two bodies in contact moving in the same and in opposite directions, see equation (4.22). The asymptotic bulk temperature numbers are listed in table 4.1.

Given the bulk temperature numbers of the two bodies in contact, the average temperature rise can be approximated by using equation (4.25).

Finally the maximum contact temperature for two bodies in contact, which have different bulk temperatures and where heat is generated in the interface, can be approximated by using equation (4.26), which is the combined result of the present and the previous chapter.

References

Abel, N.H., 1823, "Solutions de quelques problèmes à l'aide d'intégrales définies," *Oeuvres*, I **11**, 97.

Carslaw, H.S., and Jaeger, J.C., 1959, "Conduction of Heat in Solids", Oxford University Press, Oxford, UK.

Elshof, H.L.J., 1994, "Heat fluxes between semi-infinite solids", MSc. Thesis, Dept. of Mech. Eng., University of Twente, Enschede.

Hijmans, J.P.A.M., 1992, *private communications*, SKF-ERC Nieuwegein.

Holm, 1958, Electric contacts handbook, Berlin/New York.

Chapter 5

Thermal Networks

The frictional heat generated in e.g. brakes, bearings and seals, is transfered to the environment through machine parts and contacts between machine parts. This will lead to different temperature levels in the machine, depending on how well the heat is conveyed by the machine parts. A complete analysis of the heat fluxes and temperature levels in machines, i.e. solving the energy equation for the whole machine, is often very complicated, e.g. due to complicated geometries of machine parts.

However, since machines often contain a lot of standard components like shafts of which the thermal response has been determined for all kinds of thermal inputs and cooling conditions, these parts can be described as thermal resistances (stationary situation) or capacitances (non-stationary situation). By describing the machine as a thermal network, i.e. a combination of thermal resistances, capacitances and heat sources, the analysis can be simplified (see *van Heijningen*, 1986), since solving the thermal network requires a much smaller numerical effort than, e.g., the numerical simulation of the energy equation for the whole machine.

To describe a machine as a thermal network requires a characterization of the thermal behaviour of each part, e.g. based on measurements or numerical analysis. For example, the curve fit formulas derived in the preceding chapters, summarize the results of such numerical simulations in such a way that concentrated contacts can be incorporated in a thermal network as resistances. These formulas are improvements upon work conducted by *Blok* (1969), *Barber* (1970) and *Francis* (1971) who took the first steps in describing a concentrated tribological contact as a thermal resistance.

5.1 Insulated Body

Modelling the environment of a tribological contact requires knowledge of the geometry of the bodies in contact and of the heat loss characteristics of the contacting bodies. Determining the heat loss characteristics of bodies is a problem by itself

and is not the aim of this work. However without detailed knowledge of the bodies in contact, two extreme situations can be studied: perfectly cooled bodies and perfectly insulated bodies. In chapter 3 the situation of two perfectly cooled bodies has been studied. Now the situation of an insulated body in contact with a perfectly cooled body will be addressed.

In the thermal steady state, the temperature of the insulated solid will have risen to such extent that the net heat flux entering this body is zero. Since the other body is perfectly cooled, its bulk temperature will remain equal to the environmental temperature. By using the curve fit formulas derived in chapters 3 and 4, the bulk temperature of the insulated body can be calculated as well as the maximum and average contact temperature.

The rate of heat flow entering the insulated body (say body 2) is given by equation (3.32).

$$F_2 \approx \frac{\lambda/\theta_2}{1/\theta_1 + \lambda/\theta_2} F.$$

Now the zero net heat flux for the insulated body requires a bulk temperature difference between body 2 and body 1, such that it induces exactly this heat flux, but in the opposite direction, i.e. if F_m denotes the heat flux asociated with the bulk temperature difference then $F_m = F_2$. According to equation (4.20) this is accomplished by a bulk temperature, ϑ_m, of body 2 of

$$\vartheta_2 = \vartheta_m = \frac{F_2}{K_1\sqrt{ab}}(\psi_1 + \psi_2/\lambda)$$

or

$$\begin{aligned} \vartheta_2 &= \frac{\lambda/\theta_2}{1/\theta_1 + \lambda/\theta_2}(\psi_1 + \psi_2/\lambda)\frac{F}{K_1\sqrt{ab}} \\ &= \frac{\lambda\psi_1 + \psi_2}{\lambda\theta_1 + \theta_2}\theta_1\frac{F}{K_1\sqrt{ab}} \end{aligned} \tag{5.1}$$

The maximum contact temperature can be calculated from equation (4.26) which can be written as:

$$\vartheta_b + \vartheta_f \approx \frac{\psi_1}{\psi_2/\lambda + \psi_1}\vartheta_m + \frac{1}{1/\theta_1 + \lambda/\theta_2}\frac{F}{K_1\sqrt{ab}}$$

Substitution of (5.1) for ϑ_m gives

$$\begin{aligned} \vartheta_b + \vartheta_f &\approx \left(\frac{\psi_1}{\psi_2/\lambda + \psi_1}\frac{\lambda\psi_1 + \psi_2}{\lambda\theta_1 + \theta_2}\theta_1 + \frac{1}{1/\theta_1 + \lambda/\theta_2}\right)\frac{F}{K_1\sqrt{ab}} \\ &= \frac{\lambda\psi_1 + \theta_2}{\lambda\theta_1 + \theta_2}\theta_1\frac{F}{K_1\sqrt{ab}}. \end{aligned} \tag{5.2}$$

Comparing the expression for the bulk temperature (5.1) with the expression for the maximum contact temperature (5.2) shows that the maximum contact temperature is higher than the bulk temperature of the insulated body, since θ, the flash temperature number, is always larger than ψ, the mass temperature number.

5.2 Verification of Maximum Contact Temperature

In chapter 4 it was shown that the temperature rise in the contact due to a bulk temperature difference is generally non-uniform. It will be clear that by taking the average bulk temperature rise and superimposing this to the maximum local temperature rise, the maximum contact temperature can be found with the restriction that the bulk temperature rise should be small compared to the local temperature rise. However, if the bulk temperature rise is of the same order of magnitude as the local temperature rise, as for a perfectly cooled body in contact with an insulated body, the result for the maximum contact temperature as obtained in equation (5.2), i.e. the superposition of the two temperature rises, is questionable. Therefore, this result will be verified by examining the worst case, i.e. a perfectly cooled body in contact with a perfectly insulated body, moving at high speeds in opposite directions. This situation gives rise to the most un-uniform bulk temperature rise, see figure 4.2; the difference between the maximum and the average bulk temperature rise is the largest for this situation, and the maximum bulk temperature rise in the contact is of the same order of magnitude as the maximum local temperature rise.

For two equal bodies moving at high speeds in opposite directions, inserting $\theta_1 = \theta_2$, $\psi_1 = \psi_2$ and

$$\theta \rightsquigarrow \frac{\theta_s}{\sqrt{\phi P}} \quad \text{and} \quad \psi \rightsquigarrow \frac{\psi_s}{\sqrt{\phi P}},$$

see equations (3.28) and (4.21), in equation (5.1) yields:

$$\vartheta_m = \frac{\psi_s}{\sqrt{\phi P}}\frac{F}{K_1\sqrt{ab}} \tag{5.3}$$

or in dimensionless form:

$$\overline{\vartheta}_m\sqrt{\phi P} = \psi_s \tag{5.4}$$

Now that the bulk temperature difference has been determined, figure 4.2 can be used to determine the distribution of the bulk temperature rise, ϑ_b, at the line of symmetry in the contact.

The local temperature rise, ϑ_f, at the line of symmetry can be determined by solving numerically equation (3.22) for Q_1, for both a uniform and a semi-ellipsoidal heat supply. Subsequently Q_1 can be substituted in equation (3.20), which subsequently can be evaluated. This has been extensively described by *Bos and Moes*, (1995).

Figures 5.1 and 5.2 show the bulk, the local, as well as the actual temperature rise, for a uniform and a semi-ellipsoidal heat source, respectively. From these figures it is clear that the maximum actual temperature rise is only slightly higher

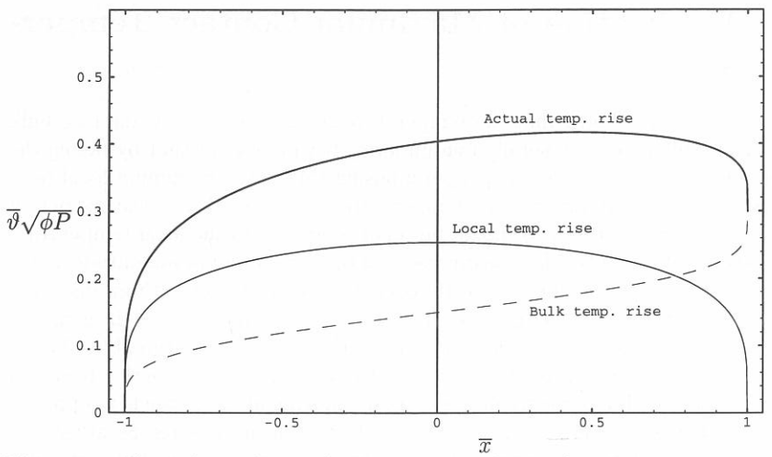

Figure 5.1: Centerline solution for local, bulk and actual contact temperature rise, uniform heat supply ($\lambda = 1$).

than the sum of the maximum local temperature rise and the average bulk temperature rise, i.e the actual temperature rise at $\overline{x} = 0$. For a uniform heat supply the difference is 3%, whilst for a semi-ellipsoidal heat supply the difference is even smaller, i.e. 1%. So, even for this extreme case, the formulas for the maximum contact temperature rise are quite accurate.

5.3 Analogy Heat versus Electricity

So far only one contact has been considered and application of the curve-fit functions was relatively easy. For more complex situations the implicitly stated analogy with electrical circuits can be exploited. The rate of heat flow, F, is the equivalent of the electrical current, the temperature is the equivalent of the potential, and the bodies are represented as resistances.

The electrical scheme for the division of heat generated in a contact is shown in figure 5.3. The electrical scheme for two bodies in contact with different bulk temperatures is shown in figure 5.4. Although both problems can be described well by electrical schemes, the two problems cannot be combined into one electrical scheme. The calculation of the heat flows and the temperatures proceeds in two steps. First for each contact, the heat flows entering the bodies in contact are calculated according to the scheme in figure 5.3. Once these heat flows are calculated they can be added to the scheme for the bulk temperature differences, shown in figure 5.4.

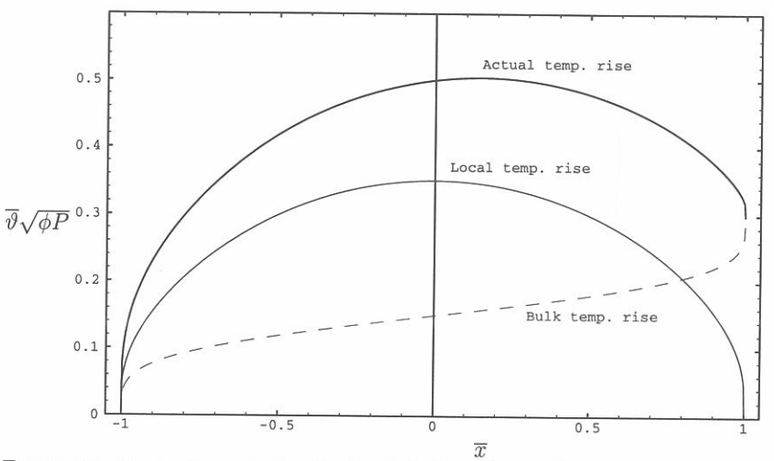

Figure 5.2: Centerline solution for local, bulk and actual contact temperature rise, semi-ellipsoidal heat supply ($\lambda = 1$).

5.4 Example: The Four Ball Tester

As an example the contact temperatures in a four ball tester, see figure 5.5, will be estimated. This apparatus is often used in Tribology to qualify lubricants in a qualitive manner. Todays lubricants often contain additives; chemical components whose activity strongly depends on the temperature. So, to get a more than qualitative insight in the characteristics of the lubricant, it is necessary to know the contact temperature. *Hsu and Klaus*, (1977) determined the contact temperature by analysing the wear debris. They used chemical reaction rate data to correlate dynamic wear tests (the four ball tester) and static, externally controlled temperature runs. The temperature, measured this way was 351 °C, much higher than

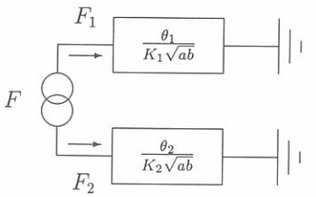

Figure 5.3: Electric scheme for the partition of the heat generated in the contact.

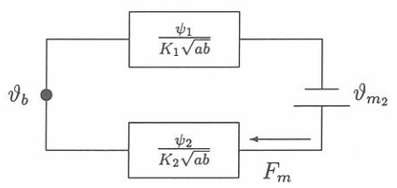

Figure 5.4: Electrical scheme for bulk temperature differences.

the Blok-Archard flash temperature relations predict (132 °C).

The Blok-Archard relations predict the local temperature rise, i.e. they assume the bodies in contact to be perfectly cooled. Naturally this leeds to lower temperatures compared to the situation where finite heat transfer coefficients are considered, as in a four ball tester. By taking into account the relation between the balls and the environment, one can expect to find higher and thus more realistic contact temperatures. Below a thermal network representing the four ball tester is introduced. Subsequently for the conditions for which Hsu and Klaus measured, the contact temperature is calculated to find out whether the difference between measured and predicted contact temperature can indeed be ascribed to the finite size of the bodies in contact.

5.4.1 Conditions of the experiment by Hsu and Klaus

Hsu and Klaus deduced a contact temperature of 351 $°C$, in a four ball tester running at 600 rpm, under a load of 400 N. The oil temperature was kept at 75 $°C$. The diameter of the measured wear scar varied during the first 100 minutes from 0.3 mm to 0.9 mm, whereas in the second 100 minutes it varied from 0.9 mm to 0.995 mm. Furthermore they report a calculated contact temperature of 132 $°C$ obtained from the Blok-Archard relations for this situation. Unfortunately, Hsu and Klaus did not report the coefficient of friction during the experiments, so the coefficient of friction has to be guessed. However, since they report substantial wear (the width of the wear scar much exceeded the width of the Hertzian contact circle; 0.3 mm) indicating incipient scuffing, a value of 0.3 seems reasonable; see *Begelinger et. al.*, (1976). Figure 5.5 shows a schematic drawing of the four ball tester. The ball at the top of the tetrahedron is rotating whilst the others are locked.

P is the load applied, i.e. 400 N. From the geometry of the equilateral tetrahedron it follows that $P_1 = P/\sqrt{6} = 163N$, $P_2 = P/3 = 133N$ and $P_3 \approx P_1 \sin 35° =$

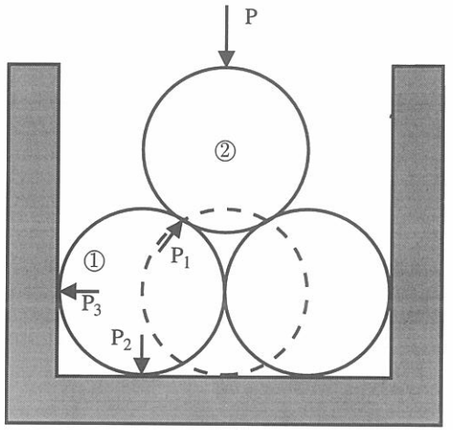

Figure 5.5: Schematic drawing four ball tester

$94N$. Because the contacts between the top ball and the 3 underlying balls are identical, we can restrict ourselves to the analysis of one of these contacts and the contact between one of these balls with the environment. The dimensions of the contacts can be calculated using Hertzian theory; the size of contact 1, however, is given by the diameter of the wear scar. It is taken as the average of the second run, i.e. a diameter of 0.948 mm. The diameters of contacts 2 and 3 have been calculated as 0.352 mm and 0.314 mm respectively.

5.4.2 Local temperature rise

The reported value of 132 $°C$ given by Hsu and Klaus for the calculated contact temperature, can be used to verify the assumption of 0.3 for the coefficient of friction. Since the Blok-Archard relations describe the local temperature rise, using the curve-fit functions from chapter 3 should result in about the same contact temperature.

First the rate of heat flow, F, generated in the contact is calculated. For the four ball tester a rpm of 600 corresponds to a linear velocity of 0.23 m/s. So the rate of heat generated in contact 1 is

$$F = \mu P_1 U = 0.3 \cdot 163 \cdot 0.23 = 11.25\ W$$

The Péclet numbers for contacts 2 and 3 are zero as well as the Péclet number of

the stationary ball in contact 1. The Péclet number of rotating ball is

$$P = \frac{0.5 \cdot D_{contact_1} U}{\kappa_{steel}} = \frac{0.5 \cdot 0.948 \cdot 10^{-3} \cdot 2.29}{13 \cdot 10^{-6}} = 84$$

Figure 5.3 can be used to calculate the maximum contact temperature and the heat fluxes going into the stationary and rotating ball. If the stationary ball is denoted by 1 and the rotating one by 2 then

$$\begin{aligned} F_1 &= \frac{\frac{\theta_2}{K_{steel}\sqrt{a_1 b_1}}}{\frac{\theta_1}{K_{steel}\sqrt{a_1 b_1}} + \frac{\theta_2}{K_{steel}\sqrt{a_1 b_1}}} F = 3.63\ W \\ F_2 &= F - F_1 = 7.62\ W \end{aligned}$$

For the values of the flash temperature numbers θ, see equation (3.28) (a semi ellipsoidal heat supply has been assumed). The maximum local temperature rise follows from:

$$\vartheta_f = \frac{\theta_1}{K_{steel}\sqrt{a_1 b_1}} F_1 = 64\ ^\circ C$$

Adding this local temperature rise to the oil temperature leads to a contact temperature of 139 $^\circ C$, which is very close to the 132 $^\circ C$ calculated by Hsu and Klaus for the same situation. So it can be concluded that the assumption 0.3 for the coefficient of friction is valid.

5.4.3 Network for the four ball tester

Taking the local temperature rise as the contact temperature, assumes the bodies to be perfectly cooled. Another extreme case is taking the bodies to be perfectly insulated, i.e. the heat flow generated in the contact between the rotating ball and the stationary ball is transfered to the environment through the contacts only. Figure 5.6 shows how the thermal resistances are connected. This figure can be used to calculate the bulk temperatures of body 1, $\vartheta_{m,1}$, and 2, $\vartheta_{m,2}$, and the bulk temperature rise of contact 1, $\vartheta_{b,1}$. The values of the resistances are given by:

$$\begin{aligned} R_1 &= \frac{\psi_{1,2}}{K_{steel}\sqrt{a_1 b_1}} = 4.8\ ^\circ C/W \\ R_2 &= \frac{\psi_{1,1}}{K_{steel}\sqrt{a_1 b_1}} = 11.7\ ^\circ C/W \\ R_3 &= R_4 = \frac{\psi_l}{K_{steel}\sqrt{a_2 b_2}} = 31.6\ ^\circ C/W \\ R_5 &= R_6 = \frac{\psi_l}{K_{steel}\sqrt{a_3 b_3}} = 35.4\ ^\circ C/W \end{aligned}$$

R_1 and R_2 form the contact resistance of contact 1 for the heat flow due to bulk temperature differences, R_3 and R_4 that of contact 2 and R_5 and R_6 that of contact 3. $\vartheta_{m,1}$ and $\vartheta_{m,2}$ are the bulk temperatures for body 1 and 2 respectively.

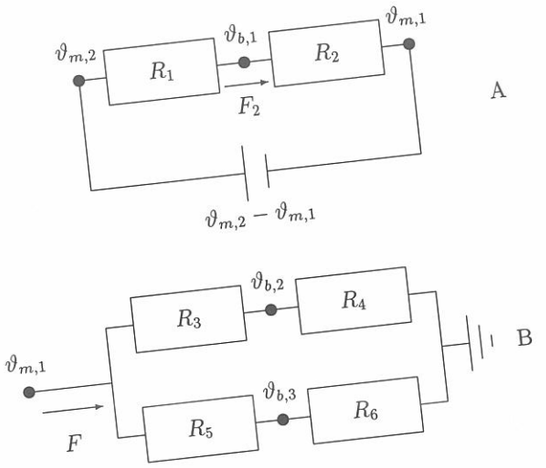

Figure 5.6: Network for the four ball tester in case the balls are insulated

The combined resistance R_v of R_3, R_4, R_5 and R_6 is 33.4 $^\circ C/W$, see figure 5.6^b. The bulk temperature of the stationary ball can now be calculated as

$$\vartheta_{m,1} = F \cdot R_v = 376\ ^\circ C.$$

From figure 5.6^a it immediately follows that $\vartheta_{b,1}$, the bulk temperature rise in contact 1, can be calculated as

$$\vartheta_{b,1} = \vartheta_{m,1} + R_2 \cdot F_2 = 465\ ^\circ C.$$

The maximum contact temperature thus follows from

$$\vartheta_c = \vartheta_f + \vartheta_{b,1} + \vartheta_{oil} = 604\ ^\circ C.$$

So the maximum contact temperature in the case of insulated bodies is almost a factor two higher then the measured value for this situation. As could have been expected, the heat loss to the oil cannot be neglected. To accurately predict the contact temperatures for the four ball tester it is necessary to determine the heat loss charateristics of the balls.

References

Barber, J.R., 1970, "The Conduction of Heat From Sliding Solids", *Int. J. Heat Mass Transfer*, Vol. 13, pp. 857-869.

Begelinger, A., and de Gee, A.W.J., 1976, "On the mechanism of lubricant film failure in sliding concentrated contacts," *ASME J. of Tribology*, Vol. 98, no. 4, pp. 575-579.

Blok, H., 1969, "The postulate about the constancy of scoring temperature," *Proc. Interdisciplinary Approach to the Lubrication of Concentrated Contacts*, 15-17 July 1969; Doc. NASA SP-237, pp. 153-248.

Bos, J., and Moes, H., 1995, "Frictional heating of tribological contacts," *ASME J. of Tribology*, Vol. 117, pp. 171-177

Francis, H.A., 1971, "Interfacial Temperature Distribution Within a Sliding Hertzian Contact," *ASLE Trans.*, Vol. 14, pp. 41-54.

Heijningen, G.J.J. van, 1986, "Tribotechniek Deel D: Temperatuur- en warmtestroomverdeling in machines en machineonderdelen", in Dutch, Delft University, The Netherlands.

Hsu, S.M., and Klaus, E.E., 1977, "Estimation of the molecular junction temperatures in four-ball contacts by chemical reaction rate studies," *ASLE Transactions*, Vol. 21, pp. 201-210.

Chapter 6

Thermal EHL Theory

In this chapter a mathematical model describing the thermal EHL line contact situation will be discussed. The running surfaces are assumed to be separated by a lubricant film and to deform elastically. The fluid flow depends on, amongst other factors, the geometry of the contact, the running conditions, i.e. the load applied and the velocities of the surfaces, and the material properties of the fluid. By comparing measured film thicknesses with calculated film thicknesses, *Venner and Lubrecht*, (1994) showed that accurate film thickness predictions can be made under the assumption of isothermal and Newtonian fluid behaviour. The differences between measured and calculated mimimum film thicknesses they found were 1ess than 10% for the cases considered (a maximum Hertzian pressure of 0.54 GPa). Under these assumptions, however, the prediction of the energy loss due to friction, i.e. viscous dissipation is highly unrealistic and is orders of magnitude too high compared with experimental results. More realistic models for the fluid and including thermal effects lead to lower predictions of the energy dissipation. A model capable of describing the thermal non-Newtonian EHL problem consists of five equations:

1. The film thickness equation for the computation of the elastic deformation of the surfaces caused by the pressure in the fluid.

2. A constitutive equation that relates the shear rate to the shear stress and the viscosity of the fluid.

3. The energy equation which relates the temperature rise in the fluid to the viscous dissipation in the fluid.

4. A generalized Reynolds equation which relates the pressure in the fluid to the geometry of the contact and the velocities of the running surfaces and

5. the force balance equation requiring equilibrium of forces.

The pressure in the lubricant is high, to such a degree that the change in material properties of the lubricant like viscosity and density cannot be neglected and must be taken into account. The viscosity and the density also depend on the temperature, even far more than on the pressure. A temperature increase of a mere 10°, reduces the viscosity of a standard oil by about a factor two. So the variation of the lubricant properties with temperature must be accounted for as well.

Empirical relations describing the variation of the viscosity and the density with pressure and temperature exist. However, for the extreme conditions under which EHL contacts operate, the accuracy of these relations is still questionable.

6.1 Film thickness equation

If the contact is small compared to the radii of curvature of the undeformed surfaces of the contacting solids, these surfaces can be approximated by parabolas and the solids can be considered as semi-infinite elastic bodies. Furthermore, if the materials are isotropic and the elastic deformations are small enough for the linear elasticity theory to apply, then the gap between the two solids can be described by:

$$h(x) = h_{00} + \frac{x^2}{2R} - \frac{4}{\pi E'} \int_{-\infty}^{\infty} \ln|x - x'| p(x') dx' \tag{6.1}$$

where:

R = reduced radius of curvature: $R^{-1} = R_1^{-1} + R_2^{-1}$

E' = reduced elastic modulus: $\frac{2}{E'} = \frac{(1-\nu_1^2)}{E_1} + \frac{(1-\nu_2^2)}{E_2}$

E = Elastic (Young's) modulus

ν = Poisson's ratio

h_{00} = a constant

For a more detailed discussion on this subject see *Johnson* (1985) and *Timoshenko* (1982).

6.2 Rheology

Over the years a lot of attention has been paid to the lubricant behaviour under EHL conditions, see for instance *Johnson and Tevaarwerk* (1977) and *Bair and Winer* (1979[a], 1979[b], 1990, 1992). Most constitutive relations derived from these studies can be written in the following form:

$$\dot{\gamma} = \frac{d\tau/G}{dt} + \frac{\tau_r}{\eta} F(\tau/\tau_r) \tag{6.2}$$

where τ_r is a representative stress and G is the shear modulus.

In this 'non-linear Maxwell' model $\frac{d\tau/G}{dt}$ denotes the contribution to the shear rate of the linear elastic element and $\frac{\tau_r}{\mu} F(\tau/\tau_r)$ the contribution of a (possibly) non-linear viscous element.

6.3 Energy Equation

A prediction of the temperature rise in the EHL contacts between machine elements is an important contribution to the engineering design process. Apart from this, the temperature rise has a significant influence on the material properties of the lubricant and thus on the performance of the contact.

The full energy equation expressing the law of conservation of energy is (*Hughes and Gaylord*, 1964)

$$\rho \left[\frac{De}{Dt} + p \frac{D}{Dt} \left(\frac{1}{\rho} \right) \right] = \frac{\partial q}{\partial t} + \Phi + \underline{\nabla} \cdot (k \, \underline{\nabla} T) - \underline{\nabla} \cdot \underline{\mathbf{q}}_r \tag{6.3}$$

where

- e = specific internal energy per unit mass
- Φ = viscous dissipation function
- $\underline{\mathbf{q}}_r$ = the radiation heat flux vector
- q = internal heat generation
- T = temperature
- t = time
- ρ = lubricant density
- p = pressure
- k = thermal conductivity

The specific internal energy can be expressed in terms of known quantities and lubricant properties. According to the first law of thermodynamics

$$de = T \, dS - p \, dv \tag{6.4}$$

where is S is the entropy and v is the specific volume, the entropy may be regarded as a function of the temperature, T, and the pressure, p. So

$$dS = \left(\frac{\partial S}{\partial T}\right)_p dT + \left(\frac{\partial S}{\partial p}\right)_T dp \tag{6.5}$$

One of Maxwell's identities states

$$\left(\frac{\partial S}{\partial p}\right)_T = -\left(\frac{\partial v}{\partial T}\right)_p \tag{6.6}$$

Therefore

$$de = T\left(\frac{\partial S}{\partial T}\right)_p dT - T\left(\frac{\partial v}{\partial T}\right)_p dp - p\, dv \tag{6.7}$$

By using the definitions for the specific heat at constant pressure, c_p, and the thermal expansion coefficient, ε:

$$c_p = T\left(\frac{\partial S}{\partial T}\right)_p, \quad \varepsilon = \left(\frac{1}{v}\frac{\partial v}{\partial T}\right)_p \tag{6.8}$$

this equation can be written as

$$de = c_p\, dT - \varepsilon\, T\, v\, dp - p\, dv = c_p\, dT - \varepsilon\, T \left(\frac{1}{\rho}\right) dp - p\, d\left(\frac{1}{\rho}\right) \tag{6.9}$$

Thus,

$$\rho\left[\frac{De}{Dt} + p\,\frac{D}{Dt}\left(\frac{1}{\rho}\right)\right] = \rho\, c_p\,\frac{DT}{Dt} - \varepsilon\, T\,\frac{Dp}{Dt} \tag{6.10}$$

Replacing the lefthand side of equation (6.3) with the righthand side of the previous equation gives:

$$\rho\, c_p\,\frac{DT}{Dt} - \varepsilon\, T\,\frac{Dp}{Dt} = \frac{\partial q}{\partial t} + \Phi + \underline{\nabla}\cdot(k\,\underline{\nabla}T) - \underline{\nabla}\cdot\underline{\mathbf{q}}_r \tag{6.11}$$

Or

$$\rho\, c_p\left[\frac{\partial T}{\partial t} + \underline{\mathbf{v}}\cdot\underline{\nabla}\,T\right] = \frac{\partial q}{\partial t} + \Phi + \underline{\nabla}\cdot(k\,\underline{\nabla}T) - \underline{\nabla}\cdot\underline{\mathbf{q}}_r + \varepsilon\, T\left[\frac{\partial p}{\partial t} + \underline{\mathbf{v}}\cdot\underline{\nabla}p\right] \tag{6.12}$$

6.3.1 Relevant Terms of the Energy Equation in Case of Elasto Hydrodynamic Lubricated Contacts

The general energy equation can be significantly reduced when applied to a lubricant film:

- Except for viscous heating, no heat is generated in the lubricant (No chemical reactions or radio activity). This cancels the $\frac{\partial q}{\partial t}$-term.
- Within the lubricant radiation can be neglected. Therefore $\underline{\mathbf{q}}_r = 0$
- For steady state situations all the time derivatives are equal to zero, this being the case when the surfaces of the bodies are considered perfectly smooth.

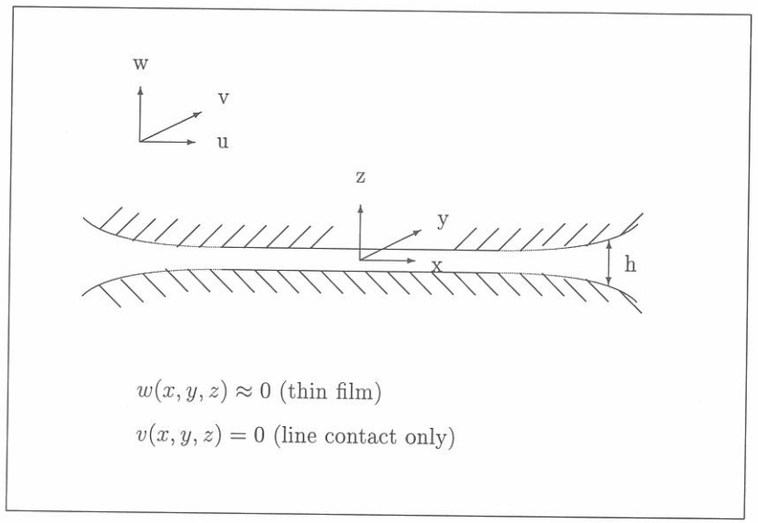

Figure 6.1: Diagrammatic representation of the lubricant film geometry

Due to the specific geometry and flow aspects of the lubricant film, further simplifications can be applied (see Figure 6.1). Since for EHL-contacts the surfaces are almost parallel, the velocity across the film, w, is generally neglected. In concentrated contacts the oil film is very thin, i.e. of the order of 10^{-3} compared to the

contact width, so:

$$\frac{\partial}{\partial x}\left(k\,\frac{\partial T}{\partial x}\right), \frac{\partial}{\partial y}\left(k\,\frac{\partial T}{\partial y}\right) \ll \frac{\partial}{\partial z}\left(k\,\frac{\partial T}{\partial z}\right) \tag{6.13}$$

Applying these simplifications to equation (6.12) results in equation (6.14):

$$\rho\, c_p \left[u\,\frac{\partial T}{\partial x} + v\,\frac{\partial T}{\partial y}\right] = \Phi + \frac{\partial}{\partial z}\left(k\,\frac{\partial T}{\partial z}\right) + \varepsilon\, T\, \left[u\frac{\partial p}{\partial x} + v\frac{\partial p}{\partial y}\right] \tag{6.14}$$

For line contacts this equation can be reduced even further, since $v = 0$ and all the derivatives in the y direction ar equal to zero:

$$\underbrace{\rho\, c_p u\,\frac{\partial T}{\partial x}}_{\text{convection}} = \underbrace{\Phi}_{\text{source}} + \underbrace{\frac{\partial}{\partial z}\left(k\,\frac{\partial T}{\partial z}\right)}_{\text{conduction}} + \underbrace{\varepsilon\, T\, u\frac{\partial p}{\partial x}}_{\text{compressive heating/cooling}} \tag{6.15}$$

6.3.2 Boundary Conditions

The heat generated in the fluid is mostly transferred to the contacting solids. Depending on the size of the contact and the surface velocities, part of the heat will flow into solid 1 and another part into solid 2. Under the assumption of infinite or semi infinite bodies it is possible to obtain an analytical expression for the surface temperatures of the solids, analoguous to the one derived in chapter 2, without solving the energy equation for both the solids as well as for the fluid.

In case of the line contact problem, the solution for the moving line source should be applied; see *Carslaw an Jaeger* (1959). Heat is emitted at some rate q per unit time per unit length along the y-axis (see figure 6.1). The distribution of the surface temperature rise of a semi infinite body moving past a heated wire at x' is given by

$$T(x) = \frac{q}{\pi k_s} e^{\frac{U}{2\kappa}(x-x')} K_0[\frac{U}{2\kappa}|x-x'|] \tag{6.16}$$

where $K_0(x)$ is the modified Bessel function of the second kind, k_s is the thermal conductivity of the body, U is the velocity relative to the heat source and κ is the diffusivity.

The heat, q, flowing into the bodies is generated in the lubricant film. Since the velocities across the film are neglected, the only means of heat transfer from the fluid to the bodies is by conduction. Therefore:

$$\begin{aligned} q_1 &= -k_f \frac{dT}{dz}|_{z=0} \\ q_2 &= k_f \frac{dT}{dz}|_{z=h} \end{aligned} \tag{6.17}$$

With these heat sources the temperature distribution at the surfaces of the bodies can be written as:

$$\begin{aligned} T_1(x) &= T_0 - \frac{1}{\pi k_{s_1}} \int_{-\infty}^{+\infty} k_f \frac{dT}{dz}(x')|_{z=0}\; e^{U_1(x-x')/2\kappa_1} K_0[U_1/2\kappa_1|x-x'|]dx' \\ T_2(x) &= T_0 + \frac{1}{\pi k_{s_2}} \int_{-\infty}^{+\infty} k_f \frac{dT}{dz}(x')|_{z=h}\; e^{U_2((x-x')/2\kappa_2} K_0[U_2/2\kappa_2|x-x'|]dx' \end{aligned}$$

When the contact is fully flooded, the temperature far away from the inlet can be considered equal to the ambient temperature:

$$T(x = -\infty) = T_0 \tag{6.18}$$

6.4 Generalized Reynolds equation

Reynolds (1886), derived the equation that relates the pressure in the lubricant film to the geometry of the gap and the velocities of the running surfaces under the following assumptions:

1. the body forces are negligible
2. the pressure is constant across the film
3. no slip occurs at the boundaries
4. the lubricant flow is laminar
5. inertia and surface tension forces are negligible compared to viscous forces
6. shear stress and velocity gradient are only significant across the lubricant film
7. the lubricant behaves like a Newtonian fluid
8. the lubricant viscosity is constant across the film
9. the surfaces bounding the lubricant flow are parallel or at small angle with respect to each other.

For EHL-problems assumptions 7 and 8 do not apply, especially when determining friction in an EHL-contact. Usually the lubricants are poor heat conductors. Therefore, when slip is important the temperature will vary across the film due to the viscous heating in the film. Since for most lubricants the viscosity strongly depends on the temperature, the viscosity will also vary across the film. Further, non-Newtonian properties of the lubricant should be included. *Yang and Wen*

(1990), derived a generalized Reynolds equation which can incorporate rheological laws of the form of equation (6.2) as well as thermal effects.

To take into account the rheological laws, the velocity gradient is expressed as:

$$\frac{\partial u}{\partial z} = f(\tau, \eta) \tag{6.19}$$

By considering the equilibrium of a small material volume of the fluid, it follows that:

$$\frac{\partial p}{\partial x} = \frac{\partial \tau}{\partial z} \tag{6.20}$$

Defining a function called the "equivalent viscosity" as:

$$\eta^* = \frac{\tau}{f(\tau, \eta)} \tag{6.21}$$

an expression for τ follows by eliminating $f(\tau, \eta)$ from (6.19) and (6.21):

$$\tau = \eta^* \frac{\partial u}{\partial z} \tag{6.22}$$

By applying this relation, *Yang and Wen* (1990) a generalized Reynolds equation can be derived in which almost all rheological laws can be incorporated and in which variations in the viscosity over the film, e.g. due to thermal effects, can be taken into account. For smooth surfaces this equation can be written as:

$$\frac{\partial}{\partial x}\left[\left(\frac{\rho}{\eta}\right)_e h^3 \frac{\partial p}{\partial x}\right] = 12\frac{\partial}{\partial x}(\rho^* u_+ h) + 12\frac{\partial}{\partial t}(\rho_e h) \tag{6.23}$$

where

$$u_+ = (U_1 + U_2)/2 \tag{6.24}$$

$$u_- = (U_1 - U_2)/2 \tag{6.25}$$

$$\left(\frac{\rho}{\eta}\right)_e = 12(\eta_e \rho_e'/\eta_e' - \rho_e'') \tag{6.26}$$

$$\rho^* = [-\rho_e' \eta_e 2u_- + \rho_e(u_+ + u_-)]/u_+ \tag{6.27}$$

$$\rho_e' = \frac{1}{h^2}\int_0^h \rho \int_0^z \frac{dz'}{\eta^*} dz \tag{6.28}$$

$$\rho_e'' = \frac{1}{h^3}\int_0^h \rho \int_0^z \frac{z' dz'}{\eta^*} dz \tag{6.29}$$

$$\rho_e = \frac{1}{h}\int_0^h \rho dz \tag{6.30}$$

$$\frac{1}{\eta_e} = \frac{1}{h}\int_0^h \frac{dz}{\eta^*} \tag{6.31}$$

$$\frac{1}{\eta_e'} = \frac{1}{h^2}\int_0^h \frac{z dz}{\eta^*} \tag{6.32}$$

and

$$\begin{aligned} p &= 0 \quad \text{at the inlet and outlet boundary} \\ p &\geq 0 \quad \text{in the contact} \end{aligned} \tag{6.33}$$

This last boundary condition is necessary since a fluid will cavitate when subjected to negative pressures. The lowest possible pressure in a fluid is its vapor pressure. However, since this pressure is very small compared to the pressures in the contact, it is neglected, i.e. set to zero. So, in the outlet zone of the contact, the fluid is described by the cavitation condition, $p = 0$. In this work transient effects, for instance due to surface roughness, will not be taken into account, therefore the last term of this equation is discarded. Further, u_+ the average velocity, is assumed to be constant.

6.4.1 The Viscosity-Pressure-Temperature Relation

In this work two different viscosity-pressure-temperature relations have been used, the Barus relation and the Roelands equation. The Barus relation, *Barus* (1893),

$$\eta(p, T) = \eta_0 \, e^{\alpha p - \gamma(T - T_0)} \tag{6.34}$$

with:

η_0 = the viscosity at ambient pressure
α = the pressure viscosity coefficient
γ = the temperature viscosity coefficient
T_0 = the ambient temperature

is used in many other EHL calculations, but is only accurate for pressures up to 0.1 GPa. A more accurate relation was proposed by *Roelands* (1966). In S.I. units this relation can be given as:

$$\eta(p, T) = \eta_0 \, e^{\left\{[\ln \eta_0 + 9.67]\left[-1 + (1 + \frac{p}{p_0})^z \left(\frac{T_0 - 138}{T - 138}\right)^{S_0}\right]\right\}} \tag{6.35}$$

where:

z = the pressure viscosity index
S_0 = the temperature viscosity index
p_0 = a constant : $p_0 = 1.96\ 10^8$

If α and γ are defined as

$$\alpha = \frac{1}{\eta}\frac{d\eta}{dp}\bigg|_{p=0, T=T_0}, \quad \gamma = \frac{1}{\eta}\frac{d\eta}{dT}\bigg|_{p=0, T=T_0} \tag{6.36}$$

the following relations are found between the Barus' and the Roelands parameters, see for instance *Houpert* (1985).

$$z = \frac{\alpha}{5.1\ 10^{-9}(\ln \eta_0 + 9.67)} \tag{6.37}$$

$$S_0 = \frac{\gamma(T_0 - 138)}{\ln \eta_0 + 9.67} \tag{6.38}$$

6.4.2 The Density-Pressure-Temperature Relation

The isothermal *Dowson* (1966) density-pressure relation has been used in this work. For the temperature variation, it is assumed that within the range of temperatures considered, a linear model applies. Therefore, the complete density relation can be expressed as

$$\rho(p,T) = \rho_0 \left(1 + \frac{A\,p}{1 + B\,p}\right)[1.0 - \varepsilon(T - T_0)] \tag{6.39}$$

where $A = 0.6\ 10^{-9}\ m^2/N$, $B = 1.7\ 10^{-9}\ m^2/N$ and ε is the thermal expansion coefficient.

6.5 Force Balance Equation

If the surfaces of the two bodies are fully separated by a lubricant film, the entire load w is carried by this film. To assure equilibrium of forces, the integral over the pressure in the film must equal the applied load, so:

$$w = \int_{-\infty}^{\infty} p(x)dx \tag{6.40}$$

References

Bair, S. and Winer, W.O., 1979[a], "Shear Strength Measurements of Lubricants at High Pressure", *ASME JOT*, Vol. 101, No. 3, pp. 251-257.

Bair, S. and Winer, W.O., 1979[b], "A Rheological Model for Elastohydrodynamic Contacts Based on Primary Laboratory Data", *ASME JOT*, Vol. 101, No. 3, pp. 258-265.

Bair, S. and Winer, W.O., 1990, "High Shear Stress Rheology of Liquid Lubricants at Pressures of 2 to 200 MPa", *ASME JOT*, Vol. 112, No. 2, pp. 246-253.

Bair, S. and Winer, W.O., 1992, "The High Pressure High Shear Stress Rheology of Liquid Lubricants", *ASME JOT*, Vol. 114, pp. 1-13.

Barus, C., 1893, "Isothermals, isopiestics and isometrics relative to viscosity", *Am. J. of Science*, Vol. 45, pp. 87-96.

Carslaw, H.S. and Jaeger, J.C., 1959, "Conduction of Heat in Solids", Oxford University Press, Oxford, UK.

Dowson, D., 1966, "Elasto-Hydrodynamic-Lubrication", Pergamon Press.

Hughes, W.F. and Gaylord, E.W., 1964, "Basic Equations of Engineering Science", McGraw-Hill Book Company.

Houpert, L., 1985, "New Results of Traction Force Calculations in Elastohydrodynamic Contacts", *ASME JOT*, Vol. 107, pp. 241-248.

Johnson, K.L., 1985, "Contact Mechanics", Cambridge University Press.

Johnson, K.L., and Tevaarwerk, J.L., 1977, "Shear behaviour of elastohydrodynamic oil films", *Proc. R. Soc. Lond*, Vol. 356A, pp. 215-236.

Reynolds, O., 1886, " On the Theory of Lubrication and its Application to Mr. Beauchamp Tower's Experiments, including an Experimental Determination of the Viscosity of Olive Oil", *Phil. Trans. Roy. Soc.*, Vol. 177, pp. 157-234.

Roelands, C.J.A., 1966, "Correlation Aspects of the Viscosity-Temperature-Pressure Relationship of Lubricating Oils", PhD. thesis, Technische Hogeschool Delft, the Netherlands, (V.R.B., Groningen, the Netherlands)

Timoshenko, S. and Goodier, J.N., 1951, "Theory of Elasticity", 3rd Edn. New York, McGraw-Hill.

Venner, C.H., Lubrecht, A.A, 1994, "Numerical Simulation of Transverse Waviness in a Circular EHL Contact, under Rolling/Sliding", 21st Leeds-Lyon Symposium on Tribology, to appear.

Yang Peiran and Wen Shizhu, 1990, " A Generalized Reynolds Equation for Non-Newtonian Thermal Elastohydrodynamic Lubrication", *ASME JOT.*, Vol. 112, pp. 631-636.

Chapter 7

Thermal Elastohydrodynamic Lubrication

In this chapter a multilevel algorithm will be described for the thermal EHL-problem. First the model equations, given in the previous chapter, will be made dimensionless using the "Optimum Similarity Analysis" (*Moes*, 1985) in order to minimize the number of independent parameters. Subsequently the resulting equations will be normalized to reduce numerical truncation errors, and finally, the equations will be discretized.

From a numerical point of view, the thermal Newtonian EHL-problem contains two extensions compared to the isothermal Newtonian EHL-problem, i.e. the coefficients in the Reynolds equation are functions of the coordinate across the lubricant film and an additional equation, the energy equation, must be solved. The multilevel approach, outlined by *Venner* (1991), for the isothermal Newtonian EHL-problem is extended in order to incorporate the two mentioned extensions. These extensions will be implemented one by one. In section 7.5 the incorporation in a multilevel solver of non-closed-form coefficients in Reynolds' equation will be described. Then, in sections 7.6.1 and 7.6.2 the incorporation of the energy equation, with its own numerical difficulties, is addressed. Finally the algorithm is tested for a simplified energy equation and some results will be shown and discussed.

7.1 Normalized Dimensionless Equations

In order to decrease the number of variables and parameters the so-called "Optimum Similarity Analysis" has been applied. With this method, which is described by *Moes*, 1985 a minimum of dimensionless numbers and variables can be determined.

$$\Theta = \frac{\bar{T}}{\bar{T}_0} = \frac{T}{T_0}$$

Substitution of these normalized variables in the equations for the auxiliary variables results in:

$$\left(\frac{\rho}{\eta}\right)_e = 12(\eta_e \rho_e'/\eta_e' - \rho_e'') \tag{7.18}$$

$$\rho^* = [\rho_e' \eta_e 2S + \rho_e(1+S)] \tag{7.19}$$

$$\rho_e' = \frac{1}{H^2}\int_0^H \bar{\rho}\int_0^Z \frac{dZ'}{\bar{\eta}^*}dZ \tag{7.20}$$

$$\rho_e'' = \frac{1}{H^3}\int_0^H \bar{\rho}\int_0^Z \frac{Z'dZ'}{\bar{\eta}^*}dZ \tag{7.21}$$

$$\rho_e = \frac{1}{H}\int_0^H \bar{\rho}dZ \tag{7.22}$$

$$\frac{1}{\eta_e} = \frac{1}{H}\int_0^H \frac{dZ}{\bar{\eta}^*} \tag{7.23}$$

$$\frac{1}{\eta_e'} = \frac{1}{H^2}\int_0^H \frac{ZdZ}{\bar{\eta}^*} \tag{7.24}$$

$$F = \frac{\bar{f}\,\bar{b}}{\bar{p}_h\,\bar{h}_h} \tag{7.25}$$

7.2.1 Normalized dimensionless equations

Substitution of the normalized variables in the governing equations results in a number of normalized dimensionless equations, in which:

$$\Omega = \frac{\bar{h}_h^2 \bar{p}_h}{\bar{b}} = \left(\frac{4M}{\pi}\right)^2$$

$$\Psi = \frac{\bar{h}_h^2}{\bar{b}} = \sqrt{\left(\frac{8M}{\pi}\right)^3}$$

$$K_{fs}^* = K_{fs}\frac{\bar{b}}{\bar{h}_h} = \frac{k_f}{k_s}\frac{R}{b}$$

$$Pe = Pec\,\bar{b} = \frac{u_+ b}{2\kappa}$$

The symbol Pe has been used for the Péclet number instead of the symbol P used in chapters 1-5, because P would be confusing since it is used for the pressure as well. The equations are:

Velocity gradient

$$\frac{\partial \bar{u}}{\partial Z} = \Omega \cdot F_x(\tau, \bar{\eta}) \tag{7.26}$$

Equilibrium equation

$$\frac{\partial P}{\partial X} = \frac{\partial \tau}{\partial Z} \tag{7.27}$$

Equivalent viscosity

$$\bar{\eta}^* = \frac{\tau}{F(\tau, \bar{\eta})} \tag{7.28}$$

Shear stress equation

$$\tau = \frac{\bar{\eta}^*}{\Omega}\frac{\partial \bar{u}}{\partial Z} \tag{7.29}$$

Reynolds equation

$$\Omega\frac{\partial}{\partial X}\left[\left(\frac{\rho}{\eta}\right)_e H^3 \frac{\partial P}{\partial X}\right] = 12\frac{\partial}{\partial X}(\rho^* H) \tag{7.30}$$

Film thickness equation:

$$H(X) = H_{00} + \frac{X^2}{2} - \frac{1}{\pi}\int_{-\infty}^{+\infty} \ln|X - X'|P(X')dX' \tag{7.31}$$

The energy equation:
By assuming that lubricant properties such as thermal conductivity, specific heat, and thermal expansivity do not vary with temperature and pressure, the energy equation can be written in dimensionless form as

$$\frac{\partial}{\partial Z}\left(\frac{\partial \Theta}{\partial Z}\right) = \bar{\rho} C_o \bar{u} \Psi \frac{\partial \Theta}{\partial X} - \Omega \Theta E \bar{u}\frac{\partial P}{\partial X} - \frac{\Omega}{\bar{T}_0}\tau\frac{\partial \bar{u}}{\partial Z} \tag{7.32}$$

The normalized dimensionless boundary conditions for the energy equation are:

$Z = 0$:

$$\Theta_1(X) = 1 - \frac{K_{fs}^*}{\pi}\int_{-\infty}^{+\infty}\frac{\partial \Theta}{\partial Z}\exp\left\{(1+S)Pe(X-X')\right\}K_0\left[(1+S)Pe|X-X'|\right]dX'$$

$Z = H$:

$$\Theta_2(X) = 1 + \frac{K_{fs}^*}{\pi}\int_{-\infty}^{+\infty}\frac{\partial \Theta}{\partial Z}\exp\left\{(1-S)Pe(X-X')\right\}K_0\left[(1-S)Pe|X-X'|\right]dX'$$

$$X = -\infty \quad : \quad \Theta = 1$$

Viscosity-pressure-temperature:
Barus:

$$\bar{\eta}_x(P, \Theta) = e^{L_\alpha \bar{p}_h P - L_\gamma \bar{T}_0(\Theta - 1)} \tag{7.33}$$

Roelands:

$$\bar{\eta}(P,\Theta) = \exp\left\{\frac{\alpha p_0}{z}\left(-1+\left(1+\frac{p_h P}{p_0}\right)^z\left(\frac{T_0-138}{T_0\Theta-138}\right)^{S_0}\right)\right\} \tag{7.34}$$

Density-pressure-temperature relationship:

$$\bar{\rho}(P,\Theta) = \left(1.0+\frac{\bar{A}\bar{p}_h P}{1.0+\bar{B}\bar{p}_h P}\right)[1.0-E\bar{T}_0(\Theta-1)] \tag{7.35}$$

The force balance equation:

$$\frac{\pi}{2} = \int_{-\infty}^{+\infty} P(X')dX' \tag{7.36}$$

7.3 Non Orthogonal Coordinate Transformation

In order to take inlet shear heating into account, the energy equation should be solved on a domain that extends beyond the contact area. This means that the energy equation is to be solved on a slightly non-rectangular domain. Since non-rectangular domains are inconvenient from a numerical point of view, this domain will be mapped onto a rectangular domain using a non orthogonal coordinate transformation. For smooth surfaces, this transformation and its consequences for the energy equation will be explained in detail in this section. For the problem at hand: solving the energy for an EHL-contact, a mapping from the non rectangular domain to a rectangular domain is established by the following coordinate transformation:

$$\zeta = \frac{Z}{H(X)}, \quad \xi = X \tag{7.37}$$

Figures 7.1 and 7.2 show the X,Z- and the ζ,ξ coordinate lines in the physical domain. Since lines of constant ξ coincide with the Z-coordinate lines $\mathbf{e}_\zeta$ is $\mathbf{e}_Z$. To determine $\mathbf{e}_\xi$ it is noted that this vector is perpendicular to the unit vector $\mathbf{n}$ that is normal to a line of constant ζ. $\mathbf{n}$ is given by:

$$\mathbf{n} = \frac{\nabla\zeta}{|\nabla\zeta|} = \frac{\mathbf{e}_X - \beta\mathbf{e}_Z}{\sqrt{\alpha}} \tag{7.38}$$

where

$$\beta = \zeta\frac{\partial H}{\partial\xi}, \quad \alpha = 1+\beta^2 \tag{7.39}$$

and therefore

$$\mathbf{e}_\xi = \frac{\mathbf{e}_Z + \beta\mathbf{e}_X}{\sqrt{\alpha}} \tag{7.40}$$

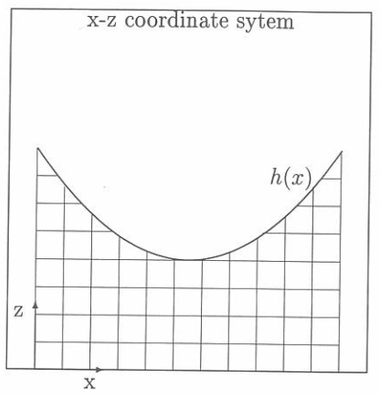

Figure 7.1: coordinate lines in the x,z coordinate sytem

The formal coordinate transformation is completed by relating the derivatives with respect to the X- and Z-coordinate in the cartesian system, to the derivative with respect to the ζ- and ξ-coordinate:

$$\begin{aligned}\left(\frac{\partial}{\partial Z}\right)_X &= \frac{1}{H}\left(\frac{\partial}{\partial\zeta}\right)_\xi \\ \left(\frac{\partial}{\partial X}\right)_Z &= -\frac{\beta}{H}\left(\frac{\partial}{\partial\zeta}\right)_\xi + \left(\frac{\partial}{\partial\xi}\right)_\zeta\end{aligned} \tag{7.41}$$

One of the assumptions made when deriving the Reynolds equation was: the lubricant boundary surfaces are parallel or at small angle with respect to each other, i.e. $\frac{\partial H}{\partial\xi} \ll 1$. So

$$\left(\frac{\partial}{\partial X}\right)_Z \approx \left(\frac{\partial}{\partial\xi}\right)_\zeta$$

7.3.1 Transformed equations

Velocity gradient

$$\frac{\partial\bar{u}}{\partial\zeta} = H\Omega\, F(\tau,\bar{\eta}) \tag{7.42}$$

Equilibirium equation

$$H\frac{\partial P}{\partial\xi} = \frac{\partial\tau}{\partial\zeta} \tag{7.43}$$

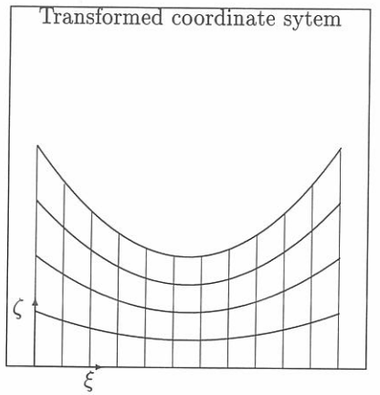

Figure 7.2: coordinate lines of the transformed coordinate system

Equivalent viscosity

$$\bar{\eta}^* = \frac{\tau}{F(\tau, \bar{\eta})} \tag{7.44}$$

Shear stress equation

$$\tau = \frac{\bar{\eta}^*}{H\Omega}\frac{\partial \bar{u}}{\partial \zeta} \tag{7.45}$$

Reynolds equation

$$\Omega\frac{\partial}{\partial \xi}\left[\left(\frac{\rho}{\eta}\right)_e H^3\frac{\partial P}{\partial \xi}\right] = 12\frac{\partial}{\partial \xi}(\rho^* H) \tag{7.46}$$

where

$$\left(\frac{\rho}{\eta}\right)_e = 12(\eta_e\rho_e^{'}/\eta_e^{'} - \rho_e^{"}) \tag{7.47}$$

$$\rho^* = [\rho_e^{'}\eta_e 2S + \rho_e(1+S)] \tag{7.48}$$

$$\rho_e^{'} = \int_0^1 \bar{\rho}\int_0^{\zeta}\frac{d\zeta^{'}}{\bar{\eta}^*}d\zeta \tag{7.49}$$

$$\rho_e^{"} = \int_0^1 \bar{\rho}\int_0^{\zeta}\frac{\zeta^{'}d\zeta^{'}}{\bar{\eta}^*}d\zeta \tag{7.50}$$

$$\rho_e = \int_0^1 \bar{\rho}d\zeta \tag{7.51}$$

$$\frac{1}{\eta_e} = \int_0^1 \frac{d\zeta}{\bar{\eta}^*} \tag{7.52}$$

$$\frac{1}{\eta_e^{'}} = \int_0^1 \frac{\zeta d\zeta}{\bar{\eta}^*} \tag{7.53}$$

(7.54)

Film thickness equation:

$$H(\xi) = H_{00} + \frac{\xi^2}{2} - \frac{1}{\pi}\int_{-\infty}^{+\infty}\ln|\xi - \xi^{'}|P(\xi^{'})d\xi^{'} \tag{7.55}$$

The energy equation:

$$\frac{\partial}{\partial \zeta}\left(\frac{\partial \Theta}{\partial \zeta}\right) = \bar{\rho}C_0\bar{u}\Psi\ H^2\frac{\partial \Theta}{\partial \xi} - H^2\Omega\Theta E\bar{u}\frac{\partial P}{\partial \xi} - \frac{H\Omega}{\bar{T}_0}\tau\ \frac{\partial \bar{u}}{\partial \zeta} \tag{7.56}$$

The normalized dimensionless boundary conditions for the energy equation are:

$\zeta = 0$:

$$\Theta_1(\xi) = 1 - \frac{K_{fs}^*}{\pi}\int_{-\infty}^{+\infty}\frac{1}{H}\frac{\partial \Theta}{\partial \zeta}\exp\left\{(1+S)Pe(\xi-\xi^{'})\right\}K_0\left[(1+S)Pe|\xi-\xi^{'}|\right]d\xi^{'}$$

$\zeta = 1$:

$$\Theta_2(\xi) = 1 + \frac{K_{fs}^*}{\pi}\int_{-\infty}^{+\infty}\frac{1}{H}\frac{\partial \Theta}{\partial \zeta}\exp\left\{(1-S)Pe(\xi-\xi^{'})\right\}K_0\left[(1-S)Pe|\xi-\xi^{'}|\right]d\xi^{'}$$

$$\xi = -\infty \quad : \quad \Theta = 1$$

The force balance equation:

$$\frac{\pi}{2} = \int_{-\infty}^{+\infty}P(\xi^{'})d\xi^{'} \tag{7.57}$$

7.3.2 Calculation of the equivalent viscosity

The generalized Reynolds equation is written in terms of the equivalent viscosity. Before this equation can be solved, the equivalent viscosity must be calculated. This is accomplished as follows: integrating the equilibrium equation (7.43) results in

$$\tau = \tau_1 + H\zeta\ \frac{\partial P}{\partial \xi} \tag{7.58}$$

where τ_1 is the shear stress on surface 1. Substituting (7.58) in (7.42) and integration over the film yields

$$\int_0^1 F_x(\tau_1 + H\zeta\ \frac{\partial P}{\partial \xi}, \bar{\eta})d\zeta = -\frac{2S}{H\Omega} \tag{7.59}$$

τ_1 is found by solving this equation for τ_1. For a Newtonian fluid this results in:

$$\int_0^1 \frac{\tau_1 + H\zeta \frac{\partial P}{\partial \xi}}{\bar{\eta}} d\zeta = -\frac{2S}{H\Omega} \tag{7.60}$$

or:

$$\tau_1 = -\frac{2S}{\Omega} \frac{F_1}{H} - \frac{\partial P}{\partial \xi} H \frac{F_1}{F_2} \tag{7.61}$$

with

$$\frac{1}{F_1} = \int_0^1 \frac{d\zeta}{\bar{\eta}} \quad , \quad \frac{1}{F_2} = \int_0^1 \frac{\zeta d\zeta}{\bar{\eta}} \tag{7.62}$$

The equivalent viscosity can subsequently be calculated by applying equation 7.44.

7.4 Discretization

The governing equations are discretized on a uniform grid with mesh size h_ξ in the ξ-direction and h_ζ in the ζ-direction, covering the calculational domain

$$\left\{(\xi, \zeta) \in I\!R^2 | \xi_a \leq \xi \leq \xi_b \wedge 0 \leq \zeta \leq 1\right\}.$$

Velocity gradient

$$\left.\frac{\partial \bar{u}}{\partial \zeta}\right|_{i,j} = H_i \Omega F_x(\tau_{i,j}, \bar{\eta}_{i,j}) \tag{7.63}$$

Equivalent viscosity

$$\bar{\eta}^*_{i,j} = \frac{\tau_{i,j}}{F(\tau_{i,j}, \bar{\eta}_{i,j})} \tag{7.64}$$

Reynolds Equation

$$h_\xi^2 \left(\epsilon_{i-\frac{1}{2}} P_{i-1} - (\epsilon_{i-\frac{1}{2}} + \epsilon_{i+\frac{1}{2}}) P_i + \epsilon_{i+\frac{1}{2}} P_{i+1}\right) - h_\xi^{-1} \left(\rho^*_i H_i - \rho^*_{i-1} H_{i-1}\right) = 0 \tag{7.65}$$

where $\epsilon_{i-\frac{1}{2}}$ and $\epsilon_{i+\frac{1}{2}}$ denote the value of $\Omega \left(\frac{\rho}{\eta}\right)_e H^3$ at the intermediate locations $\xi = \xi_a + (i - \frac{1}{2})h_\xi$ and $\xi = \xi_a + (i + \frac{1}{2})h_\xi$ respectively. They are calculated from values of ϵ in the sites i and $i-1$ or i and $i+1$. For example:

$$\epsilon_{i-\frac{1}{2}} = \frac{\epsilon_i + \epsilon_{i-1}}{2}.$$

ϵ_i is defined as:

$$\Omega \left(\frac{\rho}{\eta}\right)_{e_i} H_i^3$$

The coefficients $\left(\frac{\rho}{\eta}\right)_{e_i}$ and ρ^*_i are defined as:

$$\left(\frac{\rho}{\eta}\right)_{e_i} = 12(\eta_{e_i} \rho'_{e_i} / \eta'_{e_i} - \rho''_{e_i}) \tag{7.66}$$

$$\rho^*_i = [\rho'_{e_i} \eta_{e_i} 2S + \rho_{e_i}(1 + S)] \tag{7.67}$$

(7.68)

where

$$\rho'_{e_i} = \frac{h_\zeta}{2} \sum_{j=1}^{n_\zeta - 1} \left(\bar{\rho}_{i,j} \frac{h_\zeta}{2} \sum_{k=0}^{j-1} \left(\frac{1}{\bar{\eta}^*_{i,k}} + \frac{1}{\bar{\eta}^*_{i,k+1}} \right) + \bar{\rho}_{i,j+1} \frac{h_\zeta}{2} \sum_{k=0}^{j} \left(\frac{1}{\bar{\eta}^*_{i,k}} + \frac{1}{\bar{\eta}^*_{i,k+1}} \right) \right)$$

$$\rho''_{e_i} = \frac{h_\zeta}{2} \sum_{j=1}^{n_\zeta - 1} \left(\bar{\rho}_{i,j} \frac{h_\zeta}{2} \sum_{k=0}^{j-1} \left(\frac{k h_\zeta}{\bar{\eta}^*_{i,k}} + \frac{(k+1) h_\zeta}{\bar{\eta}^*_{i,k+1}} \right) + \bar{\rho}_{i,j+1} \frac{h_\zeta}{2} \sum_{k=0}^{j} \left(\frac{(k h_\zeta}{\bar{\eta}^*_{i,k}} + \frac{(k+1) h_\zeta}{\bar{\eta}^*_{i,k+1}} \right) \right)$$

$$\rho_{e_i} = \frac{h_\zeta}{2} \sum_{j=0}^{n_\zeta - 1} (\bar{\rho}_{i,j} + \bar{\rho}_{i,j+1})$$

$$\frac{1}{\eta_{e_i}} = \frac{h_\zeta}{2} \sum_{j=0}^{n_\zeta - 1} \left(\frac{1}{\bar{\eta}^*_{i,j}} + \frac{1}{\bar{\eta}^*_{i,j+1}} \right)$$

$$\frac{1}{\eta'_{e_i}} = \frac{h_\zeta}{2} \sum_{j=0}^{n_\zeta - 1} \left(\frac{j h_\zeta}{\bar{\eta}^*_{i,j}} + \frac{(j+1) h_\zeta}{\bar{\eta}^*_{i,j+1}} \right)$$

Film thickness equation

$$H_i = H_{00} + \frac{\xi_i^2}{2} - \frac{1}{\pi} \sum_{j=0}^{n_\xi} K_{i,j}^{h_\xi h_\xi} P_j \tag{7.69}$$

where

$$K_{i,j}^{h_\xi h_\xi} = (i - j + \frac{1}{2}) h_\xi (\ln(|i - j + \frac{1}{2}|h_\xi) - 1) - (i - j - \frac{1}{2}) h_\xi (\ln(|i - j - \frac{1}{2}|h_\xi) - 1)$$

Energy equation

$$\frac{\Theta_{i,j-1} - 2\Theta_{i,j} + \Theta_{i,j+1}}{h_\zeta^2} = \bar{\rho}_{i,j} C_0 \bar{u}_{i,j} \Psi \left(\pm H_i^2 \frac{\Theta_{i,j} - \Theta_{i \mp 1, j}}{h_\xi} \right) - H_i^2 \Omega \Theta_{i,j} E \bar{u}_{i,j} \frac{P_{i+1} - P_{i-1}}{h_\xi} - \frac{H_i \Omega}{\bar{T}_0} \tau_{i,j} \left.\frac{\partial \bar{u}}{\partial \zeta}\right|_{i,j}$$

The signs in the convection term depend on the sign of the velocity, $u_{i,j}$, and is chosen such that the discretization is upstream. The equations for the boundary conditions are discretized as:

$$\zeta = 0 \; : \; \Theta_{1_i} = 1 - \frac{K^*_{fs}}{\pi} \sum_{k=0}^{n_\xi} G1_{i,k}^{h_\xi h_\xi} \frac{\Theta_{k,0} - \Theta_{k,1}}{H_k h_\zeta}$$

$$\zeta = 1 \; : \; \Theta_{2_i} = 1 - \frac{K^*_{fs}}{\pi} \sum_{k=0}^{n_\xi} G2_{i,k}^{h_\xi h_\xi} \frac{\Theta_{k,n_\zeta} - \Theta_{k,n_\zeta - 1}}{H_k h_\zeta}$$

$$\xi = -\infty \; : \; \Theta = 1$$

where

$$G1_{i,k}^{h_\xi h_\xi} = \int_{\xi_k - h_\xi/2}^{\xi_k + h_\xi/2} \exp\left\{(1+S)Pe(\xi - \xi')\right\} K_0\left[(1+S)Pe|\xi - \xi'|\right] d\xi$$

$$G2_{i,k}^{h_\xi h_\xi} = \int_{\xi_k - h_\xi/2}^{\xi_k + h_\xi/2} \exp\left\{(1-S)Pe(\xi - \xi')\right\} K_0\left[(1-S)Pe|\xi - \xi'|\right] d\xi$$

The force balance equation

$$\frac{h_\xi}{2} \sum_{i=0}^{n_\xi - 1} (P_i + P_{i+1}) = \frac{\pi}{2} \tag{7.70}$$

This global constraint determines the value of the constant H_{00} in equation 7.69.

Equations for the calculation of the equivalent viscosity

$$\tau_{i,j} = \tau_{1_i} + H_i \, j h_\zeta \frac{P_{i+1} - P_{i-1}}{h_\xi} \tag{7.71}$$

$$\tau_{1_i} = -\frac{2S}{\Omega} \frac{F_{1_i}}{H_i} - \frac{P_{i+1} - P_{i-1}}{h_\xi} H_i \frac{F_{1_i}}{F_{2_i}} \tag{7.72}$$

with

$$\frac{1}{F_{1_i}} = \frac{h_\zeta}{2} \sum_{j=0}^{n_\zeta - 1} \left(\frac{1}{\bar{\eta}_{i,j}} + \frac{1}{\bar{\eta}_{i,j+1}} \right)$$

$$\frac{1}{F_{2_i}} = \frac{h_\zeta}{2} \sum_{j=0}^{n_\zeta - 1} \left(\frac{j h_\zeta}{\bar{\eta}_{i,j}} + \frac{(j+1) h_\zeta}{\bar{\eta}_{i,j+1}} \right)$$

7.5 Numerical Approach

In recent years it has been amply demonstrated that multigrid techniques yield fast and efficient solvers for EHL problems. Following the introduction by *Lubrecht* (1986, 1987[a], 1987[b]) they have found increasing application in EHL, e.g. *Osborn*

and Sadeghi (1992), *Kim and Sadeghi* (1991), and *Huang, et al.* (1992). A detailed explanation of these techniques and their application to the EHL line and point contact problem can be found in *Venner* (1991) and *Lubrecht* (1987[a]) and references therein. In this section attention is focussed on the questions to be answered when equations are added to the model as described by *Venner* (1991), i.e. for the isothermal Newtonian EHL problem.

The corner-stone of an efficient multilevel solver for any integro-partial differential equation is a relaxation process that effectively smooths the error. In the case of a system of equations this firstly applies to each individual equation and the variable assigned to it. At this stage matters such as anisotropy in the equations (strong coupling in one of the directions) have to be recognized and dealt with. Secondly, for a system of equations it should be investigated how, relaxing one equation for its variable, affects the residuals of the other equations. This generally depends on the strength of the coupling between the equations. A formal tool to investigate this coupling is an analysis of the determinant of the system of equations, see *Brandt* (1984).

To illustrate this point of coupling: when developing a relaxation process for Reynolds' equation and the film thickness equation, it is convenient to have the relaxation deal with each equation consecutively, e.g. first compute the entire elastic deformation and film thickness and subsequently scan the grid to improve the pressure everywhere using (the discretized) Reynolds equation. For such a relaxation (when repeated) to converge and smooth well it is essential that the changes applied to the pressure are such that their cumulative effect on the elastic deformation integrals, remains small. At low loads this is automatically the case and most standard relaxation processes will converge. However with increasing load the coupling between Reynolds' equation and the film thickness equation (via the elastic deformation integrals) becomes stronger and distributive relaxation is needed. These matters are extensively explained by *Venner* (1991).

The questions raised above need to be readdressed when adding equations to the system. Assuming there exists a stable relaxation for the energy equation (see section 7.6) the coefficients in Reynolds' equation can be evaluated using equations (7.66) and (7.67), i.e. no relaxations are needed to compute the coefficients.

The next question is that of the coupling. Compared to the isothermal problem, Reynolds' equation is changed in two places; through the coeffient in the pressure flow term and through the coefficient in the wedge term. However, the pressure flow term is, in the region where the coefficient will significantly deviate from the coefficient in the isothermal case, not the dominant term in the equation. Consequently, its changes due to relaxing the energy equation will not cause significant changes of the residual(s) of Reynolds' equation. Secondly changes appear in the so-called wedge term:

$$12\frac{\partial(\rho^* H)}{\partial \xi} \tag{7.73}$$

Here changes in the coefficient are more important, as this is the dominating term in the above mentioned region. However, of the two variables appearing in it, the 'generalized' density is the less important one (from a relaxation point of view). Because of the global character of the elastic deformation integrals, the cumulative effect of pressure changes on the film thickness will be much larger than the changes in the generalized density.
Summarizing, it can be concluded that, changes induced when relaxing the energy equation can be expected to affect the residuals of Reynolds' equation only in a moderate way. Hence, apart from appropriate linearization when relaxing Reynolds' equation, no special measures are needed and a straigthforward extension of the relaxation scheme as outlined by *Venner* (1991) can be expected to work. The resulting consecutive scheme is schematically drawn in figure 7.3^a.

Next the incorporation of the relaxation of the energy equation and the calculation of the coeffients in a multilevel solver is addressed. From a formal point of view equations are added to the system. In multilevel solvers for non-linear problems it is essential that all equations are treated according to the so-called *FAS* rules, see *Brandt* (1984). Hence, in addition to the pressure and film thickness, the coefficients in Reynolds equation and the temperature must be fully treated as a variable, e.g. transfer of residuals to the coarse grid and when returning to the fine grid it is corrected using the coarse grid result. These measures are essential for the convergence of the coarse grid correction cycle, see *Venner* (1991).

Before shifting attention to results obtained with the algorithm described above two final comments are appropriate. One might suggest that simply replacing every call for the coefficients in the original algorithm by a number of iterations of the energy equation followed by an update of the coefficients in Reynolds' equation can also do the job, i.e. calculate the temperature distribution belonging to the current pressure and film thickness and calculate the coefficients in Reynolds using these temperatures. This in effect is the same as the procedure followed so far when encountering coefficients determined by non-closed form equations in a numerical solver for the pressure and film thickness, e.g. in the case thermal and/or non-Newtonian lubricant behaviour are taken into account. An "inner" iterative loop is introduced (on the lubricant model yielding the velocities and/or temperature and thereby the coefficients ϵ_i, ρ_i^* in the discrete Reynolds equation) within the "outer" iterative loop for pressure and film thickness (that uses these coefficients). Such a scheme is schematically drawn in figure 7.3^b.

Naturally if the scheme marked by (A) converges, scheme (B) also works. However, scheme (B) is inefficient from a computational point of view. The number of iterations to satisfy the error criterion for the inner loop, should be sufficiently large, to avoid slowdown of the convergence of the pressure and film thickness.

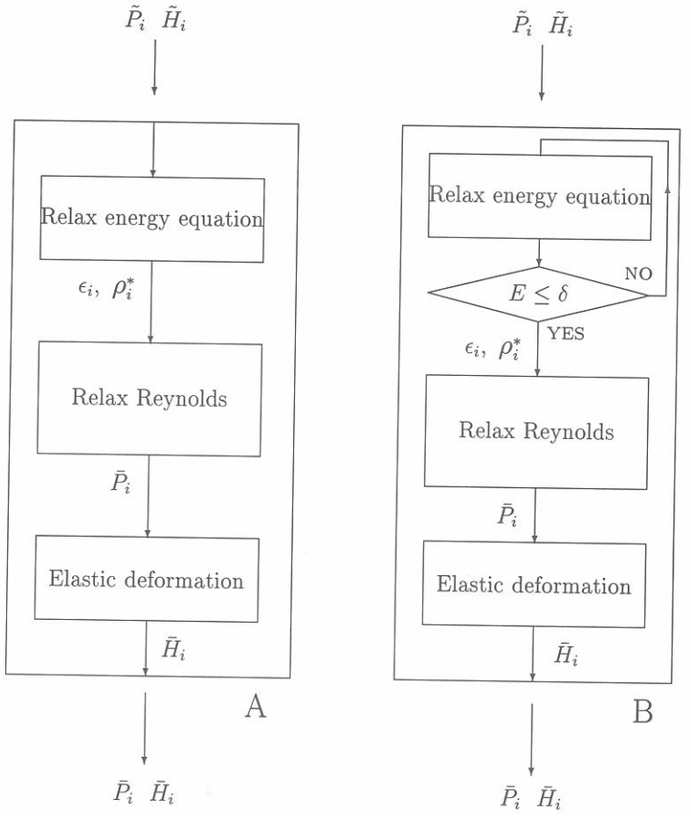

Figure 7.3: Flow diagram of the relaxtion process as proposed (A), and the (computationally inefficient) alternative with a nested loop (B)

This is particularly important if the speed of convergence of these latter variables is relatively large as characteristic for a multigrid algorithm (coarse grid correction cycle), and a single relaxation of the energy equation and an update of the coefficients as in the above algorithm is certainly not enough. In the case of scheme (B), in the process of relaxing (and solving) a set of equations, the energy equation is accurately (in practice often almost exactly) solved each sweep, even with pressure values still far away from the converged solution. This is done at the expense of many operations per gridpoint. Following the approach as outlined above however, the variable associated with the additional equation, i.e. the temperature, converges along with the pressure and film thickness.

7.6 Relaxation of the Energy Equation

As stated earlier, the corner-stone of a multilevel solver is a relaxation process that effectively smooths the error. To devise such a relaxation for the energy equation in combination with the integral boundary conditions, is not a trivial task. Therefore, first a simple model problem is constructed to study the effect of an integral boundary condition.

7.6.1 Model Problem

In order to the isolate the boundary condition problem from all kinds of additional problems that might occur when relaxing the energy equation, a model problem is constructed. The way to solve this model problem is, except from the implementation of this type of boundary condition, well known. The model problem is depicted in figure 7.4 and can be looked upon as a medium in which heat is generated at a constant rate everywhere on the unit square. On the left and right boundary this medium is thermally insulated. At the lower boundary the temperature is kept constant and at the upper boundary heat is transferred to a moving semi-infinite solid medium. The kernel G, present in the upper boundary integral condition is given by

$$G(x-x') = \exp\left(P(x-x')\right)K_0(P\sqrt{(x-x')^2})$$

where K_0 is the zero order modified Bessel function of the second kind and P is the Péclet number.

Analysis of the relaxation of the integral boundary condition

Setting the ambient temperature T_0 to unity, the upper boundary equation is discretized as:

$$T_{i,n_y} = 1 - \sum_{k=0}^{n_x} G^{hh}_{i,k}(T_{k,n_y} - T_{k,n_y-1})/h \tag{7.74}$$

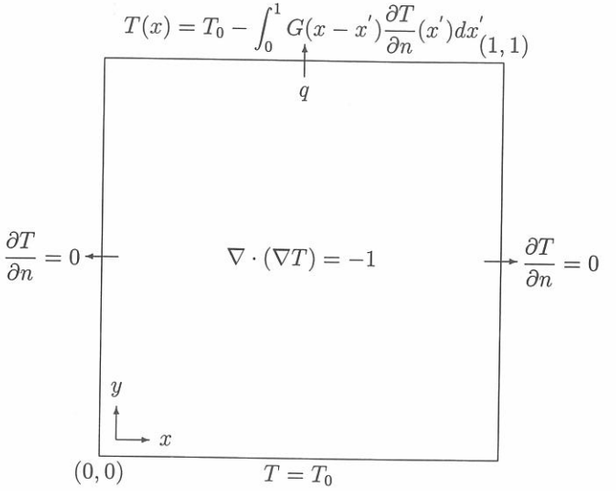

Figure 7.4: model problem

where n_x and n_y are the number of points in x- and y-direction respectively and h is the meshsize. The coefficients $G^{hh}_{i,j}$ are defined by

$$G^{hh}_{i,k} = \int_{x_k-h/2}^{x_k+h/2} G(x_i - x')dx' \tag{7.75}$$

For now, it will be assumed that somehow the exact solution to the discrete equations is known for the points T_{i,n_y-1}, $i = (0, ..., n_x)$. This assumption enables a simple analysis of the treatment of the integral boundary condition. In the following section the treatment of the boundary points will be extended to our model problem at hand in which the simultaneous relaxation of boundary and adjacent interior points is required. With the assumption just mentioned, the equation for the boundary points reduces to an one-dimensional integral equation of the form:

$$\lambda T_{i,n_y} + \sum_{k=0}^{n_x} G^{hh}_{i,k} T_{k,n_y} = f_i \tag{7.76}$$

This equation can be solved by means of the following second order distributive relaxation scheme: Given an approximation $\tilde{T}_{i,n_y}$ to T_{i,n_y}, all grid points are visited in lexicographic order and changes δ_i to be applied at sites i and adjacent sites $i-1$

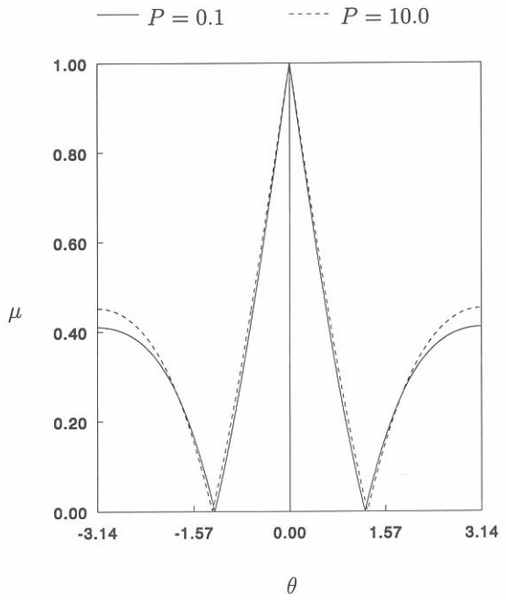

Figure 7.5: Amplitude reduction factor $\mu(\theta)$ for Jacobi second order distributive relaxation

and $i+1$ according to the following distribution:

$$\frac{1}{2}\delta_i \left[\begin{array}{ccc} -1 & 2 & -1 \end{array} \right], \tag{7.77}$$

are calculated according to:

$$\delta_i = \frac{f_i - (\lambda \tilde{T}_{i,n_y} + \sum_{k=0}^{n_x} G^{hh}_{i,k} \tilde{T}_{k,n_y})}{\lambda + \frac{1}{2}(-G^{hh}_{i,i-1} + 2G^{hh}_{i,i} - G^{hh}_{i,i+1})} \tag{7.78}$$

The changes are applied simultaneously after the sweep is completed. As a result of the distributive changes the new approximation $\bar{T}_{i,n_y}$ to T_{i,n_y} is given by:

$$\bar{T}_{i,n_y} = \tilde{T}_{i,n_y} + \delta_i - \frac{1}{2}(\delta_{i-1} + \delta_{i+1}) \tag{7.79}$$

Figure 7.5 shows the amplitude reduction factor for two different values of P and $\lambda = 0$. The case $\lambda = 0$ being a worst case situation as far as stability and error reduction are concerned. From figure 7.5 it can be seen, that apart from the almost negligible effect of the Péclet number, the second order distributive Jacobi relaxation is very effective in reducing high frequency error components. This

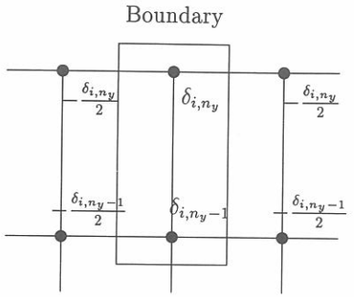

Figure 7.6: Distribution of the simultaneously calculated changes δ_{i,n_y} and δ_{i,n_y-1}

aspect makes this relaxation a suitable smoother, e.g. coarser grids can be applied to accelerate the convergence of the boundary equation given the exact solution of the discrete equations for T_{i,n_y-1}.

Combined relaxation of interior and boundary points

The interior equation is discretized using the well known 5-point stencil:

$$\frac{T_{i-1,j} + T_{i+1,j} + T_{i,j-1} + T_{i,j+1} - 4T_{i-1,j}}{h^2} = f_{i,j} \tag{7.80}$$

The upper boundary grid points are discretised as discussed in the previous section:

$$T_{i,n_y} + \sum_{k=0}^{n_x} G^{hh}_{i,k}(T_{k,n_y} - T_{k,n_y-1})/h = f_{i,n_y} \tag{7.81}$$

The treatment of Neumann boundaries is considered to be known and will not be discussed. Evidently the temperatures T_{i,n_y-1} cannot be calculated exactly without knowing in advance the temperatures on the boundary and vice versa. They have to be solved simultaneously. In order to ensure smoothness of the error in the direction perpendicular to the boundary, all the interior points adjacent to this boundary are treated in a special way. Given an approximation $\tilde{T}_{i,n_y}$ to T_{i,n_y} and $\tilde{T}_{i,n_y-1}$ to T_{i,n_y-1} , these grid points are visited and changes δ_{i,n_y} and δ_{i,n_y-1} to be applied at sites i and adjacent sites $i-1$ and $i+1$ according to figure 7.6 are calculated according to:

$$\begin{aligned} \frac{1}{h^2}\left(-5\ \delta_{i,n_y-1} + \delta_{i,n_y}\right) &= R_{i,n_y-1} \\ \delta_{i,n_y} + \Delta G^{hh}_{ii}(\delta_{i,n_y} - \delta_{i,n_y-1}) &= R_{i,n_y} \end{aligned} \tag{7.82}$$

level	# points	W(1,1)	W(2,1)	V(2,1)
3	16x16	0.09	0.06	0.13
4	32x32	0.09	0.06	0.14
5	64x64	0.08	0.04	0.17

Table 7.1: asymptotic convergence rates

where

$$R_{i,n_y} = f_{i,n_y} - (\tilde{T}_{i,n_y} + \frac{1}{h}\sum_{k=0}^{n_x} G^{hh}_{i,k}(\tilde{T}_{k,n_y} - \tilde{T}_{k,n_y-1}) \tag{7.83}$$

$$R_{i,n_y-1} = f_{i,n_y-1} - \left(\frac{\tilde{T}_{i-1,n_y-1} + \tilde{T}_{i+1,n_y-1} + \tilde{T}_{i,n_y-2} + \tilde{T}_{i,n_y} - 4\,\tilde{T}_{i-1,n_y-1}}{h^2} + 1\right)$$

$$\Delta G^{hh}_{ii} = \frac{1}{2h}(-G^{hh}_{i,i-1} + 2G^{hh}_{i,i} - G^{hh}_{i,i+1})$$

This means, solving both the boundary equation and the adjacent interior equation simultaneously, taking into account the second order distribution of the changes.

A full relaxation sweep consists of a sweep over the boundary points according to the above mentioned scheme, followed by a Red-Black sweep over the interior grid points.

Results

Table 7.1 shows the asymptotic convergence rates of different multigrid cycles on different levels. These convergence rates are close to the rates obtained for the standard 2D Poisson problem. Consequently it is concluded that, provided the appropriate measures are taken with regard to relaxation near the boundary, also in the case of an integral boundary condition the multi-grid textbook efficiency can be obtained. Figure 7.7 shows a contour plot of a solution for the model problem, for $P = 10$. Figure 7.8 shows the temperature on the boundary for this case.

7.6.2 Extension of the model problem to the real Energy Equation

The treatment of the integral boundary conditions is now well understood and therefore, the treatment of the energy equation can be addressed. If the discrete energy equation is written in operator form like

$$L^h\Theta_{i,j} = \frac{\Theta_{i,j-1} - 2\Theta_{i,j} + \Theta_{i,j+1}}{h^2_\zeta}$$

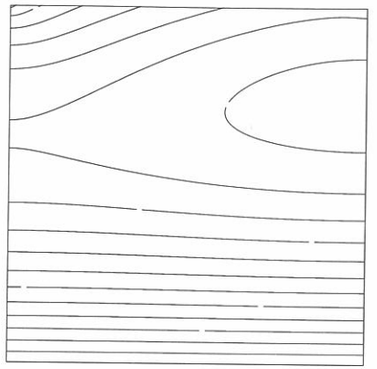

Figure 7.7: Contour lines of the temperature distribution for an example solution with $P = 10$.

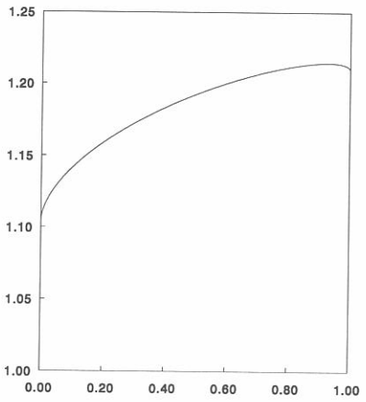

Figure 7.8: Boundary temperature.

$$- \quad \bar{\rho}_{i,j} C_0 \bar{u}_{i,j} \Psi \left(\pm H_i^2 \frac{\Theta_{i,j} - \Theta_{i\mp1,j}}{h_\xi} \right)$$
$$+ \quad H_i^2 \Omega \Theta_{i,j} E \bar{u}_{i,j} \frac{P_{i+1} - P_{i-1}}{h_\xi} + \frac{H_i \Omega}{\bar{T}_0} \tau_{i,j} \left. \frac{\partial \bar{u}}{\partial \zeta} \right|_{i,j} = 0$$

then new approximations $\overline{\Theta}_{i,j}$ of $\Theta_{i,j}$ are calculated from old approximations $\tilde{\Theta}_{i,j}$ according to

$$\overline{\Theta}_{i,j} = \tilde{\Theta}_{i,j} + \left(\frac{\partial L^h \Theta_{i,j}}{\partial \Theta_{i,j}} \right)^{-1} R_{i,j},$$

where $R_{i,j}$, the so-called dynamic residual, is defined by:

$$R_{i,j} = f_{i,j} - L^h \Theta_{i,j}.$$

The principal term (see *Brandt* 1984) of the energy equation,

$$\frac{\Theta_{i,j-1} - 2\Theta_{i,j} + \Theta_{i,j+1}}{h_\zeta^2}$$

only couples points in the j-direction. Therefore, applying a lexicographic Gauss-Seidel relaxation only smooths appropriately in this direction. In order to obtain a good smoother for the i-direction as well, a so-called line relaxation should be applied, i.e. all points on a i-line have to be solved simultaneously. By applying this relaxation the coupling in the i-direction is enhanced and provides a good smoother in both j and i-direction.

Incorporation boundary conditions

As for the model problem, the boundary equations and the adjacent interior equations should be solved simultaneously, using a second order distribution. The equations from which the changes δ must be calculated, are somewhat different though. For the boundary at $\zeta = 0$ the equations are:

$$\delta_{i,0} + \frac{K_{fs}^*}{\pi} \Delta G1_{i,i}^{h_\xi h_\eta} \frac{\delta_{i,0} - \delta_{i,1}}{h_\zeta} = f_{i,0} - \left(\tilde{\Theta}_{i,0} + \frac{K_{fs}^*}{\pi} \sum_{k=0}^{n_\xi} G1_{i,k}^{h_\xi h_\eta} \frac{\tilde{\Theta}_{k,0} - \tilde{\Theta}_{k,1}}{H_k h_\zeta} \right) \quad (7.84)$$

where $\Delta G1_{i,i}^{h_\xi h_\eta}$ is given by

$$\Delta G1_{i,i}^{h_\xi h_\eta} = \frac{1}{2} \left(-\frac{G1_{i,i-1}^{h_\xi h_\eta}}{H_{i-1}} + 2\frac{G1_{i,i}^{h_\xi h_\eta}}{H_i} - \frac{G1_{i,i+1}^{h_\xi h_\eta}}{H_{i+1}} \right),$$

and

$$f_{i,1} = \frac{(\tilde{\Theta}_{i,0} + \delta_{i,0}) - 2(\tilde{\Theta}_{i,1} + \delta_{i,1}) + \tilde{\Theta}_{i,2}}{h_\zeta^2} +$$

$$- \quad \bar{\rho}_{i,1} C_0 \bar{u}_{i,1} \Psi \left(\pm H_i^2 \frac{(\tilde{\Theta}_{i,1} + \delta_{i,1}) - (\tilde{\Theta}_{i\mp1,1} - \delta_{i,1}/2)}{h_\xi} \right)$$
$$+ \quad H_i^2 \Omega (\tilde{\Theta}_{i,1} + \delta_{i,1}) E \bar{u}_{i,1} \frac{P_{i+1} - P_{i-1}}{h_\xi}$$
$$+ \quad Source(\tilde{\Theta}_{i,1} + \delta_{i,1}) \quad (7.85)$$

where $Source(\tilde{\Theta}_{i,1} + \delta_{i,1})$ is the value of $\frac{H_i \Omega}{\bar{T}_0} \tau_{i,j} \left. \frac{\partial \bar{u}}{\partial \zeta} \right|_{i,1}$ when the change $\delta_{i,1}$ is applied. Since the source term is nonlinear, equations (7.84) and (7.85) cannot be solved exactly for $\delta_{i,0}$ and $\delta_{i,1}$, instead a local linearization of the source term is used.

Once the changes $\delta_{i,0}$ and $\delta_{i,1}$ have been determined for all i they are applied simultaneously according to the distribution displayed in figure 7.6. After the boundaries have been relaxed this way the relaxation sweep of the energy equation is completed with the line relaxation of the interior points.

7.7 Results

The algorithm described above will now be applied to a moderately loaded case, the maximum Hertzian pressure being $p_h = 1.2GPa$. A simplified energy equation is used, the only means of heat transfer is conduction, so the convection and the compresive heating/cooling terms are neglected. Table 7.2 shows the material properties of the solids and the lubricant as well as the operating conditions. All results shown have been calculated using a 289x289 grid with $\xi_a = -4.5$ and $\xi_b = 2$.

As a first check, the pure rolling case is considered. The pure rolling situation has been approximated by using a slide to roll ratio, $SR = 2\frac{U_2 - U_1}{U_2 + U_1} = 1.0e-15$. For this situation the thermal effects are due to inlet shear heating, i.e. shear heating due to compression in the inlet. The effects of inlet shear heating have been studied extensively, see for instance *Greenwood and Kauzlarich* (1973) , *Murch and Wilson* (1975) and *Wilson and Sheu* (1983). These studies show that for elastohydrodynamic contacts, inlet shear heating can result in a significant film thickness reduction, especially when high speeds or high viscosity lubricants are used. For the pure rolling situation *Wilson and Sheu* (1983) derived the following relation

$$C = \frac{1}{1 + 0.241\ L^{0.64}}, \qquad L = \frac{\eta_0 \gamma u_s^2}{k_f}$$

for the correction factor, C, which describes the reduction factor of the film thickness when compared to the isothermal case. The parameter L in this relation is the so-called thermal loading parameter. A value of ($L < 0.1$) indicates that thermal effects are negligible in the inlet and that conventional isothermal theory can be used. For ($L > 0.1$) a significant film thickness reduction can be expected.

For the case at hand the thermal loading parameter equals $L = 0.264$ which leads to a film thickness reduction factor of $C = 0.91$. The Moes' dimensionless film

Parameter	Meaning	Value	Dimension
oil:			
k_f	Thermal conductivity of the lubricant	0.12	$W.m^{-1}.K^{-1}$
ρ_{0f}	Ambient density of the lubricant	866.0	$kg.m^{-3}$
η_0	Ambient viscosity of the lubricant	0.040	$Pa.s$
γ	Temperature viscosity coefficient	0.04666	K^{-1}
ε	Thermal expansivity coefficient	6.5e-4	K^{-1}
α	Pressure viscosity coefficient	2.183e-08	$m^2.N^{-1}$
S_0	Roelands' thermoviscous parameter	1.121	–
z	Roelands' pressure-viscosity parameter	0.670	–
C_{pf}	Specific heat of the lubricant	2000.0	$J.kg^{-1}.K^{-1}$
solids:			
R	Equivalent Radius of the contact	0.01800	m
E'	Equivalent Young's modulus	2.30e+11	Pa
k_s	Thermal conductivity of the lubricant	52	$W.m^{-1}.K^{-1}$
ρ_s	density of the solid	7850	$kg.m^{-3}$
C_s	Specific heat of the solids	460.0	$J.kg^{-1}.K^{-1}$
Load Condition			
M	Moes' dimensionless load parameter	20.0	–
L	Moes' dimensionless material parameter	15.0	–
G	D-H's dimensionless material parameter	5.021e+03	–
U	D-H's dimensionless speed parameter	3.983e-11	–
W	D-H's dimensionless load parameter	1.785e-04	–
u_+	Average velocity	4.123	$m.s^{-1}$
p_h	maximum Hertzian pressure	1.226e+09	Pa
h_h	maximum Hertzian deformation	8.182e-06	m
b	half the Hertzian contact width	3.838e-04	m
T_0	Ambient temperature	293.0	K

Table 7.2: Material properties and operating conditions

thickness parameter H_{min} for this situation has been calculated as $H_{min} = 4.62$. This parameter is defined as :

$$\frac{8M_{Moes}}{\pi} \min\left(H(\xi)\right).$$

For the same situation but using isothermal theory *Venner* (1991) reports $H_{min} = 4.87$ for this parameter. Applying the the correction factor C to this value results in a value of $H_{min} = 4.42$ which is close to $H_{min} = 4.62$, the value calculated using the algorithm.

According to *Greenwood and Kauzlarich* (1975) the temperature rise at the far inlet can be approximated by

$$\Delta T \approx \frac{3}{4}\frac{\eta_0 u_s^2}{k_f}$$

which results in a temperature rise of 4.2 $°C$. Using the algorithm a maximum dimensionless inlet temperature of $\Theta_{max,inlet} = 1.014$ has been calculated. This corresponds to a maximum inlet temperature rise of 4.1 $°C$. The overall maximum temperature rise has been calculated as 5.9 $°C$ and occured in the outlet of the contact.

The coefficient of friction for this situation has been calculated as $\mu = 2.0e-4$ which corresponds to a value of $\bar{\mu} = 0.067$, a parameter defined by *ten Napel* (1975) as:

$$\bar{\mu} = \mu(2U)^{-1/4}$$

Lubrecht (1987) reports a value of $\bar{\mu} \approx 0.07$ (from graph) for this load and slip condition, so the results agree well with results from the literature in case of the pure rolling situation.

After this rolling situation, higher slip cases have been calculated. Figures $7.9^{a,b}$ show the coefficient of friction for small and large slide to roll ratios, respectively (please note the differences in scale). Although the slip curve shows the behaviour also found in experiments, i.e. a rise to a maximum followed by a monotonously fall of the coefficient of friction, the maximum value shown in the figure is far to high. This, of course, was to be expected since the lubricant has been modelled as a Newtonian fluid and in this region non-Newtonian effects are important as was shown by for instance *Johnson and Tevaarwerk* (1977) and *ten Napel et. al.* (1985).

Figure 7.10^{a} shows the maximum dimensionless temperature in the lubricant for slide to roll ratios in the range of [0,1.5]. As can be seen from this figure, the temperature rises are already substantial for small slide to roll ratios.

Another interesting result is shown in figure 7.10^{b}. From this figure it can be seen that the minimum film thickness decreases significantly with increasing slide to roll ratio; at $SR = 1.5$ it is merely more than half the value of the pure rolling case. In figure 7.11 the pressure distribution and the film profile are plotted for different SR-cases. From cases 1 and 2, i.e. $SR = 1e-15$ and $SR = 0.1$ respectively, it can be observed that the first sharp drop in mimimum filmthickness (7.10^{b}) is not accompanied by a drop in central film thickness; on the contrary, the central film thickness is even slightly larger for case 2.

This can be explained by studying the temperature rise in the contact more thouroughly. In figure 7.12 the contourlines of the dimensionless temperature distribution in the lubricant are shown. It can be seen that the inlet is not yet thermally affected for $SR = 0.1$. Also the pressure and film thickness distributions are the same in the inlet for these two cases. However the central part of the contact is heated, so the lubricant is expanded due to the temperature rise in the contact, giving rise to a larger central film thickness compared to the pure rolling case.

Looking at case 3 from figure 7.11, it can be concluded that for higher slide to roll ratios the inlet has to be thermally affected. This can be seen from figure 7.13, which shows contour lines of the dimensionless temperature distribution in the lubricant film for $SR = 1.5$. So, in the inlet, the viscosity of the lubricant is effectively lower compared to the cases 1 and 2, explaining the overall smaller film thickness.

7.8 Conclusions

It has been shown that the algorithm described in this chapter can solve the thermal EHL problem. It has been shown that the influence of shear heating at higher slide to roll ratios on the minimum film thickness and on traction is considerable and cannot be neglected.

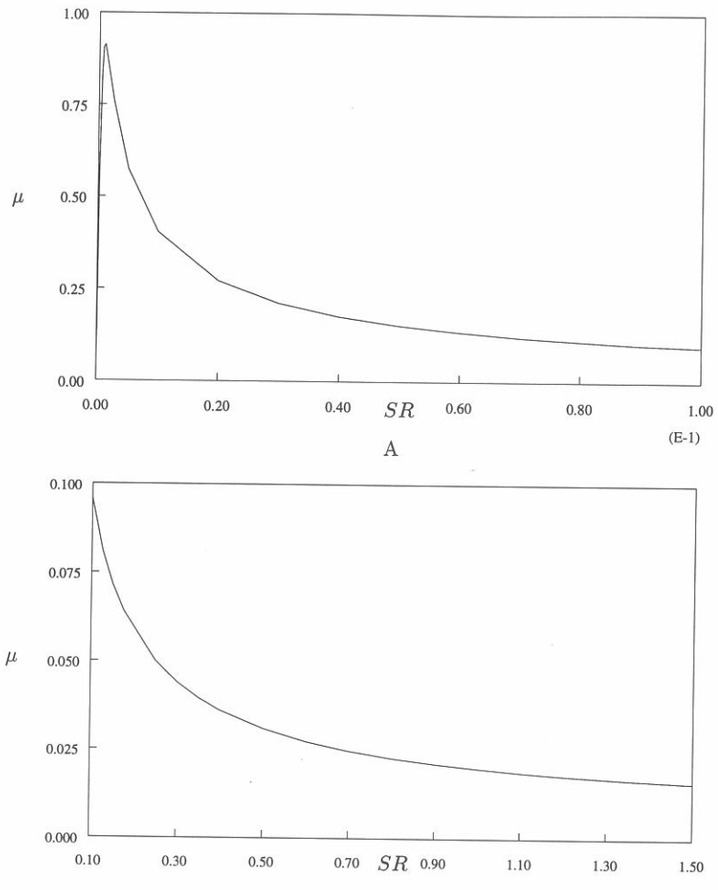

Figure 7.9: Traction, film thickness and temperature rise as function of the slide to roll ratio for the conditions given in table 7.2. A: coefficient of friction for small slide to roll ratios $[0-0.1]$, B: coefficient of friction for large slide to roll ratios $[0.1-1.5]$,

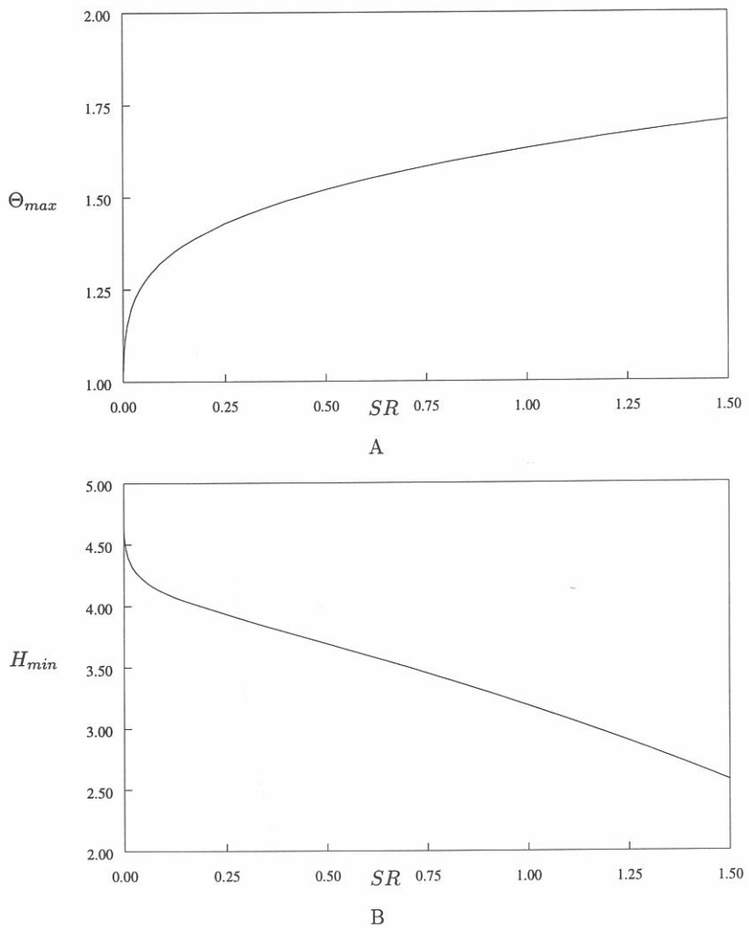

Figure 7.10: Film thickness and temperature rise as function of the slide to roll ratio for the conditions given in table 7.2. A: Maximum dimensionless contact temperature, B: Moes' dimensionless minimum film thickness parameter.

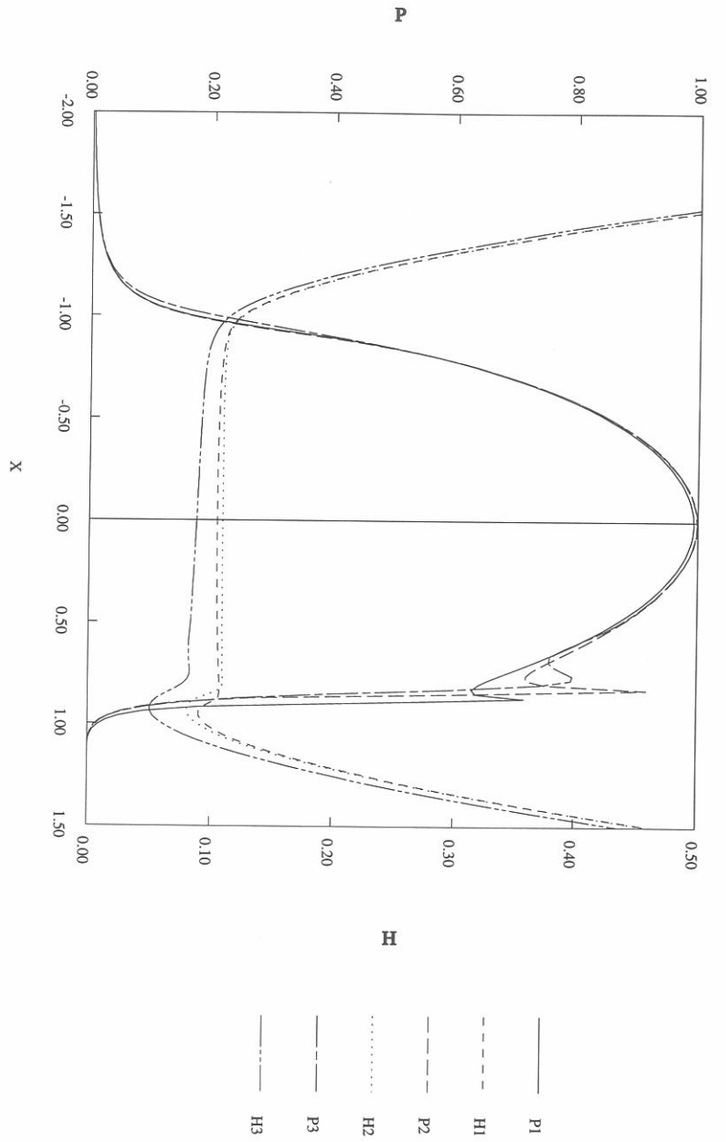

Figure 7.11: Pressure and film thickness distribution for 3 different slide to roll ratios. Case 1:$SR = 1e-15$, case 2: $SR = 0.1$ and case 3: $SR = 1.5$

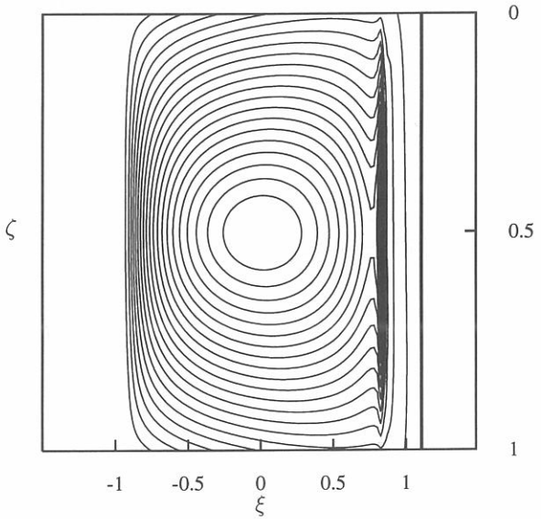

Figure 7.12: Contourlines of the dimensionless temperature distribution for $SR = 0.1$, $\Theta_{max} = 1.33$

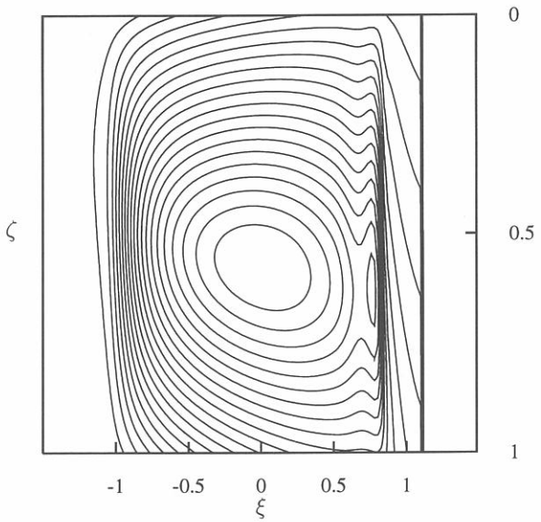

Figure 7.13: Contourlines of the dimensionless temperature distribution for $SR = 1.5$, $\Theta_{max} = 1.71$

References

Archard, J.F., and Baglin, K.P., 1975, "Nondimensional Presentation of Frictional Tractions in Elastohydrodynamic Lubrication, Part I: Fully Flooede Conditions", *ASME JOLT*, Vol. 97, pp. 398-410.

Brandt, A., 1984, "1984 Multigrid Techniques: 1984 Guide with applications to Fluid Dynamics," GMD Studien No. 85, *Gesellschaft für Mathematik und Datenverarbeitung MBH, Bon, Germany*

Greenwood, J.A. and Kauzlarich, J.J., 1973, "Inlet Shear Heating in Elastohydrodynamic Lubrication," *ASME Journal of Lubrication Technology*, Vol. 95, No. 4, pp. 417-426.

Huang, C., Wen, S., and Huang, P., 1992, "Multilevel Solution of the Elastohydrodynamic Lubrication of Concentrated Contacts in Spiroid Gears," to appear in *ASME JOT*, Preprint 92-TRIB-17.

Johnson, K.L., and Tevaarwerk, J.L., 1977, "Shear behaviour of elastohydrodynamic oil films", *Proc. R. Soc. Lond*, Vol. 356A, pp. 215-236.

Kyung Hoon Kim, and Sadeghi, F., 1991, "Non-Newtonian EHL of Point Contact," *ASME JOT*, **113**, 703-709.

Lubrecht, A.A., ten Napel, W.E., and Bosma, R., 1986, "Multigrid, An Alternative Method for Calculating Film Thickness and Pressure Profiles in Elastohydrodynamically Lubricated Line Contacts," *ASME JOT*, **108**, 551-556.

Lubrecht, A.A., 1987[a], "The numerical solution of the elastohydrodynamically lubricated line- and point contact problem using multigrid techniques," PhD. Thesis, University of Twente, Enschede, ISBN 90-9001583-3. Available from University of Twente, Central Library, P.O. Box 217, 7500 AE Enschede, The Netherlands.

Lubrecht, A.A., ten Napel, W.E., and Bosma, R., 1987[b], "Multigrid, an alternative method of solution for two-dimensional elastohydrodynamically lubricated point contact calculations," *ASME JOT*, **109**, 437-443.

Murch, L.E., and Wilson, W.R.D., 1975, "A Thermal Elastohydrodynamic Inlet Zone Analyses," *ASME Journal of Lubrication Technology*, Vol. 97, pp. 212-216.

ten Napel, W.E. Moes, H. and Bosma, R., 1975, "Discussion on *Archard and Baglin*, 1975", *ASME JOLT*, Vol. 97, pp. 410-411.

ten Napel, W.E., Klein Meuleman, P, Lubrecht, A.A., Houpert, L. and H. and Bosma, R., 1985, "Traction in elastohydrodynamic lubrication at very high contact pressures", *Proc. 4^{th} European Tribology Conference, Eurotrib '85*, Lyon, France.

Osborn, K.F., and Sadeghi, F., 1992 "Time Dependent Line EHD Lubrication using the Multigrid/Multilevel Technique," *ASME JOT*, **114**, 68-74.

Yang Peiran, and Wen Shizhu, 1990, "A generalized Reynolds equation for non-Newtonian thermal elastohydrodynamic lubrication," *ASME JOT*, **112**, 631-636.

Venner C.H. ten Napel W.E. and R. Bosma., 1990, "Advanced multilevel solution of the ehl line contact problem," *ASME JOT*, **112**, 426–432.

Venner, C.H., 1991, "Multilevel solution of the EHL line and point contact problems," PhD. Thesis, University of Twente, Enschede, The Netherlands. ISBN 90-9003974-0. Available from University of Twente, Central Library, P.O. Box 217, 7500 AE Enschede, The Netherlands.

Venner, C.H., and ten Napel, W.E., 1992, Advanced Multilevel Solution of the EHL circular contact problem, part I : Theoretical formulation and algorithm. *WEAR*, **152**, 351-367.

Wilson, W.R.D., and Shue, S., 1983, "Effect of inlet shear heating due to sliding on elastohydrodynamical film thickness," *ASME Journal of Lubrication Technology*, Vol. 105, pp. 187-188.

Recommendation for future research

The algorithm described in chapters 2 - 4 offers the possibility to numerically simulate multiple contact heat sources where the contacts are close together, i.e. when the heat flow through one contact influences the temperature rise in neighbouring contacts. This would be an important next step towards the simulation of realistic engineering contact configurations.

The model used in chapters 2 - 4 assumes that the bodies in contact are homogeneous However, in practice often hardened or coated bodies are used. It is clear that a surface layer with different thermal properties than the bulk material will have a substantial effect on the contact temperature. Therefore an important extension of the model would be the inclusion of surface layers with different thermal properties.

The algorithm described in chapter 7 can be extended in several directions. First of all the full energy equation should be used, i.e. convection and compressive heating and cooling should be taken into account.

Secondly, another direction for future research could be the inclusion of a more realistic (non-Newtonian) model of the lubricant. The algorithm described allows for non-Newtonian behaviour of the lubricant and the implementation should be straightforward, as long as no-slip boundary conditions are assumed. This limits the lubricant behaviour to fluids. However, extension to situations where the lubricant solidifies and slip occurs between the surfaces of the bodies and the "lubricant" is more involved.

In this work the EHL-line contact problem is treated. Future research might be directed towards the extension of the algorithm to point contacts. This would lead to an interesting application of the algorithm described in chapter 2, i.e. as boundary condition of the energy equation for the lubricant.

Acknowledgements

I would like to thank everyone who contributed to this thesis.

I would like to thank the members of the tribology group of the faculty of Mechanical Engineering of the University of Twente for their cooperation and support during the past four years and making it a pleasant place to work: prof. A.W.J. de Gee, ir. W.E. ten Napel, ir. H. Moes, dr. ir. C.H. Venner, dr. ir. D.J. Schipper, ir. P.H. Vroegop, ir. D.J. Ligterink, ing. E.G. de Vries, Mr. L.J. de Boer and Mrs. D. Vrieze-Zimmerman van Woesik. Special thanks to my fellow PhD. students: ir. R. ter Haar, ir. R.H.M. van der Steege, ir. H. Lubbinge, ir. E.R.M. Gelinck, ir. M. de Rooy, ir. H. Visser and ir. Y.H. Wijnant for their interest and enthousiasm.

I especially thank ir. W.E. ten Napel for the many useful discussions and suggestions as well as for creating a perfect working atmosphere, e.g. by minimizing teaching tasks.

Special thanks to dr. ir. C.H. Venner for continuous support, not only concerning multilevel algorithmic problems and the writing of this manuscript but also concerning every day things being my room mate.

I am indebted to ir. H. Moes for his co-work in much that has been reported in this thesis. The function fits presented in this thesis are his initiative and without his effort this thesis wouldn't be nearly as useful as it is now.

I owe ir. H.L.J. Elshof much. He worked with me for his M.Sc. thesis. During the period of his research I really had a partner and his results have been of great value for my own research.

I would like to thank my friend and fellow PhD. student ir. H.F. Bulthuis, for the many fun hours of studying each others problems and after work discussions.

I would like to thank the members of the "promotie-begeleidings" committee: prof. ir. A.W.J. de Gee, ir. W.E. ten Napel, dr. ir. D.J. Schipper, prof. dr. ir. L. van Wijngaarden, dr. ir. C.H. Venner and dr. ir. A.A. Lubrecht and the members of the "gebruikers" committee: prof. ir. A.W.J. de Gee, ir. W.E. ten Napel, ir. S.P.H.I. Bongers, drs. H. Mulder, ing. W. van Dam and dr. J.H. Tripp for their helpful suggestions and discussions.

Part of the research was carried out during a visit at the Weizmann institute of Science, Rehovot, Israel. I thank prof. Dr. A. Brandt for his hospitality and dr. ir. C.H. Venner for arranging everything that was needed for the visit. Furthermore I like to thank him and his wife Carole van Ruitenbeek for making it a very pleasant visit.

I gratefully acknowledge the support of the Technology Foundation STW. Due to this support I have been a "rich" PhD. student who could visit many abroad conferences and could use good computer facilities.

I would like to thank my parents for ensuring that I looked at the work in the right perspective and their encouragement.

Finally I would like to thank my girl-friend Petra Wicherink for her care, encouragement and patience in many respects.

Appendix A

Reduction of double integral to a line integral

The integral

$$I = \int_{y_m}^{y_p} \int_{x_m}^{x_p} \frac{du\ dv}{\sqrt{u^2+v^2}} \exp\left(-\frac{P}{2}\left(\sqrt{u^2+v^2}-u\right)\right) \tag{A.1}$$

can be reduced to a line integral in the following steps:

- First

$$\begin{aligned} t &= \frac{P}{2}\left(\sqrt{u^2+v^2}-u\right) \\ dt &= \frac{P}{2}\left(\frac{u}{\sqrt{u^2+v^2}}-1\right) du \end{aligned}$$

  is substituted into A.1. This leads to

$$\begin{aligned} I &= \int_{y_m}^{y_p} \left\{ \int_{\frac{P}{2}\left(\sqrt{x_m{}^2+v^2}-x_m\right)}^{\frac{P}{2}\left(\sqrt{x_p{}^2+v^2}-x_p\right)} \frac{\exp(-t)}{\sqrt{u^2+v^2}} \frac{dt}{\frac{P}{2}\left(\frac{u}{\sqrt{u^2+v^2}}-1\right)} \right\} dv \\ &= -\int_{y_m}^{y_p} \left\{ \int_{\frac{P}{2}\left(\sqrt{x_m{}^2+v^2}-x_m\right)}^{\frac{P}{2}\left(\sqrt{x_p{}^2+v^2}-x_p\right)} \frac{\exp(-t)}{t} dt \right\} dv \end{aligned}$$

- secondly using

$$E_1(x) = \int_x^\infty \frac{\exp(-t)}{t} dt \quad \text{and} \quad \int_a^b f(x)\ dx = \int_a^\infty f(x)\ dx - \int_b^\infty f(x)\ dx$$

  the integral is rewritten as:

$$I = -\int_{y_m}^{y_p} \left\{ E_1\left(\frac{P}{2}\left(\sqrt{x_m{}^2+v^2}-x_m\right)\right) - E_1\left(\frac{P}{2}\left(\sqrt{x_p{}^2+v^2}-x_p\right)\right) \right\} dv \tag{A.2}$$

- Next the first term of A.2 is treated (the second one can be treated the same way).

$$\begin{aligned}
I_1 &= -\int_{y_m}^{y_p} E_1(\frac{P}{2}\,(\sqrt{{x_m}^2+v^2}-x_m))\,dv \\
&= -\Big[v\;E_1(\frac{P}{2}\,(\sqrt{{x_m}^2+v^2}-x_m))\Big]_{y_m}^{y_p} + \int_{y_m}^{y_p} v\;dE_1(\frac{P}{2}\,(\sqrt{{x_m}^2+v^2}-x_m))\,dv \\
&= -\Big[v\;E_1(\frac{P}{2}\,(\sqrt{{x_m}^2+v^2}-x_m))\Big]_{y_m}^{y_p} + \\
&\quad \int_{y_m}^{y_p} v\;d\int_{\frac{P}{2}\,(\sqrt{{x_m}^2+v^2}-x_m)}^{\infty} \frac{\exp(-t)}{t}dt \\
&= -\Big[v\;E_1(\frac{P}{2}\,(\sqrt{{x_m}^2+v^2}-x_m))\Big]_{y_m}^{y_p} + \\
&\quad \int_{y_m}^{y_p} -v\;\frac{P}{2}\;\frac{v}{\sqrt{{x_m}^2+v^2}}\;\frac{\exp(-\frac{P}{2}\,(\sqrt{{x_m}^2+v^2}-x_m))}{\frac{P}{2}\,(\sqrt{{x_m}^2+v^2}-x_m)}\;dv
\end{aligned}$$

where in the last step Leibnitz' rule for the differentiation of integrals is used. The last result can be simplified to:

$$\begin{aligned}
I_1 &= -y_p\;E_1(\frac{P}{2}\,(\sqrt{{x_m}^2+{y_p}^2}-x_m)) + y_m\;E_1(\frac{P}{2}\,(\sqrt{{x_m}^2+{y_m}^2}-x_m)) + \\
&\quad -\int_{y_m}^{y_p} \frac{v^2}{\sqrt{{x_m}^2+v^2}}\;\frac{\exp(-\frac{P}{2}\,(\sqrt{{x_m}^2+v^2}-x_m))}{\sqrt{{x_m}^2+v^2}-x_m}\;dv \qquad \text{(A.3)}
\end{aligned}$$

In the same way the second term of A.2 can be calculated as:

$$\begin{aligned}
I_2 &= \int_{y_m}^{y_p} E_1(\frac{P}{2}\,(\sqrt{{x_p}^2+v^2}-x_p))\,dv \\
&= y_p\;E_1(\frac{P}{2}\,(\sqrt{{x_p}^2+{y_p}^2}-x_p)) - y_m\;E_1(\frac{P}{2}\,(\sqrt{{x_p}^2+{y_m}^2}-x_p)) + \\
&\quad \int_{y_m}^{y_p} \frac{v^2}{\sqrt{{x_p}^2+v^2}}\;\frac{\exp(-\frac{P}{2}\,(\sqrt{{x_p}^2+v^2}-x_p))}{\sqrt{{x_p}^2+v^2}-x_p}\;dv \qquad \text{(A.4)}
\end{aligned}$$

- So finally, the total integral can be written as:

$$\begin{aligned}
I &= y_p\;E_1(\frac{P}{2}\,(\sqrt{{x_p}^2+{y_p}^2}-x_p)) - y_m\;E_1(\frac{P}{2}\,(\sqrt{{x_p}^2+{y_m}^2}-x_p)) + \\
&\quad -y_p\;E_1(\frac{P}{2}\,(\sqrt{{x_m}^2+{y_p}^2}-x_m)) + y_m\;E_1(\frac{P}{2}\,(\sqrt{{x_m}^2+{y_m}^2}-x_m)) + \\
&\quad -\int_{y_m}^{y_p} \frac{v^2}{\sqrt{{x_m}^2+v^2}}\;\frac{\exp(-\frac{P}{2}\,(\sqrt{{x_m}^2+v^2}-x_m))}{\sqrt{{x_m}^2+v^2}-x_m}\;dv + \\
&\quad +\int_{y_m}^{y_p} \frac{v^2}{\sqrt{{x_p}^2+v^2}}\;\frac{\exp(-\frac{P}{2}\,(\sqrt{{x_p}^2+v^2}-x_p))}{\sqrt{{x_p}^2+v^2}-x_p}\;dv
\end{aligned}$$

Appendix B

If the function G is defined as:

$$G(\nu,\xi) \equiv \int_0^1 \frac{|x-\xi|^{2\nu-1}}{x^\nu(1-x)^\nu}dx, \quad 0<\nu<1.$$

then

$$G(\nu,\xi) = \frac{\pi}{\sin(\pi\nu)}, \quad \text{for} \quad 0 \le \xi \le 1$$

In the following proof by Dr. ir. J.P.A.M. Hijmans the notation c.f. Handbook of Mathematical Functions (HMF) (1965) is used.

Proof

Consider the the cases $0 < \xi < 1$:

$$G(\nu,\xi) = \int_0^\xi \frac{(\xi-x)^{2\nu-1}}{x^\nu(1-x)^\nu}dx + \int_\xi^1 \frac{(x-\xi)^{2\nu-1}}{x^\nu(1-x)^\nu}dx$$

In the first integral substitute $t = x/\xi$ and in the second $t = (1-x)/(1-\xi)$, then after some reductions this equation can be written as:

$$\begin{aligned} G(\nu,\xi) \quad &= \quad \xi^\nu \int_0^1 \frac{(1-t)^{2\nu-1}}{t^\nu(1-\xi t)^\nu}dt \\ &+ \quad (1-\xi)^\nu \int_0^1 \frac{(1-t)^{2\nu-1}}{t^\nu(1-(1-\xi)t)^\nu}dt \\ &\text{(HMF 15.3.1)} \\ &= \quad B(1-\nu,2\nu)\ \xi^\nu\ F(\nu,1-\nu;1+\nu;\xi) \\ &+ \quad B(1-\nu,2\nu)\ (1-\xi)^\nu\ F(\nu,1-\nu;1+\nu;1-\xi) \end{aligned}$$

where

$$B(1-\nu,2\nu) = \frac{\Gamma(1-\nu)\Gamma(2\nu)}{\Gamma(1+\nu)}.$$

By using (HMF 15.5.3)

$$F(\alpha,\beta;\gamma;z) = (1-z)^{\gamma-\alpha-\beta}\ F(\gamma-\alpha,\gamma-\beta;\gamma;z)$$

it follows:

$$G(\nu,\xi) = B(1-\nu,2\nu)\ \xi^{\nu}\ (1-\xi)^{\nu}\ \{F(1,2\nu;1+\nu;\xi) + F(1,2\nu;1+\nu;1-\xi)\}$$

Define, $p = \xi - \frac{1}{2}$ (due to symmetry around $\xi = \frac{1}{2}$), then it follows that

$$G(\nu,\xi) = B(1-\nu,2\nu)\ 4^{-\nu}\ (1-4p^2)^{\nu}\ S(\nu,p)$$

with

$$\begin{aligned}
S(\nu,p) &= F(1,2\nu;1+\nu;\frac{1}{2}+p) + F(1,2\nu;1+\nu;\frac{1}{2}-p) \\
S(\nu,p) &\quad \text{is an even function of } p \\
S(\nu,p) &= 2\sum_{k=0}^{\infty} C_{2k}\ p^{2k} \quad \text{with} \\
C_{2k} &= \frac{1}{(2k)!}\left[\frac{\partial^{2k}}{\partial p^{2k}} F(1,2\nu;1+\nu;\frac{1}{2}+p)\right]_{p=0} \\
&= \frac{(2\nu)_{2k}}{(1+\nu)_{2k}} F(1+2k,2\nu+2k;1+\nu+2k;\frac{1}{2}).
\end{aligned}$$

According to (HMF 15.2.2)

$$\frac{d^n}{dz^n} F(\alpha,\beta;\gamma;z) = \frac{(\alpha)_n(\beta)_n}{(\gamma)_n} F(\alpha+n,\beta+n;\gamma+n;z).$$

With $\gamma = \frac{1}{2}(\alpha+\beta+1) \neq 0,-1,-2,\cdots$ the following holds (HMF 15.1.2):

$$F(\alpha,\beta;\gamma;\frac{1}{2}) = \sqrt{\pi}\ \frac{\Gamma(\gamma)}{\Gamma(\frac{\alpha+1}{2})\Gamma(\frac{\beta+1}{2})}$$

therefore

$$\begin{aligned}
C_{2k} &= \frac{(2\nu)_{2k}}{(1+\nu)_{2k}}\ \sqrt{\pi}\ \frac{\Gamma(1+\nu+2k)}{k!\Gamma(\nu+\frac{1}{2}+k)} \\
&= \sqrt{\pi}\ \frac{\Gamma(1+\nu)}{\Gamma(\nu+\frac{1}{2})}\frac{1}{k!} 2^{2k}(\nu)_k
\end{aligned}$$

so

$$\begin{aligned}
S(\nu,p) &= 2\sqrt{\pi}\ \frac{\Gamma(1+\nu)}{\Gamma(\nu+\frac{1}{2})} \sum_{k=0}^{\infty} \frac{1}{k!}(\nu)_k 2^{2k} p^{2k} \\
&= 2\sqrt{\pi}\ \frac{\Gamma(1+\nu)}{\Gamma(\nu+\frac{1}{2})} F(\nu,1;1;4p^2) \\
&= 2\sqrt{\pi}\ \frac{\Gamma(1+\nu)}{\Gamma(\nu+\frac{1}{2})} (1-4p^2)^{-\nu} \quad \text{(HMF 15.1.8)}
\end{aligned}$$

Combining everything results in:

$$\begin{aligned}
G(\nu,\xi) &= B(1-\nu,2\nu)\ 4^{-\nu}\ 2\sqrt{\pi}\ \frac{\Gamma(1+\nu)}{\Gamma(\nu+\frac{1}{2})} \\
&= \frac{\pi}{\sin(\pi\nu)}
\end{aligned}$$

To arrive at this result equations (HMF 6.1.17 and 6.1.18) have been used to rewrite the Γ-function.

Finally consider the cases $\xi = 0$ and $\xi = 1$:

$$\begin{aligned}
G(\nu,0) &= G(\nu,1) = \int_0^1 \frac{x^{\nu-1}}{(1-x)^{\nu}} dx \\
&\quad \text{(HMF 6.2.1)} \\
&= B(\nu,1-\nu) = \frac{\Gamma(\nu)\ \Gamma(1-\nu)}{\Gamma(1)} = \frac{\pi}{\sin(\pi\nu)}
\end{aligned}$$

which concludes the proof.

References

Abramowitz, M. and Stegun, I.A., 1965 (eds), Handbook of Mathematical Functions, New York.